

Institute for Automation

Department Product Engineering,

Montanuniversität Leoben



**Modelling, Simulation and Control
of a Hydraulic System with
Individual Meter-in and Meter-out**

MASTER THESIS

Goran Stojanoski

Field of Study:
Mechanical Engineering

Supervisor:

ASS.PROF. DIPL.-ING. DR.MONT. GERHARD RATH

O.UNIV.-PROF. DIPL.-ING. DR.TECHN. PAUL O'LEARY

November, 2017

Acknowledgements

This project was funded by EIT Raw-Materials project Rock Vader and carried out in cooperation with Sandvik Mining and Construction GmbH located in Zeltweg, Austria.

There are several people who have helped in the preparation of this thesis and to whom in this occasion I wish to express my deepest gratitude. Firstly, I want to thank my mentor Ass.Prof. Dipl.-Ing. Dr.mont. Gerhard Rath for his support, shared knowledge and for giving me the opportunity to work on such project, as well as O.Univ.-Prof. Dipl.-Ing. Dr.techn. Paul O'Leary for supervising this thesis. I would also like to thank my Macedonian Professor Dr. Emil Zaev for all of his support and help during my studies here.

Thanks to the company Sandvik Mining and Construction GmbH for providing all the necessary components to make this thesis possible. Further more, I would like to thank Hubert Kargl for giving me the opportunity to work on this project, Uwe Restner the coordinator of the Rock Vader project and Martin Gimpel and Wolfgang Richter for all their support, help and time during my period at Sandvik.

Finally, I would like to thank my family for their support, love and understanding. Without my mother Snezana, my father Pece and my brother Goce I wouldn't have accomplished half of what I have accomplished today.

Zusammenfassung

Ziel dieser Arbeit war es, ein Computer-Simulationsmodell für einen servo-gesteuerten hydraulischen Antrieb zu entwickeln, der auf einem Prüfstand verwendet wird, um verschiedene Strategien zur Bewegung von großen mechanischen Lasten zu testen. Das mechanische System, bestehend aus starren Körpern und Gelenken, wurde in SimMechanics[®], einer graphisch orientierten Umgebung zur Mehrkörpersimulation, entwickelt. Die numerische Lösung des hydraulischen Systems basiert auf den gewöhnlichen Differentialgleichungen (ordinary differential equations, ODE). Beide Modelle werden innerhalb von Simulink[®] in einer Co-Simulation mithilfe des "prismatic translational interface" zusammengeführt. Das verwendete Hydraulikventil enthält ein komplexes eingebettetes System und verwendet Druck- und Wegsensoren, sowie mathematische Modelle zur Durchflussberechnung, um logische und regeltechnische Entscheidungen zu treffen. Ein Schwerpunkt dieser Arbeit war es daher auch, dieses Verhalten am Computer nachzuvollziehen. Alle wesentlichen Ergebnisse sind graphisch dargestellt und werden mit Messdaten, die am Prüfstand aufgenommen wurden, verglichen. Die Resultate sind konsistent und stimmen gut mit den realen Daten überein. Das Simulationsmodell kann in Zukunft zur Einschulung in das Prinzip der getrennten Steuerkanäle verwendet werden, zum Testen von neuen Regelstrategien, sowie zur Fehlersuche an der realen Maschine, indem Abweichungen vom normalen Verhalten in der Simulation nachvollzogen werden.

Abstract

The aim of this thesis is to develop a dynamic model for simulation of a hydraulic servo drive on a test rig, built for the purpose of testing different control strategies for the motion of inertial loads. The mechanical system, which consists of rigid bodies and joints, is modelled in SimMechanics[®], which is a dedicated environment for three-dimensional multi-body simulation, including kinematics and dynamics. The model of the hydraulic system is based on the numerical solution of ordinary differential equations (ODE). Both models were combined within the Simulink[®] environment in the sense of Co-Simulation, using the prismatic translational interface. The hydraulic valve used for the application is controlled by a complex embedded system providing two main modes for individual meter-in and meter-out control. For this purpose, it uses integrated pressure sensors, displacement sensors and mathematical models for oil-flow estimation for making decisions. Consequently, one focus of this work was to include this behaviour into the simulation model. All essential results are presented in graphs and compared with measurements of the real system. The simulation results are consistent and match well with the measurements. The simulation model developed in this work can be used in the future to explain the principle of independent metering in education, to verify new control strategies and to find causes of problems in the real machine by reproducing deviations from the normal behaviour.

Statutory declaration

I declare in lieu oath, that I wrote this thesis and performed the associated research myself, using only literature cited in this volume.

Eidesstattliche Erklärung

Ich erkläre an Eides statt, dass ich diese Arbeit selbständig verfasst, andere als die angegebenen Quellen und Hilfsmittel nicht benutzt und sonst keiner unerlaubten Hilfsmittel bedient habe.

Leoben, Tue 28th Nov, 2017

Goran Stojanoski

Symbols

dx_a	Derivative of the piston position
dt	Time derivative
F_{load}	Load force [N]
F_f	Friction force [N]
m_a	Piston mass [kg]
p_1	Pressure piston side [Pa]
p_2	Pressure rod side [Pa]
A_1	Area piston side [m ²]
A_2	Area rod side [m ²]
F_p	Resultant force for one double acting cylinder [m ³]
Q_1	Flow piston side [m ³]
Q_2	Flow rod side [m ³]
β_f	Bulk modulus of the fluid [Nm ⁻²]
ρ	Density [kgm ⁻³]
dp	Pressure differential [Pa]
v_1	Velocity piston side [ms ⁻¹]
v_2	Velocity rod side [ms ⁻¹]
g	Acceleration of the gravity [ms ⁻²]
v_I	Velocity at the entrance of the orifice (cross-section I) [ms ⁻¹]
v_v	Velocity at the cross - section v (vena contracta) [ms ⁻¹]
p_I	Pressure at the cross - section I [Pa]
p_v	Pressure at the cross - section v [Pa]
C_v	Contraction coefficient
A_I	Area at the cross-section I [m ²]
A_v	Area at the cross-section v [m ²]
A_d	Area at the cross-section d [m ²]
C_d	Discharge coefficient
u	Control variable
u_b	Bias variable(reset)
P_L	Load pressure [Pa]
P_s	Supply pressure [Pa]
x_v	Maximal valve stroke[m]
K_q	Flow gain [m ³ s ⁻¹]

w	Area gradient [m]
x_v	Spool position [m]
Δ_p	Pressure difference [Pa]
C_r	Radial clearance [m]
D	Piston head diameter [m]
x	Piston position [m]
\dot{x}	Piston velocity [ms^{-1}]
μ	Absolute viscosity [Nsm^{-2}]
ν	Kinematic viscosity [m^2s^{-1}]
θ	Temperature [K]
B	Viscous friction coefficient
h	Piston stroke [m]
A	Piston area [m^2]
D_T	Pitch diameter [m]
α	Swivel angle [$^\circ$]
α_{max}	Max. swivel angle [$^\circ$]
V_g	Geometrical displacement [$\text{cm}^3\text{rev}^{-1}$]
Q	Volume flow [lmin^{-1}]
n	Speed [$\text{rev} \cdot \text{min}^{-1}$]
η_{vol}	Volumetric efficiency
η_{meh}	Mechanical efficiency
η_t	Overall efficiency
P	Hydraulic pump power [W]
M	Hydraulic pump torque [Nm]
Q_N	Nominal volume flow [lmin^{-1}]
Δ_{pN}	Nominal pressure differential [Pa]
x_{vmax}	Maximal opening of the orifice [m]
V	Total volume [m^3]
ΔV	Change in volume [m^3]
ΔP	Change in pressure [Pa]
v_a	Velocity of the piston [ms^{-1}]
C_h	Hydraulic capacitance [m^5N^{-1}]
A_{in}	Area piston side(actuator entrance) [m^2]
A_{out}	Area rod side(actuator exit) [m^2]
y	Measured value
y_{sp}	Set point
e	Error value
e_0	Error value
K	Proportional gain
T_i	Integral time
T_d	Derivative time

K_c	Flow pressure gain [$\text{m}^3\text{s}^{-1}\text{Pa}^{-1}$]
K_p	Pressure sensitivity [$\text{Pa} \cdot \text{m}^{-1}$]
K_P	Proportional gain
K_a	Acceleration feedback gain
Q_L	Load flow [lmin^{-1}]
K_{q0}	Null flow gain [m^3s^{-1}]
A_{ratio}	Area ratio

Abbreviations

<i>SMISMO</i>	Single meter - in single meter - out concept
<i>PV</i>	Conditioning Valve
<i>CV</i>	Pivot valve
<i>PCLS</i>	Pressure compensation load sensing systems
<i>LVDT</i>	Linear variable differential transformer
<i>PVA</i>	Position velocity acceleration controller
<i>DE</i>	Discrete event model
<i>CT</i>	Continuous time model
<i>UFC</i>	Universal flow control
<i>IFC</i>	Intelligent flow control
<i>RMDS</i>	Rapid mine development system
<i>LS</i>	Load sensing

Contents

1	Introduction	1
2	Mechanical System	3
2.1	Mechanical Model	3
2.1.1	Modelling of Mechanical Systems	3
3	Basic Principles of the Hydraulic Systems	9
3.1	Hydraulic Actuators	9
3.1.1	Hydraulic Cylinder	9
3.1.2	Double Acting Cylinder	10
3.1.3	Friction in Hydraulic Cylinders	11
3.2	Hydraulic Valves	13
3.2.1	Flow through Orifices	13
3.2.2	Directional Control Valves	14
3.2.3	Modelling of 2/2 Directional Valve	15
3.2.4	3/3 Valve with Different Valve Centres	16
3.2.5	Modelling of 4/3 Directional Valve	17
3.3	Hydraulic Pumps	18
3.3.1	Axial Piston Pumps	19
4	Hydraulic Servo Systems	21
4.1	Non Linear Model of Servo Hydraulic System	21
4.1.1	Hydraulic Valve Coefficients	23
4.2	Hydraulic Capacity	24
4.3	Passive and Active Loads	24
4.3.1	Passive Loads	25
4.3.2	Active Loads	25
4.4	Independent Metering Systems	26
4.4.1	Pressure Compensation Load Sensing Systems (PCLS)	26
4.4.2	Independent Metering Valve (Eaton CMA90)	26
5	Control of Hydraulic Systems	28
5.1	Classical Feedback Control Design	28
5.2	PID Controller	28

5.2.1	Proportional Action	29
5.2.2	Integral Action	29
5.2.3	Derivative Action	30
5.3	Acceleration Feedback	30
5.4	Position Feedback	31
5.5	Pressure Feedback	31
6	Simulation of the Model	32
6.1	Co - Simulation and Co - Modelling of Hydraulic and Mechanical Systems . . .	32
6.2	Modelling of the System	33
7	Simulation and Results	45
7.1	Test Rig Model with UFC Control Mode	45
7.2	Test Rig with IFC Control Mode	51
8	Verification of the Results	65
8.1	Measurement Instruments	65
8.2	Verification of the Model	67
9	Conclusion and Future Recommendations	71
A	Code	73

List of Figures

1.1	Sandvik Mine Development System MX650 (courtesy of Sandvik)	2
1.2	RMDS test rig (courtesy of Sandvik)	2
2.1	I beam after DIN1025 - 1	4
2.2	Cross section and cross section points	4
2.3	Double bracket	5
2.4	I Beam with connection points	6
2.5	Hydraulic cylinder	6
2.6	Mechanical cylinder - piston connection	7
2.7	Mechanical system	7
2.8	Simulated hydraulic cylinder	8
3.1	Hydraulic model from double acting cylinder	10
3.2	Cylinder piston	12
3.3	Example of static friction models [19]	12
3.4	Flow through orifice	13
3.5	2/2 Directional Valve	15
3.6	3/3 Directional Valve with zero lapping	16
3.7	Open and closed valve centre by 3/3 Directional Valve	16
3.8	Flow gain of different centre types [23]	17
3.9	Three land four way spool valve	18
3.10	Variable axial piston pump of swashplate design [16]	19
4.1	Hydraulic system, servo control cylinder	21
4.2	Pressure - flow curve for a 4 port critical centre valve	23
4.3	Passive Load	25
4.4	Active Load	25
4.5	Independent metering twin spool valve Eaton CMA90	27
5.1	Feedback Control System	28
5.2	PID controller	29
6.1	Co - simulation solution cycle	33
6.2	Hydraulic cylinder in Simulink®	34

6.3	Connection of the hydraulic cylinder with the mechanical system	35
6.4	Hydraulic directional valve in Simulink® (Eaton CMA90)	36
6.5	$Sqrt_{Abs}$ block	37
6.6	UFC gains	37
6.7	UFC control logic (adopted from [7])	38
6.8	IFC control logic (adopted from [7])	39
6.9	IFC control logic in Simulink®	40
6.10	UFC control logic in Simulink®	41
6.11	Simulink® model of load sensing pump	41
6.12	Simulink® model of the test trek with IFC control mode	43
6.13	Simulink® model of the test rig with UFC control mode	44
7.1	UFC Flow control K_p	46
7.2	UFC Flow control K_p, K_d	47
7.3	UFC position control	48
7.4	UFC position control (sinus input)	48
7.5	UFC position control with acceleration feedback	49
7.6	UFC position control with acceleration feedback (sinus input)	49
7.7	Position control $UFC=0.1-1.5$	50
7.8	Pressures $UFC=0.5-1.5$	51
7.9	IFC flow control 20 - 80 l/min	52
7.10	IFC pressure control [60bar]	53
7.11	IFC pressure control [80bar]	53
7.12	IFC position control $K_p=50,100$	54
7.13	IFC position control $K_p=150,200$	54
7.14	IFC position control $K_p=400,600$	55
7.15	IFC position control with step function input $K_p=30, 60, 100$	55
7.16	IFC position control with acceleration feedback $K_p=600, 800$	56
7.17	IFC position control with acceleration feedback (step function input) $K_p=100, 200$	56
7.18	IFC position control with acceleration feedback $K_p=1200$	57
7.19	IFC position control with acceleration feedback $K_p=800, m=4000kg$	57
7.20	IFC pressure control with acceleration feedback $K_p=800, m=4000kg$	58
7.21	IFC position control with acceleration feedback $K_p=800, m=8000kg$	58
7.22	IFC pressure control with acceleration feedback $K_p=800, m=8000kg$	59
7.23	IFC position control with acceleration feedback $K_p=800, m=12000kg$	59
7.24	IFC pressure control with acceleration feedback $K_p=800, m=12000kg$	60
7.25	IFC control logic	61
7.26	IFC position control with acceleration feedback and vibration $K_p=800, m=3000kg$	62
7.27	IFC pressure control with acceleration feedback and vibration $K_p=800, m=3000kg$	63
7.28	IFC control logic with acceleration feedback and vibration $K_p=800, m=3000kg$	63
8.1	Acceleration sensor on test rig	66

8.2	Eaton block	67
8.3	Test rig	67
8.4	Verification of the position	68
8.5	Pressure piston side verification	69
8.6	Pressure rod side verification	69

List of Tables

2.1	Double bracket parameters	5
2.2	Cylinder parameters	7
7.1	UFC control block parameters	46
7.2	IFC control block parameters	51

Chapter 1

Introduction

Fluid power control i.e. transmission and control of energy by means of pressurized fluid is an old and well recognized discipline [18, p. 1]. Fluid power technology traces can be found back in ancient times when the first water watches were invented [18]. With the fast growth of technology, the hydraulic control systems evolved rapidly during a short period of time. In parallel, the requirements for hydraulic system simulation have increased. The new software generations offer a lot of new types of future by employing The Physical Network Approach which differs from the standard Modelling Approach and suits the systems consisting of real physical components.

The road and tunnel cutting machines are machines that are used to excavate a tunnel or cut a road through variety of soils and rocks. Such a machine is the Sandvik MX650 (Sandvik Mine Development System) for rock cutting for roadway development mine, which consists system of two individual but identical cutter heads. This cutter heads are driven with the cutter gearboxes vertically and with hydraulic cylinders horizontally. A new Eaton CMA control valve was used, which uses the Separate meter in and Separate meter out (SMISMO) hydraulic concept, in order to achieve better performance and stiffer system. This valve offers few control modes which were implemented and tested accordingly. Since this is the first time that such a control concept was implemented on this machine, a test rig was constructed in order to learn more and explore the possibilities of this concept Fig. 1.2.

Previous works on this types of systems and this test rig were done in [28]. In his dissertation thesis he investigates some possible improvements of the control of the SMISMO system, as a better damping systems in order to achieve better energy efficiency.

The article [8] discusses different types of independent metering systems and the advantages of this systems in comparison with the meter - in and meter - out systems.



Figure 1.1: Sandvik Mine Development System MX650 (courtesy of Sandvik)

The aim of this master thesis is the simulation of the mechanical, hydraulic and control systems of the Sandvik Mine Development System with the help of Matlab Simulink[®] in order to achieve better performance and control. For this purpose the Matlab[®] 2016b software was used, further the Simulink[®] and Simscape libraries.

Simulink[®] is a very powerful dynamic system modelling and simulation software package for Matlab[®], which provides a complete and flexible visual design and debugging environment for the user's modelling and simulation process and contains a wealth of functional modules in many professional fields [12].

By using simulation of different control modes it will be tested which of them emphasizes the difference between the flow and pressure control systems.

Test rig is built and simulated in order to get to know the SMISMO concept and to improve the control of the system.

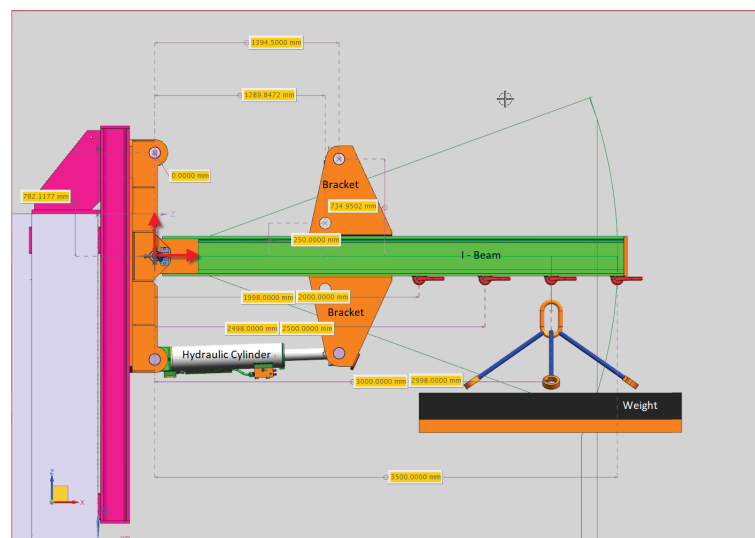


Figure 1.2: RMDS test rig (courtesy of Sandvik)

Chapter 2

Mechanical System

The following chapter focuses on the most important components of the mechanical system and the basic principles of how these components work.

The new SimMechanics block-set provides a multi-body simulation environment for 3D mechanical systems. With the help of the bodies, joints, constrains and the other elements given in the SimMechanics library you can easily construct the 3D model needed and SimMechanics will formulate and solve the equations of motion for the mechanical systems. The moment of inertia is also automatically calculated by the software with the given geometry and mass (density) of the bodies included in the mechanical system.

2.1 Mechanical Model

Figure 1.2 shows that the mechanical model consists of an I-Beam which is fixed to a concrete block, a few brackets, hydraulic cylinder and weight. In order to simulate and build this parts a complex system of systems and subsystems was created Fig. 2.7.

A dynamic mechanical model is built by using the second generation of SimMechanics. The changes in the mechanical system are measured with several sensors like vibration sensor, position sensor, velocity and acceleration sensor.

2.1.1 Modelling of Mechanical Systems

Figure 1.2 shows that the mechanical model has 1 degree of freedom. The gravity force is in z axis. As mentioned in the previous Chapter 2.1 our mechanical system consists of several subsystems, the I beam subsystem, the two double bracket subsystems and the subsystem for the weight and the rope that connects it to the I beam.

The construction process of the mechanical model is done in the software in several steps. Firstly, the rotation points are defined at the start of the I-Beam and the start of the cylinder (zero position). As mentioned in Chapter 2.1 the system consists of single and compound rigid bodies. The single rigid body uses a single solid block but the compound rigid body connects multiple rigid bodies to have the rigid body modelled. They are both connected to revolute joints in order to achieve

rotation in z - axis. The I-Beam dimensions were given according to DIN1025-1 standard for I300 profile.

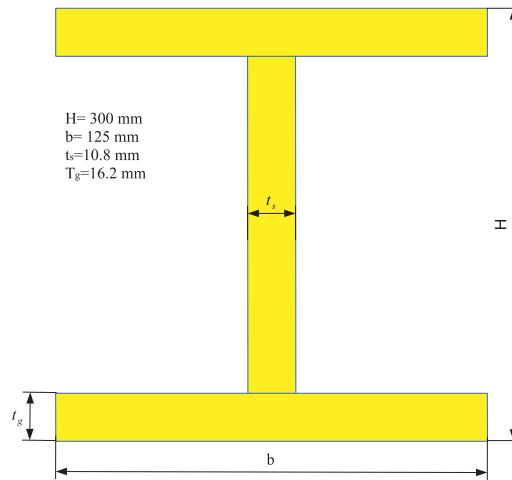


Figure 2.1: I beam after DIN1025 - 1

Figure 2.1 shows the model of the beam we are to build in our simulation. In order to achieve that, there are several parameters that we need to define first. To represent the beam geometry, the cross section and its coordinates are to be defined.

With the dimensions given in Fig. 2.1 and the cross sections points defined with the equations in figure 2.2 implemented in the mask of the subsystem, we can easily construct the I beam shown in Fig. 2.4. The length of the I beam is 3500 mm.

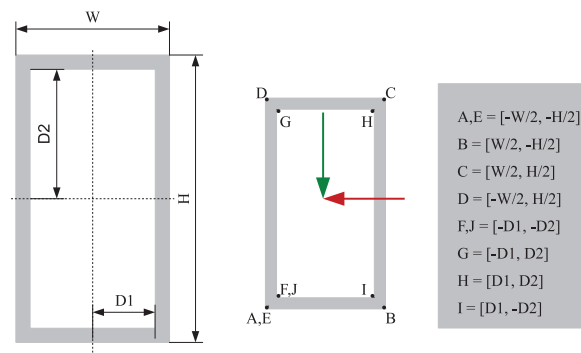


Figure 2.2: Cross section and cross section points

Figure 1.2 shows that the I beam is connected with two pairs of brackets, hydraulic cylinder, weight and external force which is implemented on top of it. After modelling the I-Beam six different connecting points were defined on it accordingly. Two for the bracket pairs, one for the mass, the position of the beam and the external force that will be applied on top of the Beam.

The two bracket points are connected to the beam in two different positions with the following coordinates: $[0 \ 155 \ -355.5]$ and $[0 \ -155 \ -355.5]$. In order to build these parts in the simulation model we need to define the dimensions of the brackets shown on Fig. 2.3 .

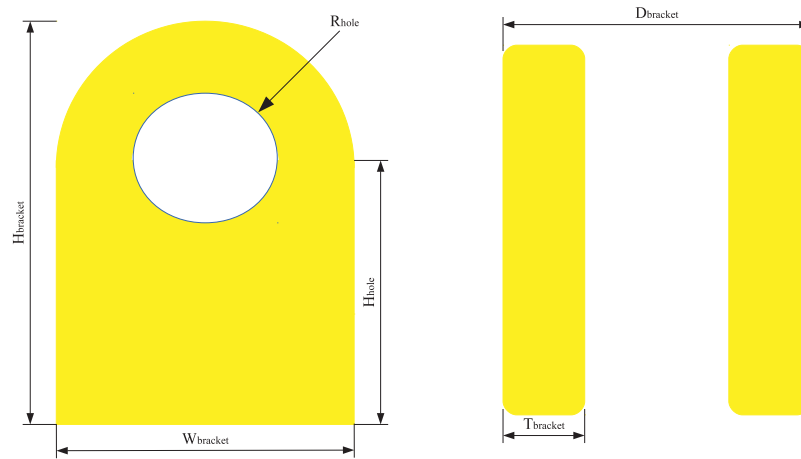


Figure 2.3: Double bracket

The dimensions of the brackets used in the simulation are given in following table.

Bracket	Parameters
Height	Hbracket
Width	Wbracket
Depth	Tbracket
Height hole	Hhole
Radius hole	Rhole
Diameter	Dbracket

Table 2.1: Double bracket parameters

The external force is implemented at the same location as the vibration motor was implemented on the real system (3400mm from the beginning of the I beam). The idea is to observe the behaviour of the control system during vibrations. Mass is applied to the beam at 3000-mm distance. The mass weight will be between 0 to 12000 kg. It is connected to a revolute joint in order to move freely when the beam moves. It is important to mention that all the point orientations need to be modified in that way that z axis always remains the axis in which the gravitational force has direct influence on the system. This is very important for the mechanical system of the simulation as well as for the hydraulic system.

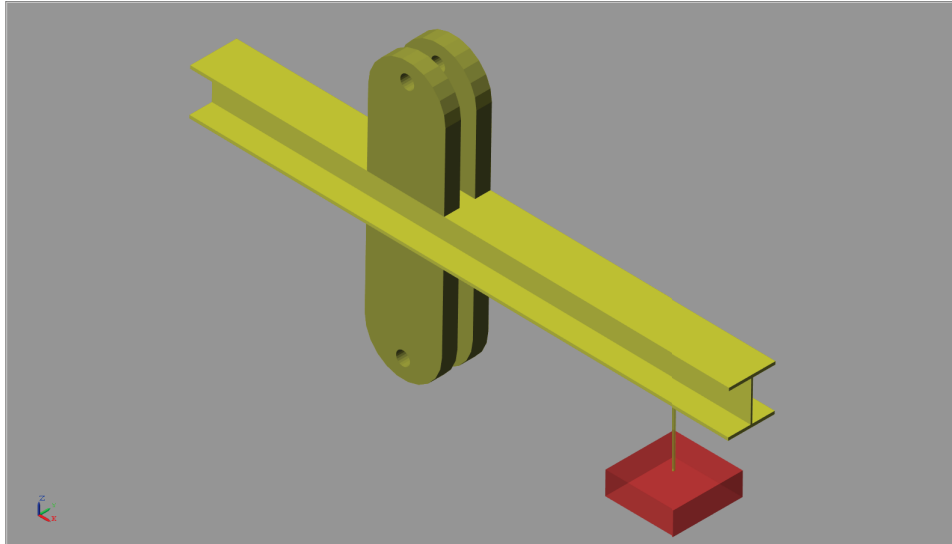


Figure 2.4: I Beam with connection points

The last part that needs to be simulated is the hydraulic cylinder. The mechanical part of the hydraulic cylinder is separated into piston and rod which are connected with a prismatic joint where the force from the hydraulic cylinder is applied. This force is calculated in the hydraulic block within the hydraulic cylinder which will be explained in the following Chapter 6.2. In order to simulate the cylinder properly we need to define the dimensions of the piston and rod side. Figure 2.5 shows the parameters of the cylinder with which it was build.

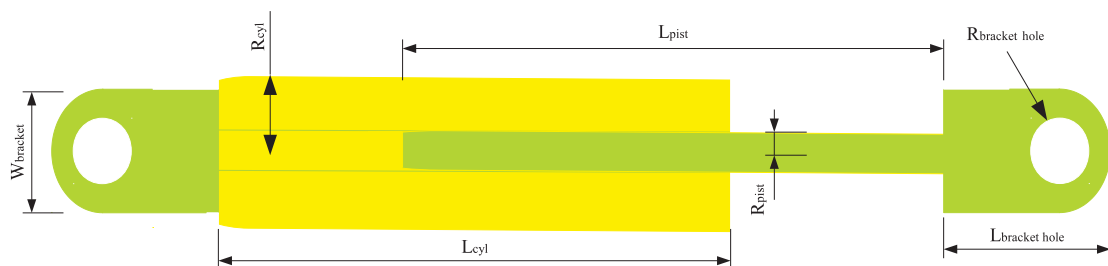


Figure 2.5: Hydraulic cylinder

The values of these parameters used in the simulation model are given in following table. Figure 2.6 shows the connection between the cylinder and the piston. The connection is done with a prismatic joint which moves the piston with the force that is applied. It is important to emphasize that for all simulated parts the inertia moments are calculated in the simulation model based on the given geometry and the density of the material used. In our case it is steel with density of $\rho = 7800 \text{ kg/m}^3$.

Cylinder	Parameters
Length cylinder	Lcyl
Radius cylinder	Rcyl
Length piston	Lpist
Radius piston	Rpist
Height bracket	Hbracket
Width bracket	Wbracket
Depth bracket	Tbracket
Height bracket	Hhole
Radius bracket	Rhole
Diameter bracket	Dbracket

Table 2.2: Cylinder parameters

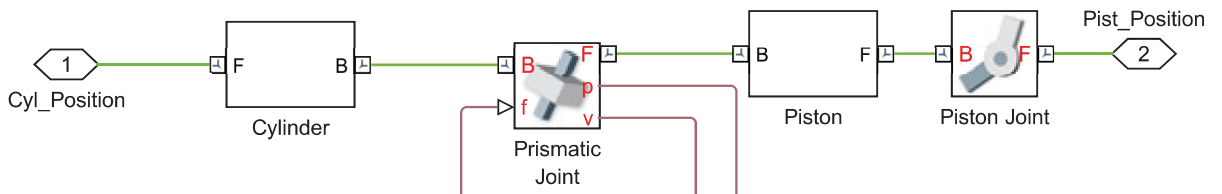


Figure 2.6: Mechanical cylinder - piston connection

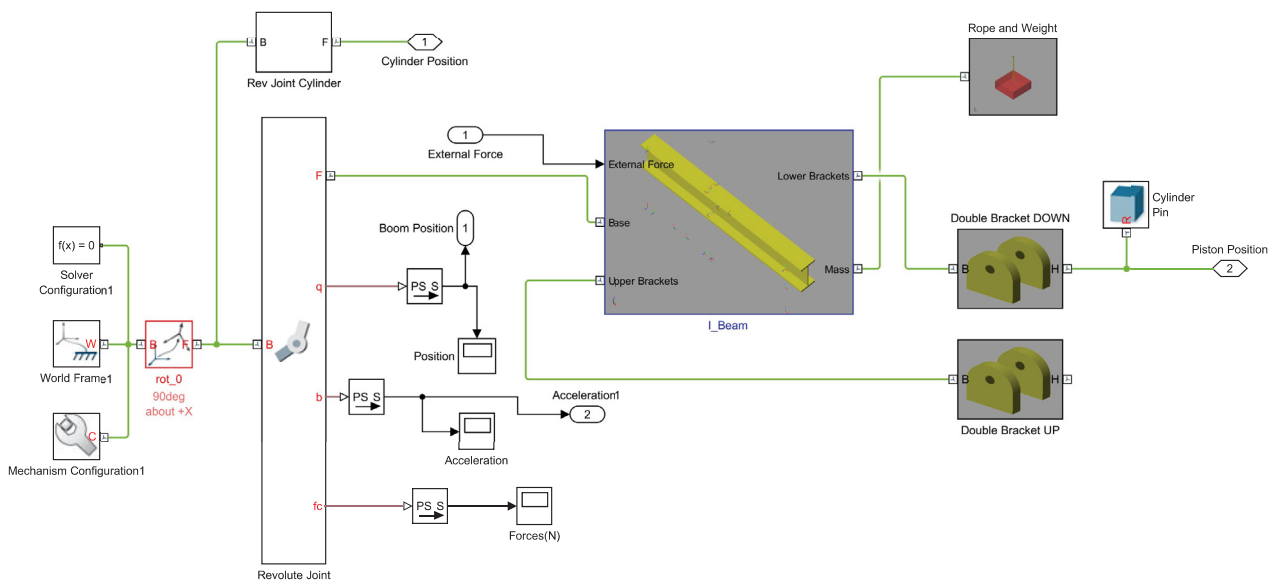


Figure 2.7: Mechanical system

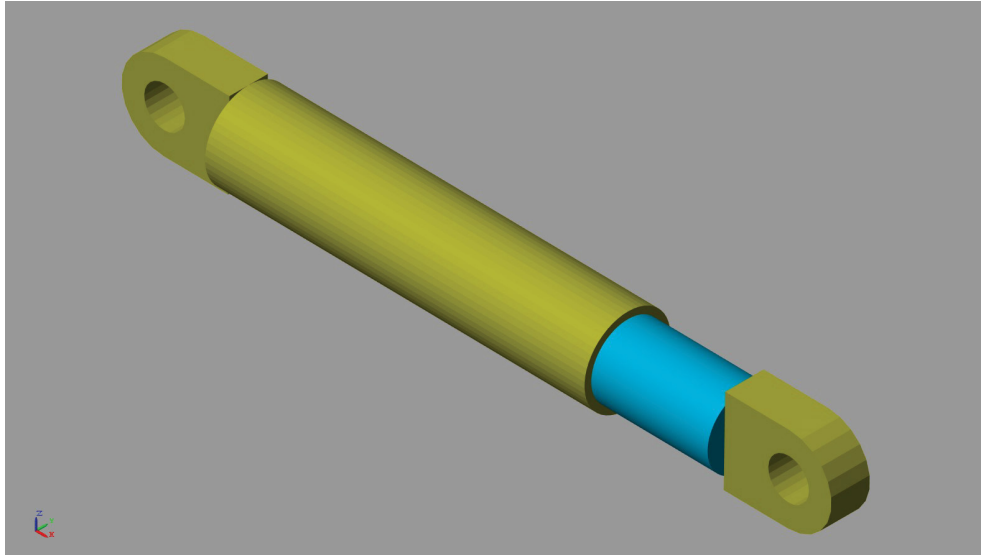


Figure 2.8: Simulated hydraulic cylinder

Chapter 3

Basic Principles of the Hydraulic Systems

This chapter explains the basic principles of hydraulic parts modelling. The main emphasis is on the physical explanation of the double acting cylinder, Chapter 3.1.2, the variable displacement axial pump in Chapter 3.3.1, the flow through orifices in Chapter 3.2.1 and the modelling of the hydraulic valve in Chapter 3.2.

3.1 Hydraulic Actuators

The hydraulic systems have the ability of transformation the hydraulic energy into mechanical motion energy and vice versa. This energy exists in the hydraulic systems in the form of flow and pressure [9].

3.1.1 Hydraulic Cylinder

A hydraulic cylinder is a device which converts the fluid power into linear mechanical motion and force. The hydraulic cylinder consists of a moving part piston, a piston rod and a plunger which operates within the cylinder.

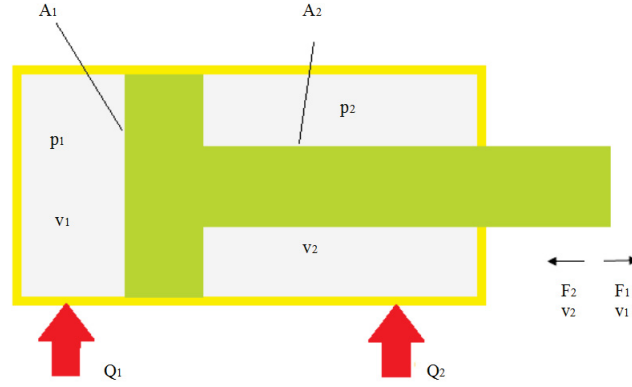


Figure 3.1: Hydraulic model from double acting cylinder

The equations for the second Newton motion Law regarding Fig. 3.1 are

$$\frac{dx_a}{dt} = v_a, \quad \frac{dv_a}{dt} = \frac{p_1 \cdot A_1 - p_2 A_2 - F_f - F_{load}}{m_a}, \quad (3.1)$$

where x_a is the position of the piston, v_a the speed of the piston, F_f the friction force which is proportional to the speed and the load forces. For the basic examinations it is assumed that they are constant ($F_{load} = F_{ext}$). The friction force can be illustrated with the linear equation $F_f = Bv_a$ where B is the coefficient for viscous friction. More attention to the friction force and the different friction models is given in the Chapter 3.1.3.

3.1.2 Double Acting Cylinder

The most commonly used cylinder in hydraulic systems is the double acting cylinder. It consists of two separate chambers, which are filled with oil and separated by the piston. With the transfer of the feeding hydraulic fluid via the ports "1" and "2" the piston may transfer pulling and pushing forces in both stroke directions [9]. So the cylinder has two pressures for the two chambers p_1 and p_2 , two volumes V_1 and V_2 , two flows Q_1 and Q_2 and two areas A_1 and A_2 . The resultant force for one double acting cylinder is

$$F_p = p_1 A_1 - p_2 A_2, \quad (3.2)$$

where the equations for the piston and rod side areas are

$$A_1 = \frac{\pi d_1^2}{4}, \quad (3.3)$$

$$A_2 = \frac{\pi(d_1 - d_2)^2}{4}. \quad (3.4)$$

The equations for the flow in the both directions are

$$Q_1 = v_1 A_1, \quad (3.5)$$

$$Q_2 = v_2 A_2, \quad (3.6)$$

where v_1 is the speed of extending and v_2 the speed of retracting the cylinder. The flow continuity equation emphasizes that mass can neither be destroyed nor created. According to [3], the conservation of mass requires that the sum of the mass change rate within the control volume (cv) and the net rate of mass outflow through the control surface (cs) should be zero

$$0 = \frac{\delta}{\delta t} \int_{cv} \rho dV + \int_{cs} \rho \vec{V} dA. \quad (3.7)$$

If there is a pre-given control fluid volume, the continuity equation can be written 3.7

$$\rho_{in} Q_{in} - \rho_{out} Q_{out} = \frac{\delta}{\delta t} (\rho V). \quad (3.8)$$

If the mean density ρ is assumed, then the equation can be expanded 3.8

$$\rho_{in} Q_{in} - \rho_{out} Q_{out} = \frac{\delta V}{\delta t} + \frac{V}{\rho} \frac{d\rho}{dt}. \quad (3.9)$$

By adding the bulk module equation 3.10 to the 3.9 we get the final look at the continuity equation 3.11

$$\frac{d\rho}{\rho} = \frac{dp}{\beta_f} \quad (3.10)$$

$$\rho_{in} Q_{in} - \rho_{out} Q_{out} = \frac{dV}{dt} + \frac{V}{\beta_f} \frac{dp}{dt}, \quad (3.11)$$

where β_f is the bulk module and ρ is the fluid density. The continuity equation 3.11 can be for extending and retracting of the cylinder. After few modifications this equation gets the following forms for extending 3.12 and retracting 3.13 of the cylinder

$$\frac{dp_1}{dt} = \frac{\beta_f}{V_1} (Q_1 - A_1 v) \quad (3.12)$$

$$\frac{dp_2}{dt} = \frac{\beta_f}{V_2} (A_2 v - Q_2). \quad (3.13)$$

By moving the cylinder the volumes of the piston and rod side will change accordingly. The volume changes can be disregarded for linear simulation but for non-linear simulation model these variations must be taken into account. The Coulomb friction model usually is used to describe the friction force dependence on the piston velocity .

3.1.3 Friction in Hydraulic Cylinders

The friction force is a phenomenon which opposes movement to surfaces in contact. A very important factor of this phenomenon is the fluid viscosity. Viscosity is very significant for the fitting surfaces in many of the hydraulic components. Figure 3.2 shows part of a hydraulic actuator which moves in the shown direction x , where C_r is the radial clearance, D the piston diameter, L the piston head length, μ is the absolute viscosity and F_f is the frictional force.

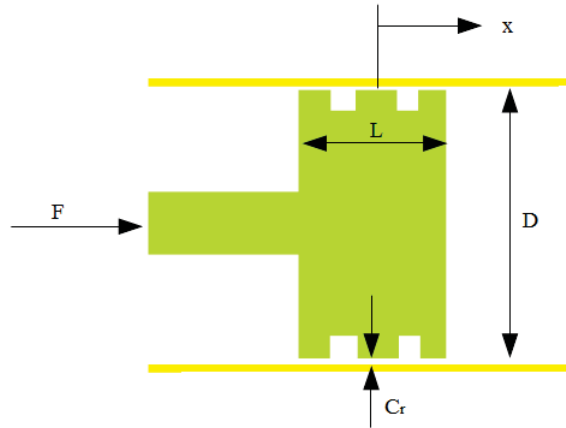


Figure 3.2: Cylinder piston

The cylinder is filled with oil. According to Newton, external force is needed in order to move the piston. This force in Eqn. 3.14 is a result of the fluid friction or its resistance to shear and it is proportional to the area in contact and the velocity and it is inversely proportional to the film thickness [17].

$$F_f = \mu A \frac{\dot{x}}{C_r} \tag{3.14}$$

The ratio between the dynamic viscosity and the fluid density is used in many equations and it is easily measured. This correspondence is also known as kinematic viscosity of the fluid Eqn. 3.15.

$$\nu = \frac{\mu}{\rho} \tag{3.15}$$

Modern studies and the different friction models show that the friction can be dependent not only on the velocity of the actuator \dot{x} but also on the pressure difference Δ_p across the piston, on the piston position x and the temperature θ .

$$F_f = F_f(x, \dot{x}, \Delta_p, \theta, t) \tag{3.16}$$

The general characteristics of the friction force as a function of the velocity are given in Fig. 3.3.

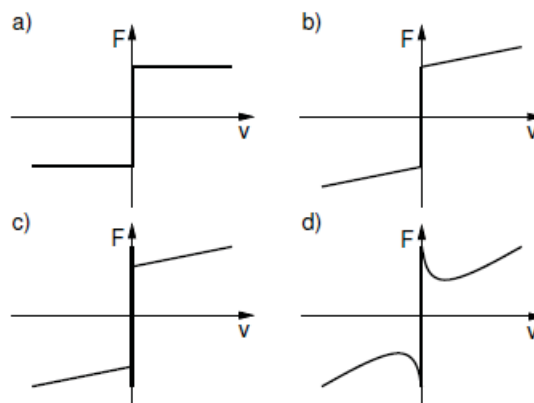


Figure 3.3: Example of static friction models [19]

The graph a) in Fig. 3.3 shows the Coulomb friction model, where the friction is constant and independent from the velocity and the contact area. The viscous friction and the Coulomb friction are shown together in graph b) Fig. 3.3. Here we can see the linear characteristic of the friction and the velocity $F_f = Bv_a$. Stiction (short for static friction) introduces the idea that the friction force at rest is higher than the Coulomb friction level [19]. This shows that even though the friction force counteracts external forces, by bigger external forces the friction force cannot prevent motion (graph c) Fig. 3.3). The graph d) shows how the friction force may decrease continuously from the static friction level. This friction curve is the combination of the three previous curves under a), b) and c). According to [6] it is common in the study of friction to refer to a curve of combined friction as a function of velocity by Stribeck friction curve or simply Stribeck curve.

3.2 Hydraulic Valves

The hydraulic valves are one of the most important parts in hydraulics nowadays. They can control the source of fluid power with the help of mechanical motion. The hydraulic valves can control the direction in which the flow occurs. In the following chapter the basic principles and equations of flow through orifices will be given. At the end the equations for 2/2, 3/3 and 4/3 a directional valve will be explained.

3.2.1 Flow through Orifices

Orifices are restrictions of short length (ideally zero length for a sharp edged orifice) in the flow passage and may have fixed or variable area [13]. Their basic use is to control the flow or to create pressure difference, which is also the basic use of the hydraulic valves.

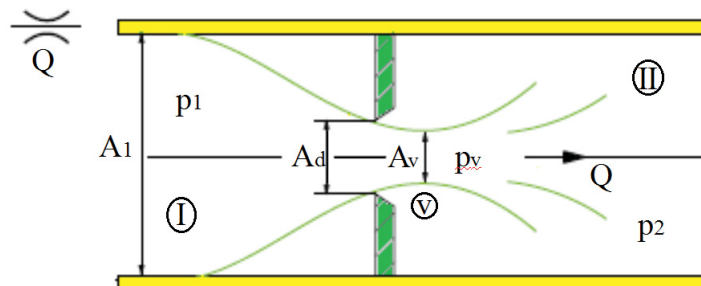


Figure 3.4: Flow through orifice

We will observe flow from one fluid through the hydraulic orifice with entrance diameter of A_1 , orifice diameter of A_d and exit diameter of A_2 which is given with Fig. 3.4. It shows that the area of the issuing jet is smaller than the orifice whereas the particles have inertia and are moving in a curve path at the opening [17]. This point where the area is minimum A_v is called *vena contracta*. The Bernoulli's theorem 3.17 affirms that by increasing the fluid velocity, the pressure drops simultaneously. Therefore, the total energy flow loss is obtained from the heat energy caused

by the friction of the particles.

$$\frac{v^2}{2} + gz + \frac{p}{\rho} = \text{constant} \quad (3.17)$$

In Eqn. 3.17 v is the velocity of the fluid, g is the acceleration of gravity, z is the elevation of the point above the reference plane, p the pressure and ρ the density of the fluid. According to the Bernoulli theorem Eqn. 3.17, the Bernoulli equation for our orifice at Fig. 3.4 for the cross-section ① and ② is

$$\frac{\rho(v_I)^2}{2} + p_I = \frac{\rho(v_v)^2}{2} + p_v \rightarrow (v_v)^2 - (v_I)^2 = \frac{2}{\rho}(p_I - p_v), \quad (3.18)$$

where v_I is the velocity in the cross-section ① and v_v is the velocity at the cross section ② (vena contracta). The area ratio at the vena contracta can be described with the coefficient C_v

$$C_v = \frac{A_v}{A_d}, \quad (3.19)$$

where A_v is the area at the vena contracta cross section and A_d is the the area at the cross section ② on Fig. 3.4. With the implementation of the continuity equation with constant density ρ

$$Q = A_1 v_1 = A_v v_v = A_d v_v C_v, \quad (3.20)$$

where Q is the volume flow for the orifice 3.4. With the transformation of Eqn. 3.20 with the Bernoulli Eqn. 3.18 for the cross-sections ① and ②, the volume flow for the orifice is

$$Q = A_d C_v \sqrt{\frac{1}{\frac{1}{v_v^2}}} = A_d C_v \sqrt{\frac{\frac{2}{\rho}(p_I - p_v)}{\frac{2}{\rho}(p_I - p_v) \frac{1}{v_v^2}}} = A_d C_v \sqrt{\frac{\frac{2}{\rho}(p_I - p_v)}{1 - (\frac{v_1}{v_v})^2}} \quad (3.21)$$

$$= A_d \frac{C_v}{\sqrt{1 - (\frac{v_1}{v_v})^2}} \sqrt{\frac{2}{\rho}(p_I - p_v)}, \quad (3.22)$$

where the expression in the blue represents the discharge coefficient C_d . In the cross section between ② and ③ the kinetic energy as a result of the turbulent flow is converted into heat of the fluid (heat) and $p_v = p_2$ [17]. So the equation for flow through orifice will have the following form

$$Q = A_d C_d \sqrt{\frac{2}{\rho}(p_I - p_v)} \quad \text{where} \quad C_d = \frac{C_v}{\sqrt{1 - (C_v \frac{A_d}{A_1})^2}}. \quad (3.23)$$

3.2.2 Directional Control Valves

The main role of the directional valve is to change direction in which the fluid moves. With the direction valves the pressure and flow can be easily controlled. There are two types of directional valves: seat valve (pocket valve) or spool valve (sliding valve). In our case as in the most of the hydraulic systems the spool valve is used. This valves can be classified by number of criteria like:

a) the "ways" in which the fluid can enter or leave the valve,

- b) the number of lands or ports,
- c) the type of centre when the valve is in neutral position.

If we observe the first criterion, in the most commonly used valves the fluid can move in one, two, three and four ways. The same is with the second criterion. The most commonly used valves can have three, four, five even six ports. As for the third criterion when the valve is in neutral position we can differ three different positions (centers):

- 1) underlapped valve or valve with open center,
- 2) zero lapped valve or valve with critical center,
- 3) overlapped valve or valve with closed center.

3.2.3 Modelling of 2/2 Directional Valve

As explained in the Chapter 3.2.2 the directional control valves can be classified depending on the ways in which the fluid can enter or leave and the number of ports. According to DIN ISO 1219-1 standard the valves can be designated depending on the number of connections A and the number of valve positions W

A/W - Directional valve.

Therefore, in this way we can expect that the 2/2 directional valve will have two connections (ways in which the fluid can enter or leave) and two lands or positions.

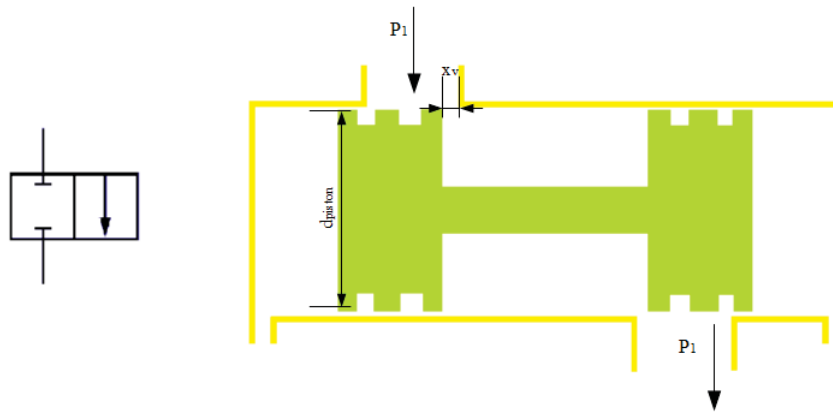


Figure 3.5: 2/2 Directional Valve

With the movement of the valve the area cross section with the piston diameter d_{piston} and the cross section opening x_v changes accordingly. The cross section area is square, so the equation for the area $A(x_v)$ is

$$A(x_v) = wx_v. \quad (3.24)$$

The equation for the flow from 1 to 2 of this 2/2 directional valve can be written from the orifice equation 3.23 where the pressure difference is $\Delta_p = p_1 - p_2$ and $A_d = A(x_v)$

$$Q = \text{sign}(\Delta_p) A(x_v) C_d \sqrt{\frac{2|\Delta_p|}{\rho}}. \quad (3.25)$$

The discharge coefficient C_d is dimensionless and $C_d=0,61$ according to [17]. This coefficient depends on the Reynolds number, the dimension of the edges (sharp or round) and the direction of the flow.

3.2.4 3/3 Valve with Different Valve Centres

According to the previous Chapter 3.2.2 the 3/3 valve should have 3 connections(ways in which the valve enter or leave) and 3 positions.

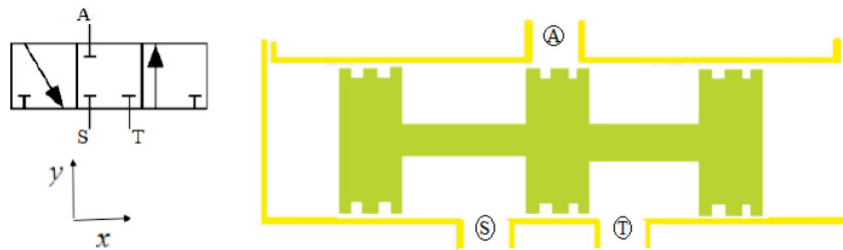


Figure 3.6: 3/3 Directional Valve with zero lapping

By combining two 2/2 valves we can get one 3/3 directional valve. In Fig. 3.6 we can see one 3/3 directional valve with critical centre or zero lapped. This means that the land width is identical to the port width. \textcircled{S} is the supply - port, \textcircled{T} is the tank - port and \textcircled{A} is the work port. Figure 3.7 describes the open and closed (over- and underlapped valve) centre.



Figure 3.7: Open and closed valve centre by 3/3 Directional Valve

When the land width is smaller than the port width $\xi < 0$ then we get open centre or underlapped valve, and when the port width is smaller than the land width $\xi > 0$ we get closed centre or overlapped valve. The most important characteristic of the valves is the flow gain. The vast majority of the valves are manufactured with critical centre because of the emphasis on the linear flow gain [17]. The use of the open centre valves is very popular in applications which require continuous flow and satisfactory fluid temperature. However, the use of the open centre valves is

limited because of big energy loss in neutral position and it is restricted to being used in special applications [23]. The use of the closed centre valves is not desirable because of the dead-band characteristic in the flow gain, which can often lead to a steady state error.

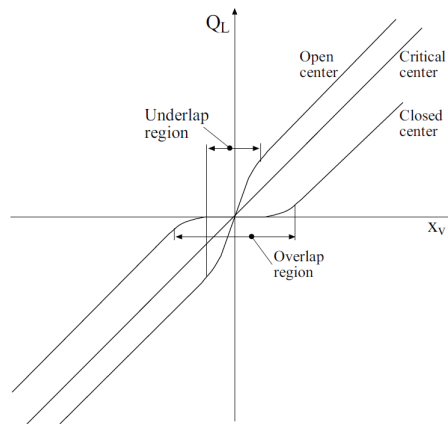


Figure 3.8: Flow gain of different centre types [23]

In Fig. 3.8 on the x - axis is the position of the spool x_v and on the y axis is the load flow Q_L .

3.2.5 Modelling of 4/3 Directional Valve

The 3- land 4- way-directional-hydraulic valve is one of the most commonly used in hydraulics. The arrow in Fig. 3.9 shows the assumed direction of the flow. The orifices in most commonly used valves are matching and symmetric, which indicates that for the matching orifices the following equations are used

$$\begin{aligned} A_1 &= A_3 \\ A_2 &= A_4, \end{aligned}$$

where as for the symmetrical orifice these equations apply

$$\begin{aligned} A_1(x_v) &= A_2(-x_v) \\ A_3(x_v) &= A_4(-x_v), \end{aligned}$$

where at the neutral position $A_1(0) = A_2(0)$ and A_1, A_2, A_3, A_4 are the areas of the four orifices in Fig. 3.9 . Being only interested in the steady - state characteristics the compressibility flows are zero and the continuity equations for the two valve chambers in Fig. 3.9 are

$$Q_L = Q_1 - Q_4 \quad Q_L = Q_2 - Q_3, \tag{3.26}$$

where Q_L is the load flow and Q_1, Q_2, Q_3, Q_4 are the flows of the four orifices accordingly [17]. By definition the load pressure $P_L = P_1 - P_2$, which is the pressure drop across the load.

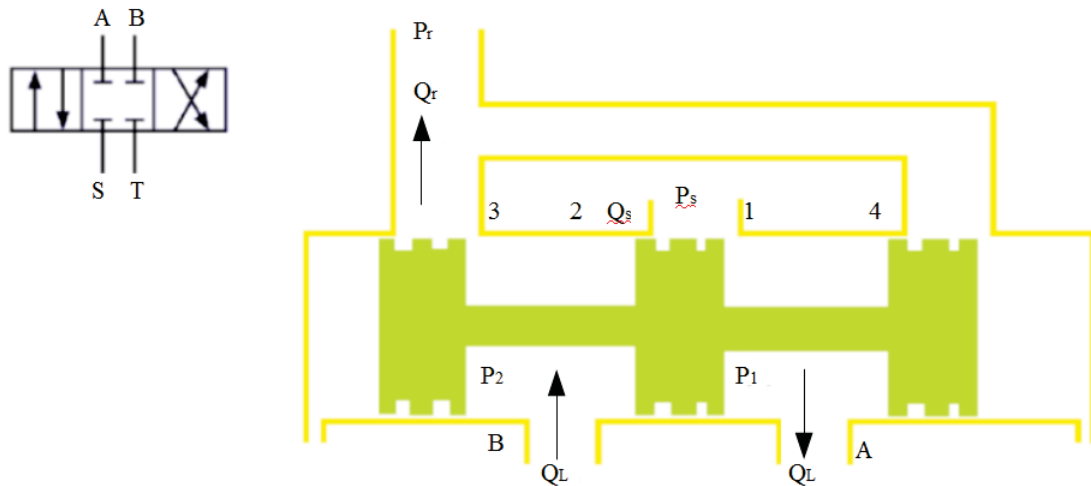


Figure 3.9: Three land four way spool valve

If we take into consideration the Eqn. 3.23 for flow through orifice we can easily write the equations for the 4 orifices in our valve

$$Q_1 = C_d A_1 \sqrt{\frac{2}{\rho} (P_s - P_1)} \quad (3.27)$$

$$Q_2 = C_d A_2 \sqrt{\frac{2}{\rho} (P_s - P_2)} \quad (3.28)$$

$$Q_3 = C_d A_3 \sqrt{\frac{2}{\rho} (P_2)} \quad (3.29)$$

$$Q_4 = C_d A_4 \sqrt{\frac{2}{\rho} (P_1)}. \quad (3.30)$$

3.3 Hydraulic Pumps

The hydraulic pumps are used to convert mechanical energy (torque) into hydraulic energy (flow, pressure) [17] [9]. They play crucial role in every hydraulic system. According to [15], they can be referred as the 'heart' of the hydraulic system. As in most applications the inlet side of the pump in our application is connected with a tank of fluid (oil) and the pressured side is connected with a hydraulic valve. They can be classified into two main groups:

- a) positive displacement pumps
- b) non positive displacement pumps.

For our model we used variable axial piston pump with swash plate design from the positive displacement group with load sensing. This chapter gives the focus on the axial piston pumps in Chapter 3.3.1 and the variable displacement pumps in Chapter 3.3.1.

3.3.1 Axial Piston Pumps

As mentioned in Chapter 3.3 the axial piston pumps belong to the positive displacement pumps group. Normally, they are equipped with number of pistons located in the cylinder block in the circular array. The pistons are connected with the swash plate which can be fixed or variable. Depending on the type of the swash plate the axial piston pumps can be separated into two groups:

- axial piston pump with fixed displacement
- axial piston pump with variable displacement.

Variable Displacement Axial Piston Pump

The axial piston pump is a rotation hydraulic machine in which the working chambers rotate in relation to the rotor axis where the axis of the pistons is parallel to the rotation axis [1]. Figure 3.10 shows Rexroth model of variable displacement axial piston pump with swash plate design,

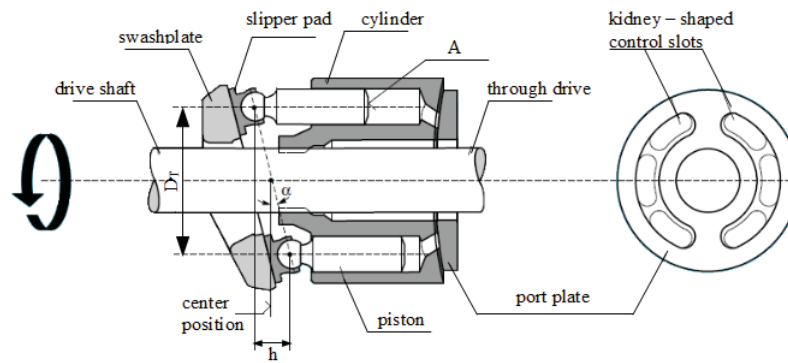


Figure 3.10: Variable axial piston pump of swashplate design [16]

where h is the piston stroke, A the piston area, D_T pitch diameter when $\alpha = 0$, α the swivel angle. As shown in Fig. 3.10, α represents the angle between the swash plate and the pistons. If the angle α is zero, no displacement takes place at all, which means that the flow Q is proportional to the angle between the swash plate and the cylinder

$$Q = \frac{V_g \cdot n \cdot \tan \alpha \cdot \eta_{vol}}{1000 \cdot \tan \alpha_{max}}, \quad (3.31)$$

where V_g is the geometrical displacement, n the speed, η_{vol} the volumetric efficiency and α_{max} the maximum swivel angle.

$$h = D_T \cdot \tan \alpha; \quad V_g = x \cdot A \cdot h; \quad V_g = x \cdot A \cdot D_T \cdot \tan \alpha \quad (3.32)$$

With Eqn. 3.31 the volume flow of the pump can be affected by changing the swivel angle. However, according to [15] the maximum swivel angle is generally limited to $17,5^\circ$. With the help of the previous equations 3.31 and 3.32 we can write the equations for power of the variable axial piston pump with

$$P = \frac{2 \cdot \pi \cdot M \cdot n}{60000} = \frac{M \cdot n}{9549}, \quad (3.33)$$

or

$$P = \frac{Q \cdot \Delta_p}{600 \cdot \eta_{vol} \cdot \eta_{meh}} = \frac{Q \cdot \Delta_p}{600 \cdot \eta_t}. \quad (3.34)$$

where η_{meh} is the mechanical hydraulic efficiency and $\eta_t = \eta_{meh} \cdot \eta_{vol}$ is the overall efficiency coefficient and M is the torque of the drive of the hydraulic pump.

According to [27], the variable displacement piston pumps are based on the pressure compensator control, which means that when the discharge pressure rises to a present level, the compensator valve is actuated to reduce the discharge pressure and feed it to the control piston. Here the control piston reduces the swivel angle, which according to equation 3.31 will decrease the output flow. The use of the pressure compensator from these pumps reduces the need of pressure relief valve in the hydraulic system.

Chapter 4

Hydraulic Servo Systems

The use of the closed loop hydraulic servo systems first began to appear in industry, where the applications required very high performance [23]. With the development of technology and the need of more accurate and faster control of high power levels these systems became very popular in variety of industries. These systems have a lot of advantages like:

- good stiffness characteristics
- low wear costs
- flexibility.

This chapter will explain the basic principles of how one hydraulic servo valve works in Chapter 4.1, hydraulic capacity in Chapter 4.2, passive and active loads in Chapter 4.3 and independent metering systems in Chapter 4.4.

4.1 Non Linear Model of Servo Hydraulic System

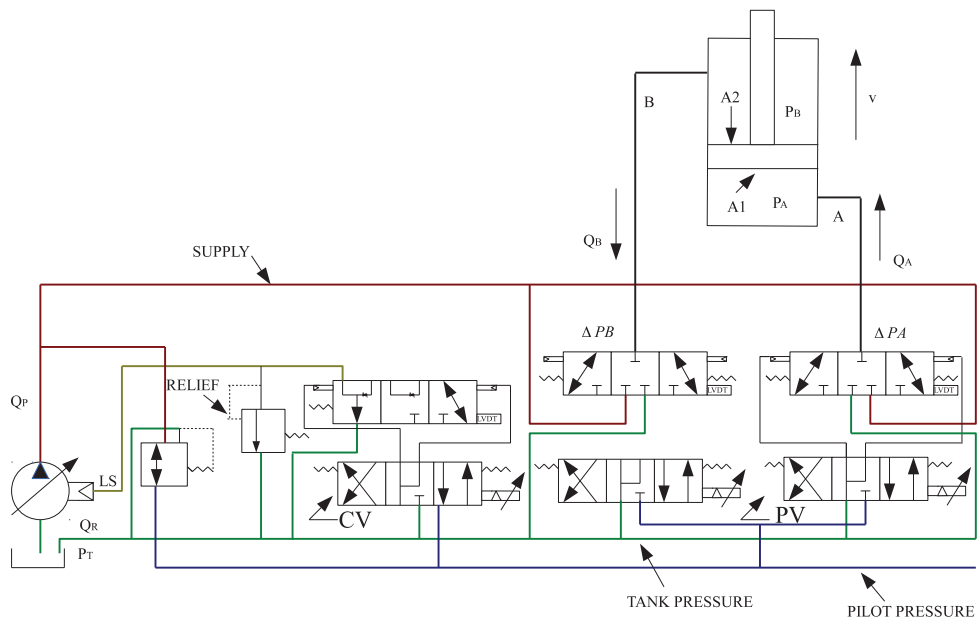


Figure 4.1: Hydraulic system, servo control cylinder

Figure 4.1 shows the model of the Eaton CMA90 valve simplified schematics that was used in the simulation. As explained in Chapter 1 a non-linear model of the servo valve with a hydraulic cylinder is used in the machine MX6501.1 as in the test rig. The goal is to test the servo valve with the cylinder to simulate its behaviour at different control modes. The valve consists of two valves, the CV and the PV. PV is the pilot valve which is built of two 4/3 proportional valves and CV is the conditioning valve which is built of one 4/3 proportional valve. In order to simplify our simulation the CV valve part is simulated together with the pump as the basic role of the CV and the pump is to maintain a constant flow to the PV with constant LS margin. Detailed explanation about the valve and its possibilities will be given in the Chapter 4.4.2.

There are a lot of effects that can influence the work of the system when modelling non linear servo valves with cylinder. The Newton Second Equation 3.1 applies to this system as the equations for flow through orifice 3.23. According to Eqn. 3.23 the equation for flow through orifice in this system are the following:

$$Q_A = C_d w x_v(t) \sqrt{\frac{2(p_s - p_a)}{\rho}} = C_v x_v(t) \sqrt{p_s - p_A}; \quad C_v = C_d w \sqrt{\frac{2}{\rho}} \quad (4.1)$$

$$Q_B = C_d w x_v(t) \sqrt{\frac{2(p_B - p_T)}{\rho}} = C_v x_v(t) \sqrt{p_B - p_T} \quad (4.2)$$

where the C_v can be calculated from the catalogue given data Q_N , Δp_N and x_{vmax} .

$$C_v = \frac{Q_N}{\sqrt{\frac{\Delta p_N}{2}}} \frac{1}{x_{vmax}} \quad (4.3)$$

x_{vmax} is the maximum opening of the orifice, Q_N the nominal flow and Δp_N the nominal pressure differential. The hydraulic fluid characteristics play vital role in the development of the dynamic equations. The elastic bulk module of the fluid can be described with

$$E = -\frac{\Delta p}{\Delta V} V, \quad (4.4)$$

where V is the total volume, ΔP change in pressure and ΔV change in volume. By rearranging of Eqn. 4.4 and writing it as a function of time we get

$$\frac{dp}{dt} = \frac{E}{V} \frac{\Delta V}{dt}. \quad (4.5)$$

According to [28] in any given instant of time the rate in which the volume V is being compressed ($\frac{\Delta V}{dt} < 0$) can be given with Eqn. 3.8. When we take Eqn. 3.8 and Eqn. 4.5 into account, the volume change given with Eqn. 3.12 and Eqn. 3.13 for this system will have the form

$$\frac{dp_A}{dt} = \left(\frac{E}{V_1 + A_1 x_a} \right) (Q_A - A_1 v_a), \quad (4.6)$$

$$\frac{dp_B}{dt} = \left(\frac{E}{V_2 + A_2 (l_a - x_a)} \right) (A_2 v_a - Q_B). \quad (4.7)$$

In order to describe this system we require 4 differential equations, Eqn. 3.1, Eqn. 4.1, Eqn. 4.2 , Eqn. 4.6 and Eqn. 4.7. These equations are known as state variables. According to [11] the state variable are first order differential equations which describe the motion of the dynamic system. In these equations the variables that appear as first derivative on the left side \dot{x}_a , \dot{p}_A , \dot{p}_B and \dot{v}_a are the state variables.

4.1.1 Hydraulic Valve Coefficients

As explained in the previous Chapter 4.1 the hydraulic behaviour of the valve and the system can be described with 4 steady state equations. In the literature for servo hydraulic systems the valve coefficients are often used to describe the behaviour of the systems. In order to obtain these coefficients we need to take a look at the pressure - flow curves 4.2 and the flow equation 4.9.

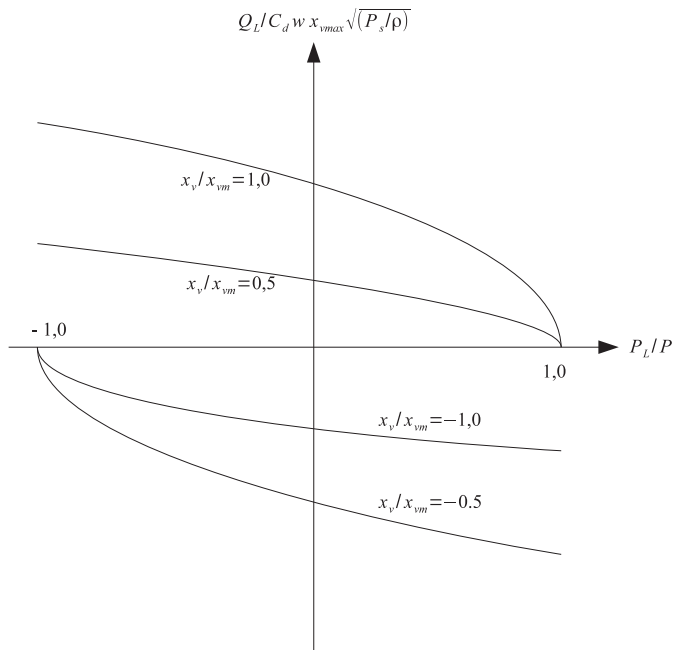


Figure 4.2: Pressure - flow curve for a 4 port critical centre valve

Taken into consideration the equations for the valve coefficient C_V 4.3 we can write the equation for the flow through the valve in this way

$$Q_v = K_v \cdot y \cdot \sqrt{\Delta p_v}; \quad K_v = \frac{Q_n}{y_{max} \sqrt{\Delta p_n}}, \quad (4.8)$$

where the Q_N is the nominal flow and p_n is the nominal pressure. These are usual parameters for the valve and can be very easily found in the valve catalogue. y is the valve electrical input signal in voltage [V], and Δp_n the pressure drop across the valve. Similar to the flow through orifice equation 3.22 the equation for the valve load flow with rectangular ports will have this form

$$Q_L = C_d w x_v \sqrt{\frac{1}{\rho} (P_s - \frac{x_v}{|x_v|} P_L)}, \quad (4.9)$$

where Q_L is the load flow, P_S is the supply pressure and P_L is the load pressure. The value x_{vm} on Fig. 4.2 is the maximum valve stroke. With the differentiation of the pressure - flow curves equation 4.9 we get the most important valve parameters. The flow gain is

$$K_q = C_d w \sqrt{\frac{1}{\rho} (P_S - P_L)}. \quad (4.10)$$

The flow - pressure coefficient is

$$K_c = \frac{C_d w x_v \sqrt{\frac{1}{\rho} (P_S - P_L)}}{2(P_S - P_L)}, \quad (4.11)$$

and the pressure sensitivity is

$$K_p = \frac{2(P_S - P_L)}{x_v} = \frac{K_q}{K_c}. \quad (4.12)$$

The null valve flow gain can be written as [17]:

$$K_{q0} = 70w\sqrt{P_S} \quad (4.13)$$

4.2 Hydraulic Capacity

Hydraulic capacitance in engineering is an alternative term for compression. It relates the rate of change of volume to the rate of change of capacitive pressure [29] with

$$C_h = \frac{Q}{\dot{p}} = \frac{dV}{dp}. \quad (4.14)$$

If we combine the last equation 4.14 with the bulk module equation 4.4 we get

$$C_h = \frac{V}{E}, \quad (4.15)$$

which can be also referred to as the inverse elastance. By reordering Eqn. 4.14 the volume flow becomes proportional to the first derivative of the pressure

$$Q = C_h \dot{p}. \quad (4.16)$$

4.3 Passive and Active Loads

In every day work the hydraulic drives and actuators try to overcome different loads (forces, moments), which, depending on the design of the hydraulic system, can have different effect. There is a difference between passive and active loads.

4.3.1 Passive Loads

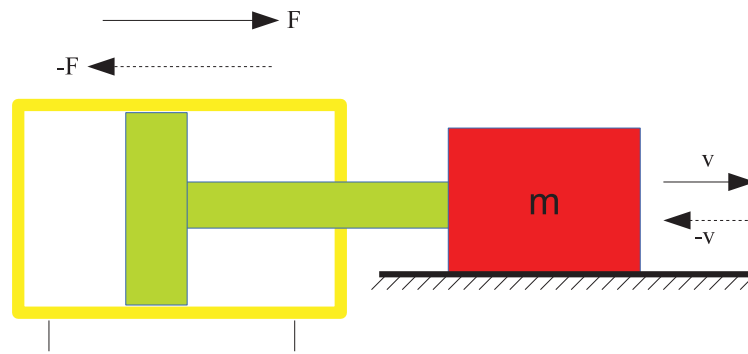


Figure 4.3: Passive Load

In Fig. 4.3 there is a hydraulic cylinder as part of a hydraulic system trying to overcome given load (in this situation the mass and the cylinder are positioned horizontally), which means that the force of the gravity acceleration has no influence to the system.

Passive load acts in the opposite direction of the movement of the working cylinder. A typical example of a passive load in this picture is the friction force which has opposite direction to the movement of the cylinder. As a result, it can be concluded that the passive load cannot inject energy into the hydraulic system.

4.3.2 Active Loads

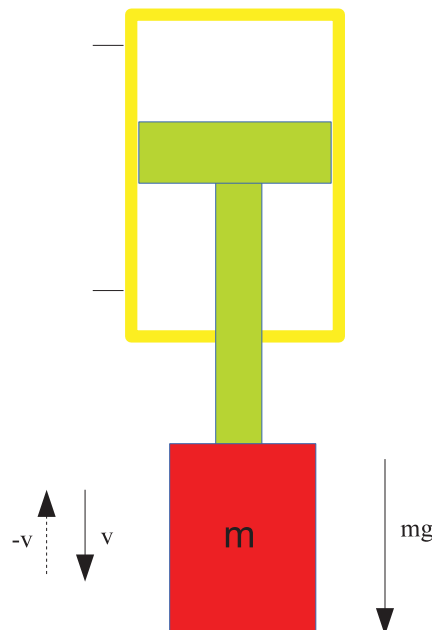


Figure 4.4: Active Load

Figure 4.4 represents the same system as Fig. 4.3, but here the cylinder and the load are vertically positioned. This means that the force of gravity will have impact on the hydraulic system.

According to [26] the active loads act by stationary movements independently of the motion direction and by standstill always in one direction. Therefore, by changing the direction of motion there is no change in the force direction on the piston side. Taking into account the previous, this system will need a throttle (single meter out throttle valve) on the rod side in order to maintain constant flow and pressure. Which leads us to the conclusion that the active loads inject energy into the system.

4.4 Independent Metering Systems

According to [8], independent metering is just an umbrella term for systems where the meter-in and meter-out orifice are independently controlled. This gives the opportunity to control the inlet and the outlet of the actuator separately. In most cases these systems are used with pressure compensation load sensing systems PCLS, which according to [2] increase the energy efficiency of the system.

One of the biggest advantages of these systems is the variety of variables that can be controlled independently on both sides of the valve (pressures, flows, position, velocity). A big disadvantage of this system is the complexity of the control system that needs to be implemented in order to achieve better performance. Such valve used in our simulation is the Eaton CMA90.

4.4.1 Pressure Compensation Load Sensing Systems (PCLS)

The pressure compensation load sensing systems are often known to have better control characteristics than the normal open centre systems. The main goal of the pressure compensator is to control the pressure drop over the control orifice. The load sensing is a margin that is predefined from the system. This means that the pump must be pre-set in order to obtain the pressure margin beyond the highest sensed load pressure. Variable displacement axial pumps explained in the Chapter 3.3.1 are often used in this type of systems. According to [2], these systems can save power by the virtue of having two degrees of freedom systems and being able to control the pressure in the return chamber in addition to the speed of the actuator. The advantages of these systems are the energy efficiency and the handling qualities (pressure compensator suppresses cross - talk between different functions [8]). One of the biggest weakness of these systems are the oscillations which can be suppressed by implementing a good damping system (input shaping).

4.4.2 Independent Metering Valve (Eaton CMA90)

Chapter 4.4 explains the main characteristics of the independent metering systems. Figure 4.1 shows the schematics of the hydraulic system and the valve used in this system. As explained in the previous chapter the independent metering valves use the flexibility of controlling multiple variables simultaneously in the hydraulic system. By using regular proportional valves we have one degree of freedom, which limits us from controlling multiple parameters on one side. The valve used in our application is the Eaton CMA90 valve.

The Eaton CMA90 control valve is a CAN controller independent metering spool valve with two

spools [7]. As mentioned in Chapter 4.1 the valve consists of two separate valves, the CV and the PV. This conditioning valve has two margins, one is the CV margin which is added to the highest sensed load pressure and another is the LS margin for each PV. The LS margin is normally set to 20 bar and the CV margin to 5 bar. The PV consists of two independently controlled spools (twin spool architecture 4.5) where on each side we have integrated pressure, position and temperature sensors.

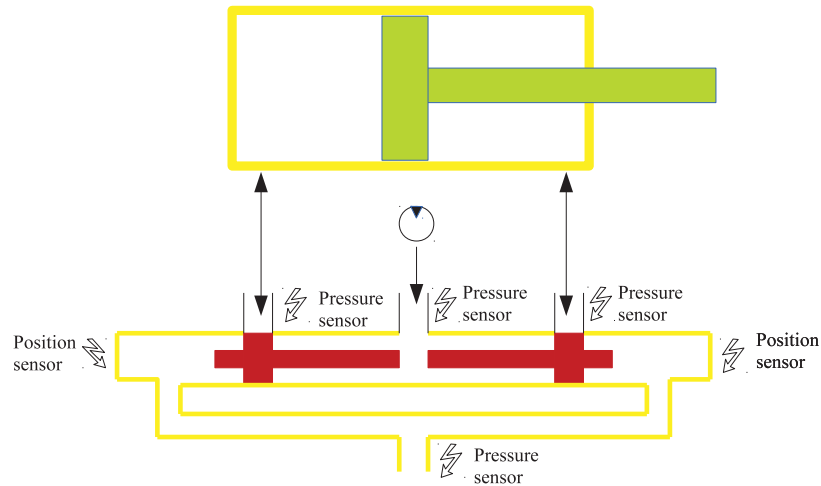


Figure 4.5: Independent metering twin spool valve Eaton CMA90

The position of the spools is measured with LVDT, which depends on the pressure difference across the valve and the flow demand. As explained in section 4.3 the passive and active loads can be a challenge in hydraulic systems. This valve eliminates that problem quite easily, when there is passive load the meter-out valve is normally commanded to open or control some low back pressure needed to reduce the pressure which moves the load. The meter-out valve is usually controlled in this way when there is active(overrunning) load in order to maintain the needed flow as well as the pressure which is determined by the load. This is done with the help of the continuity equations 3.12 and 3.13 where if the input flow is constant, the output flow must be the same but corrected with the area ratio.

$$\frac{\delta p_{in}}{\delta t} = \frac{\beta_f}{V} (Q_{in} - \frac{A_{in}}{A_{out}} Q_{out}) \quad (4.17)$$

This valve can have up to eight separate sections (PV's) on a single bank. The maximum flow that this valve can supply is 90 l/min and the nominal pressure is set to be $P_N = 14$ bar. The maximum pressure that this valve can supply is $P_{max} = 440$ bar. More detailed explanation about the control modes and the abilities of this valve will be given in Chapter 6.2.

Chapter 5

Control of Hydraulic Systems

The standard approach to control hydraulic servo systems is to apply linear feedback control design methods [13]. In this thesis we will discuss several basic approaches of the linear feedback control design methods. The purpose of this chapter is to explain the basic and standard feedback control methods in Chapter 5.1, the PID controllers in Chapter 5.2, acceleration feedback in Chapter 5.3, position feedback in Chapter 5.4 and pressure feedback systems in Chapter 5.5.

5.1 Classical Feedback Control Design

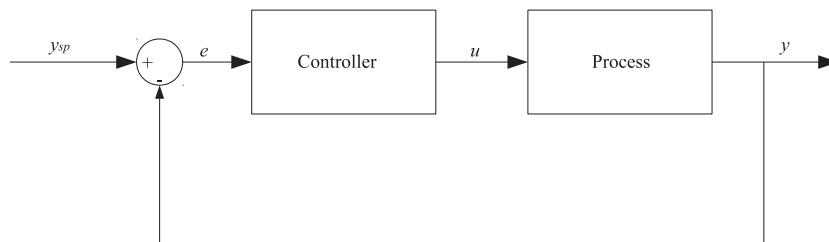


Figure 5.1: Feedback Control System

Figure 5.1 shows a diagram of simple block system. This system consists of two main elements, a controller and a process block. The controller has an input value e , which represents the error between the set point y_{sp} and the measured value y ($e = y_{sp} - y$). The output value y is measured with sensor and then that value is compared with the set point value. The error value then enters the controller where it is modified. After that the controller sends its output value u or also known as controlled variable to the process or the plant. According to [4], the main purpose of this feedback loop system is to keep the process variable close to the desired value.

5.2 PID Controller

The PID controllers are one of the most commonly used in modern control industry. The combination of the three parts, the proportional, integral and derivative, makes them very suitable for a

lot of systems and applications. With the development of the feedback control systems these controllers became very popular. They have an excellent control dynamics with fast response (short rise time), zero steady state error, no oscillations and higher stability.

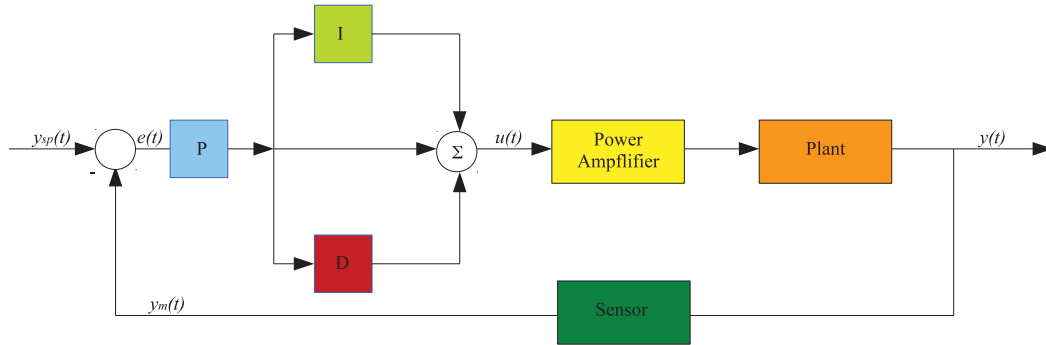


Figure 5.2: PID controller

Figure 5.2 shows the PID controller within a closed feedback controlled loop. The algorithm of this controller can be described with the following equations:

$$u(t) = K \left(e(t) + \frac{1}{T_i} \int_0^t e(\tau) d\tau + T_d \frac{de(t)}{dt} \right) \quad (5.1)$$

where u is the control variable, e the control error. P represents the proportional term (which is proportional to the error), I the integral term (which is proportional to the integral of the error) and D the derivative term (which is proportional to the derivative of the error) [4]. The parameter K represents the proportional gain, T_i the integral time and T_d the derivative time.

5.2.1 Proportional Action

As mentioned in Chapter 5.2 the proportional gain K is proportional to the error, hence

$$u(t) = Ke(t) + u_b, \quad (5.2)$$

where the variable u_b is a bias or a reset. Equation 5.2 shows that if the error is zero, then $u = u_b$. By increasing the gain, the rise time decreases and after certain amount of time the steady state error decreases as well. It can also reach smaller amplitude and phase margin and according to [24] it can reach satisfying wider frequency band and larger noise sensitivity. P controller can cause oscillation and overshooting at high values for the gain which will be shown in the following simulations of the hydraulic model.

5.2.2 Integral Action

With the proportional controller there will always be an error in the steady state. The integral part of the controller in figure 5.2 helps to eliminate zero steady state error. Taking into account the proportional and integral term

$$u_0 = K \left(e_0 + \frac{e_0}{T_i} t \right), \quad (5.3)$$

we can assume that as long as the error is $e_0 \neq 0$, the control signal will be a constant [4]. This leads us to the conclusion that the integral action always leads to zero steady state error for constant set value.

When combined together with proportion controller we get the well-known PI controller which is mostly used in applications where the speed of the system is not important. This controller has the ability to eliminate the steady state error but by further increase of the gain it can lead to oscillation and overshooting (instability) as it does not have the derivative part to predict the error.

5.2.3 Derivative Action

As mentioned in the previous chapter the purpose of the derivative action is to predict the error before it happens and act accordingly. In order to avoid sudden change in the error signal by PD controller, the extrapolation of the error is taken from the tangent of the error curve [4]. The algorithm of this controller is

$$u(t) = K \left(e(t) + T_d \frac{de(t)}{dt} \right). \quad (5.4)$$

The properties of this controller are well- known and tested. According to [24], by increasing the derivative action the overshooting decreases as well as the settling time. This leads us to the conclusion that the derivative action has a damping effect on the signal up to some limit value. If we increase the gain above this value, then the oscillations come back.

5.3 Acceleration Feedback

The acceleration feedback in the hydraulic systems is closely related to the pressure difference [13]. Since the measuring of the acceleration in the hydraulic systems can be very costly and very complicated it is not widely used. It can be calculated as second derivative from the position of the hydraulic actuator. However, the derivative of this signal can often be very noisy and can have a phase delay which can disturb our system and cause oscillation. But in simulations the acceleration feedback can be easily implemented and measured. Fitzsimmons in his paper [10] discusses the effect of the acceleration feedback with the implementation of PVA controller (position velocity acceleration). He explains that the acceleration feedback in hydraulic systems has a damping effect and it can be used to achieve higher frequency range. Similar results were presented by Welch, in his paper regarding the use of derivative pressure feedback [25]. He explains that by increasing the acceleration gain K_a the damping effect increases thus contributing for the system stability. The damp effect of the acceleration feedback will be shown in the simulation model included in Chapter 7, Fig. 7.5 and Fig. 7.16. The controlled variable is

$$u(t) = K_p(1 + K_a s^2). \quad (5.5)$$

Eqn. 5.5 represents a proportional gain with included acceleration feedback, where K_p represents the proportional gain and K_a represents the acceleration feedback gain.

5.4 Position Feedback

The position feedback is one of the most widely used feedback controllers. This feedback control type is very easily implemented and measured. In the hydraulic systems the use of the position feedback is very common and has various effects on the system performance. According to [13], in order to provide both stability and damping, the position feedback needs to be selected in order to meet the so called $M=1,3$ criterion.

In our system the implementation of the position feedback is done on the position of the I Beam. This control process and its effects are shown in Figures 7.13 and 7.3.

5.5 Pressure Feedback

The pressure feedback in the servo hydraulic systems is very old and well-studied area [23]. Since the measurement of the pressure in the hydraulic parts (valve, cylinder) is very simple and cheap procedure, it is used in almost every hydraulic system. As the pressure parameter changes in the course of time and it is one of the state variables, Eqn. 4.6 and Eqn. 4.7, it is very important to have a good and stable measured value. As it is shown in Fig. 4.5 our valve can control the pressure on both sides as well as on the inlet.

According to [23], the pressure feedback increases the hydraulic damping but it can have some negative effects on the steady state stiffness.

Chapter 6

Simulation of the Model

As explained in Chapter 1 the simulation of hydraulic power systems has evolved rapidly in the last few decades. The fluid power systems can very often interact with mechanical systems, combustion engines, electrical power systems and controllers [22]. In order to achieve this the terms 'co - modelling' or 'co - simulation' need to be introduced.

This chapter will describe the basic understanding of the terms 'co - modelling' or 'co - simulation' by applying different simulation approaches as well as the construction of different parts of the simulation model which will be explained with the help of the previous chapters in which the basic working principles of these types of systems are given. The modelling of the system used for our simulations will be explained in Chapter 6.2.

6.1 Co - Simulation and Co - Modelling of Hydraulic and Mechanical Systems

The co - simulation and co - modelling approach makes it possible for different types of systems to be modelled and simulated in one environment. In our situation there is a combination of mechanical, hydraulic and control system. The systems which contain computing and physical elements can also be called embedded systems. John F. in his paper about collaborative design for embedded systems [14] introduces an interesting approach of dealing with this type of systems. He divides the embedded systems into two models, the discrete event modelling(DE) which represents the digital hardware or the communication part of the system and the continuous time model which represents the analogue circuit and the physical process. He goes further into explanation of the importance of the syntactic and semantic consistency of the models in order to have accurate results and valid simulation.

The connection between the models in Simulink® can be obtained with the introduction of 'Prismatic Translational Interface' elements between the hydraulic and the mechanical model of the system [5]. This system will be explained in more detail in Chapter 6.2.

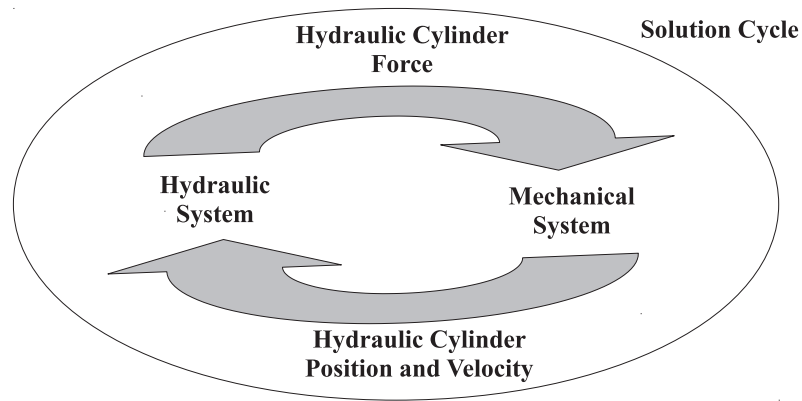


Figure 6.1: Co - simulation solution cycle

The simulation of the model was done in Matlab[®] Simulink[®] 2016b.

6.2 Modelling of the System

As explained in the previous chapters the system consists of 3 parts: mechanical, hydraulic and control system. The construction of the mechanical system was explained in Chapter 2.1.1 as well as the building process of the separate parts of the mechanical system.

The hydraulic cylinder and the hydraulic valve are included in the hydraulic part. The construction of the hydraulic cylinder and the connection to the mechanical system was achieved by following the principle explained in Fig. 6.1. The hydraulic cylinder can be separated in two parts, the piston side and the rod side. Figure 6.2 shows the hydraulic cylinder.

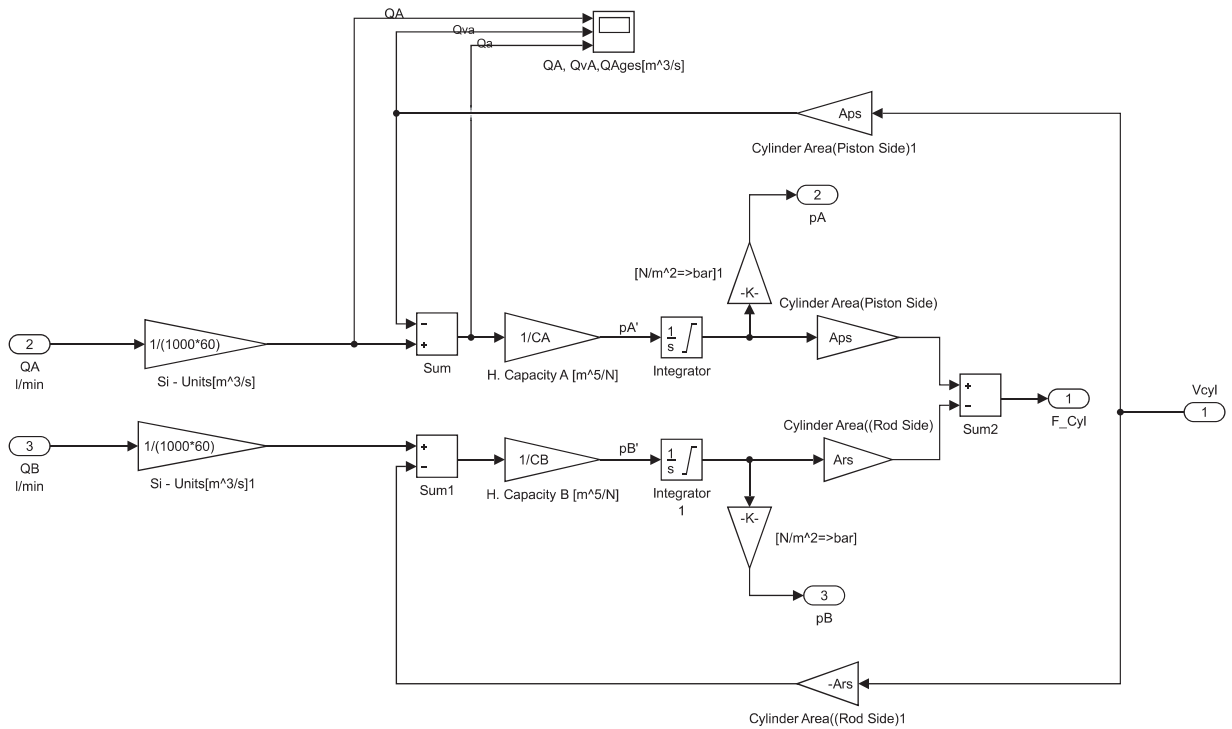


Figure 6.2: Hydraulic cylinder in Simulink®

In Fig. 6.2 we can see the working principle of the hydraulic cylinder. The set or the target values of the flow in the piston and rod side are preset from the controller in order to achieve constant velocity and enough flow to achieve the desired position.

On the other hand, the velocity of the piston measured in the prismatic joint shown in Fig.6.3 is multiplied with the areas from both sides Eqn. 3.5 and Eqn. 3.6, in order to calculate the actual value of the flow. Then these two values are compared and divided with the hydraulic capacitance according to 4.15. The bulk module of the oil is $E = 1.4 \cdot 10^9 \frac{N}{m^2}$. As a result of Eqn. 4.16 we get the first derivative of the pressure for both sides which then is integrated in order to get the values for the pressure in Pa for both sides. With the implementation of Eqn. 3.2 in this situation we get the force needed to move the piston on the cylinder, or as shown in the cylinder block F_{Cyl} .

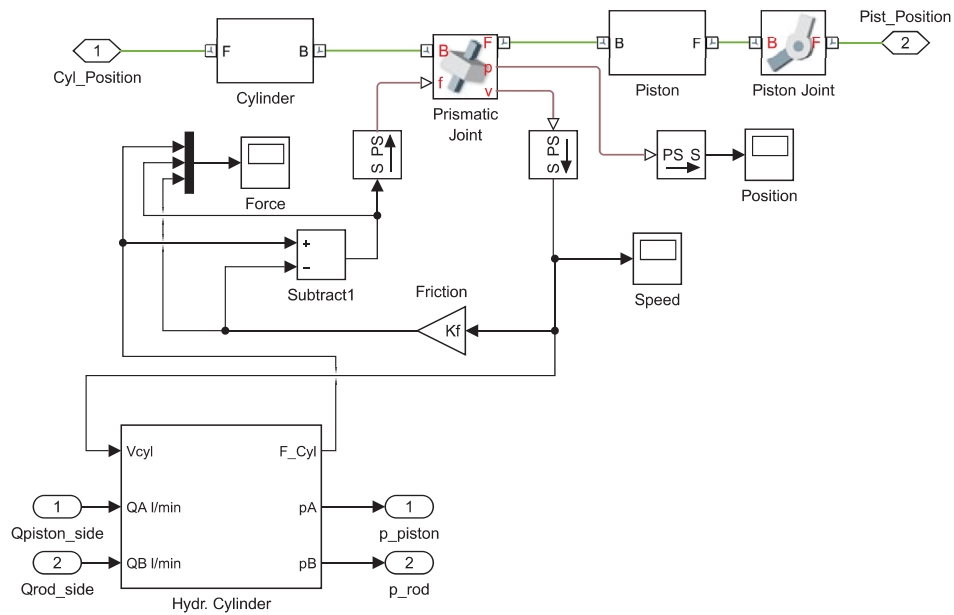


Figure 6.3: Connection of the hydraulic cylinder with the mechanical system

Figure 6.3 describes the 'Prismatic Translational Interface'. Here, the pressures of the piston and rod side are calculated in stand still in order to keep the position and the velocity constant. The pressure is then converted into the hydraulic force as shown in Fig. 6.2 which is then fed to the mechanical prismatic joint in order to achieve the desired position of the mechanical system. On the other hand, the prismatic joint velocity and position sensor feed back the information about the new position of the piston in the cylinder and compare it with the desired position. In each solution the cycle given in Fig. 6.1 is repeated until the desired position is achieved. Fig. 6.3 also shows the effect of the friction force. As explained previously in Chapter 3.1.3 the friction force is proportional to the velocity Eqn. 3.14 and the friction coefficient K_f . We then subtract the friction force from the actual actuator force (because it has opposite direction) which normally has damping effect on the system. This effect will be shown in Chapter 7.

The hydraulic valve tends to change the direction of flow into the hydraulic actuator whenever needed. The basic principles of the hydraulic valve are explained in Chapters 3.2, 3.2.2. In our situation there is an independent metering Eaton CMA90 valve Fig. 4.1, Fig. 4.5. As explained in Chapter 4.1 this valve has a CV and a PV valve. In our simulation we included the PV valve which is built of two 4/3 proportional valves and the control modes that this valve offers.

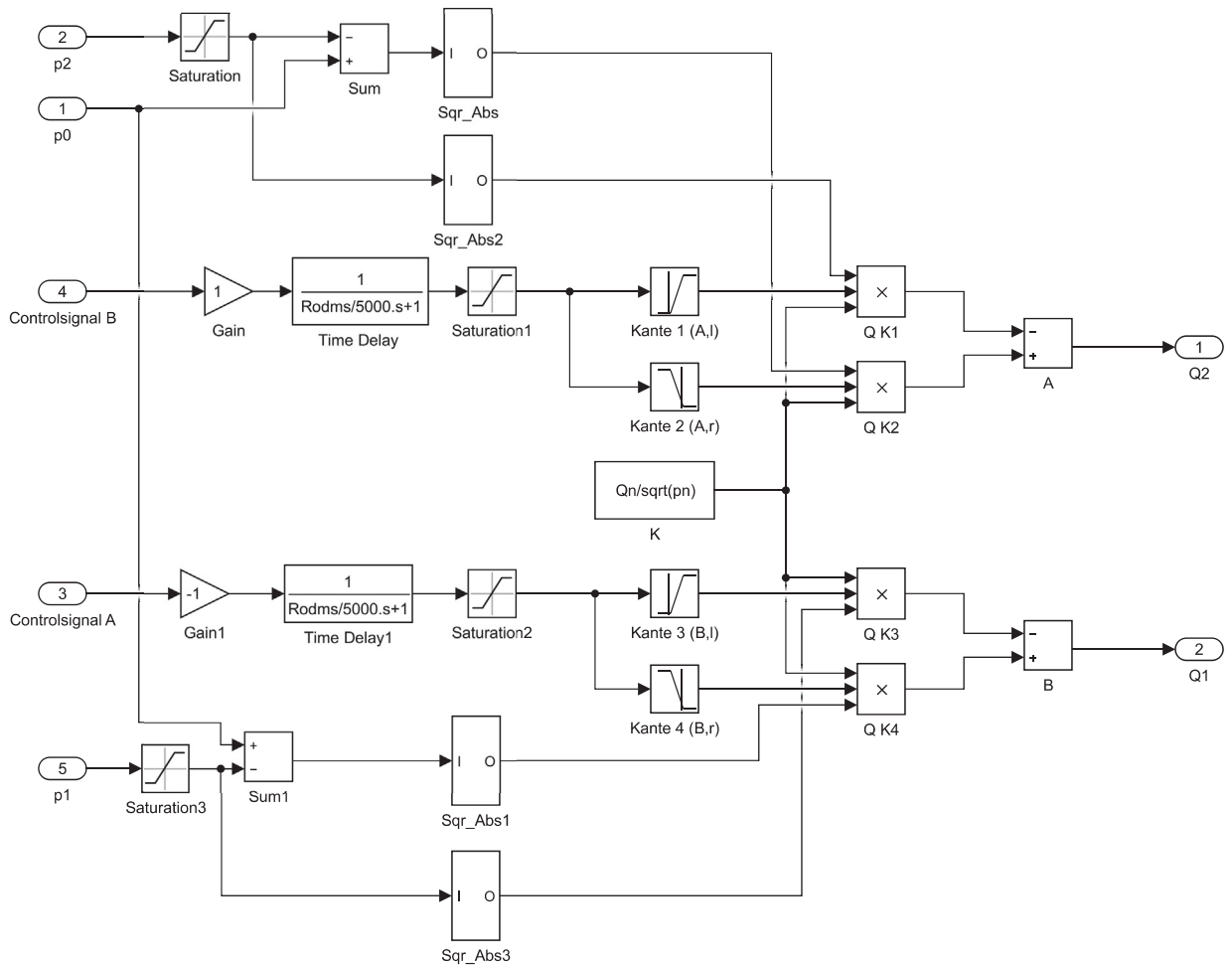


Figure 6.4: Hydraulic directional valve in Simulink® (Eaton CMA90)

Figure 6.4 shows the simulation block of the hydraulic cylinder in Simulink®. Here, p_0 is the supply pressure, p_1 is the pressure that is connected with the rod side of the cylinder and the p_2 is the pressure that is connected with the piston side of the cylinder. The flow equations for this valve are described with the Eqn. 3.30. If we implement the equation of the valve coefficient Eqn. 4.8 and multiply it with the valve input signal y , we get the equation for the flow through the valve Eqn. 4.8. The lookup blocks are designed so that the flow curve of the valve can be of critical center type. The control signals in the simulation are defined in the control block of the valve. In the flow equation for valve Eqn. 4.8 there is a square root from the pressure differences across the valve. Because this value Δp_v can also be negative and knowing that the square root of a negative value is an imaginary number we need to implement a block which will solve this issue.

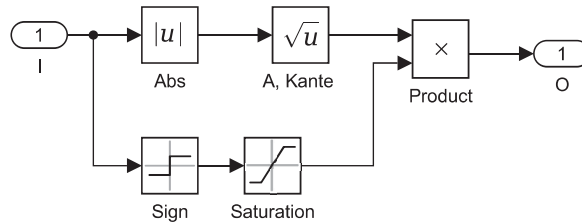
Figure 6.5: $Sqrt_{Abs}$ block

Figure 6.4 shows that these four blocks are implemented on the 4 pressure lines accordingly. This problem is solved by firstly taking the absolute value of the pressure and then taking the square root of the absolute value of the pressure. On the other hand, we take the sign of the pressure at this particular moment and we multiply it at the end with the square root value of the pressure in order to get the correct direction in which the fluid moves. The control signals of the valve depend on the control system implemented in the control logic block.

In order to understand the control block of the system we need to explain the control modes that this valve offers and try to understand what distinguishes every one of them. The Eaton valve offers three different control modes:

1. UFC (Universal flow control)
2. IFC (Intelligent flow control)
3. Single spool control mode

The UFC is the basic twin spool control mode that is available for this valve. However, its limited complexity can be a strength as well as a weakness [7]. The basic working principle of this mode is to try and match the flow in with the flow out of the valve. For this reason two UFC gains are defined in order to control the flow in and the flow out of the valve.

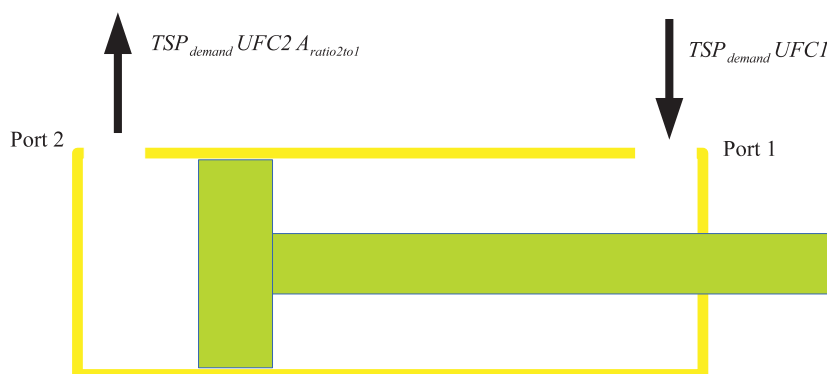


Figure 6.6: UFC gains

If we increase the gain for one port above unity, we ask for more flow out than what theoretically comes into the port. As a result, we reduce the pressure in the port which can lead to cavitation and low stiffness. On the other hand, when we lower the gain at a port we restrict the flow out which will build pressure in the cylinder. This will have very positive effect on the stiffness but it will have negative effect on the system power efficiency. Therefore, when using these

control modes we need to be careful and try to find a balance between the hydraulic stiffness and the energy efficiency of the system. In order to understand how this control mode works we need to examine Fig. 6.7.

The UFC control logic is a flow control logic, which means that the pressure is not controlled or relevant in this control loop. Figure 6.7 begins at the flow demand of the valve. If there is no flow demand, then the spool positions are centred and there is no flow entering or leaving the valve ($TSP_{demand} = 0$). If the demand is bigger or smaller than zero, then the valve can move the cylinder in two directions, from port one to port two (>0) or from port two to port one (<0). The next decision that the valve needs to make is whether the load is passive or overrunning, as explained in Chapter 4.3.

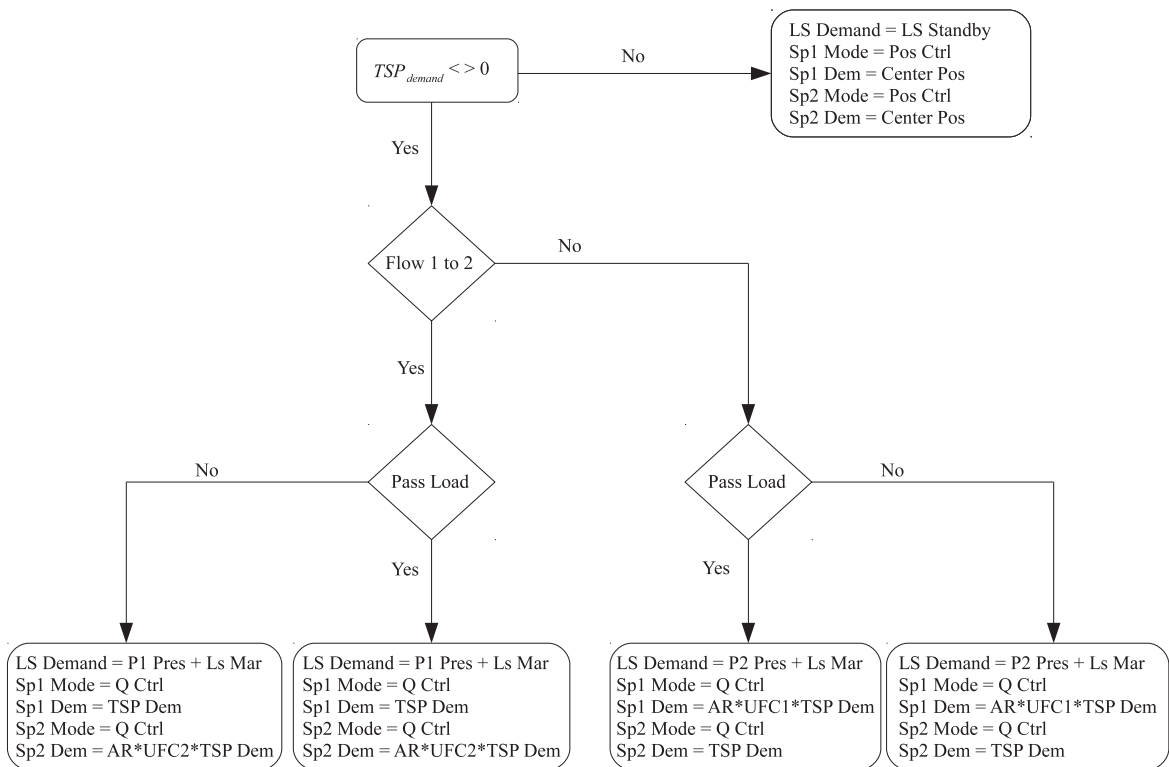


Figure 6.7: UFC control logic (adopted from [7])

This is made by implementation of two margins, one for the passive and the other for the overrunning (active) load and by implementation of a control logic which can easily determine these two loads. If we examine Fig. 3.1 and we assume that the area ratio is $A_{ratio} = \frac{A_1}{A_2}$ than we can define the following margins:

$$If \quad \frac{P_2}{A_{ratio}} - P_1 > \text{Overrunning Margin} \quad (6.1)$$

then

Differential Load = overrunning,
 else
 Differential Load = passive.

$$If \frac{P_2}{A_{ratio}} - P_1 < \text{Passive Margin} \tag{6.2}$$

then

Differential Load = passive,
 else
 Differential Load = overrunning.

If the pressure is passive or overrunning, the control logic can be separated into four control blocks. If we examine further, we can see that the UFC control mode utilizes flow control on both sides regardless of the load conditions [7]. This can in some situations lead to inconsistency in velocity as to cavitation and low energy efficiency. The control mode that take the load into account and deals with it properly is IFC or also know as the "intelligent flow control".

The initial setup for this control mode is to set the desired pressures for each port. Another positive thing is that this control mode takes the loads into consideration. The load is calculated with the Eqn. 6.1 and the Eqn. 6.2 and determines how will the valve react accordingly. What is different in this control logic is that there are flow and pressure controllers on both sides. Therefore, we can see in Fig. 6.8 that when the flow is overrunning, the valve activates the pressure control on one side in order to maintain the constant velocity. One of the interesting features of this control mode is the Anti - Fallback, which acts when the valve receives a non-zero flow demand for a passive load. In this situation the valve spool positions itself in the centre in order not to allow the load from falling backwards and stays in that position until the supply pressure is bigger than the load pressure.

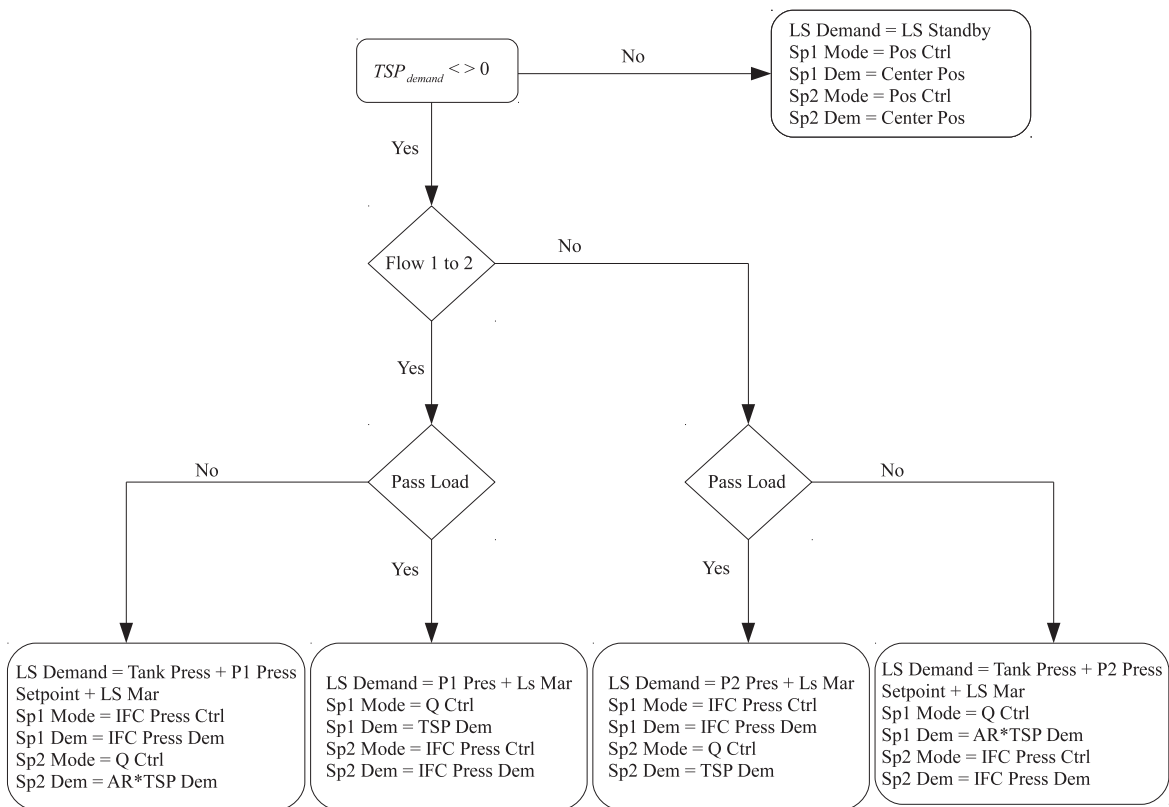


Figure 6.8: IFC control logic (adopted from [7])

The single spool flow control is the third mode that this valve offers. This control mode was not implemented in our simulations for a few reasons. Firstly, this control mode gives us the possibility to program and control both spools in manner that we desire and need. This is very interesting option for much simpler models and machines where the demand and precision of the valve needed are not big and the complexity of the system is smaller.

As explained before we implemented two of the control modes that this valve offers in our simulation, the UFC and the IFC control mode. The implementation of these control modes in the simulation model is shown in Fig. 6.9.

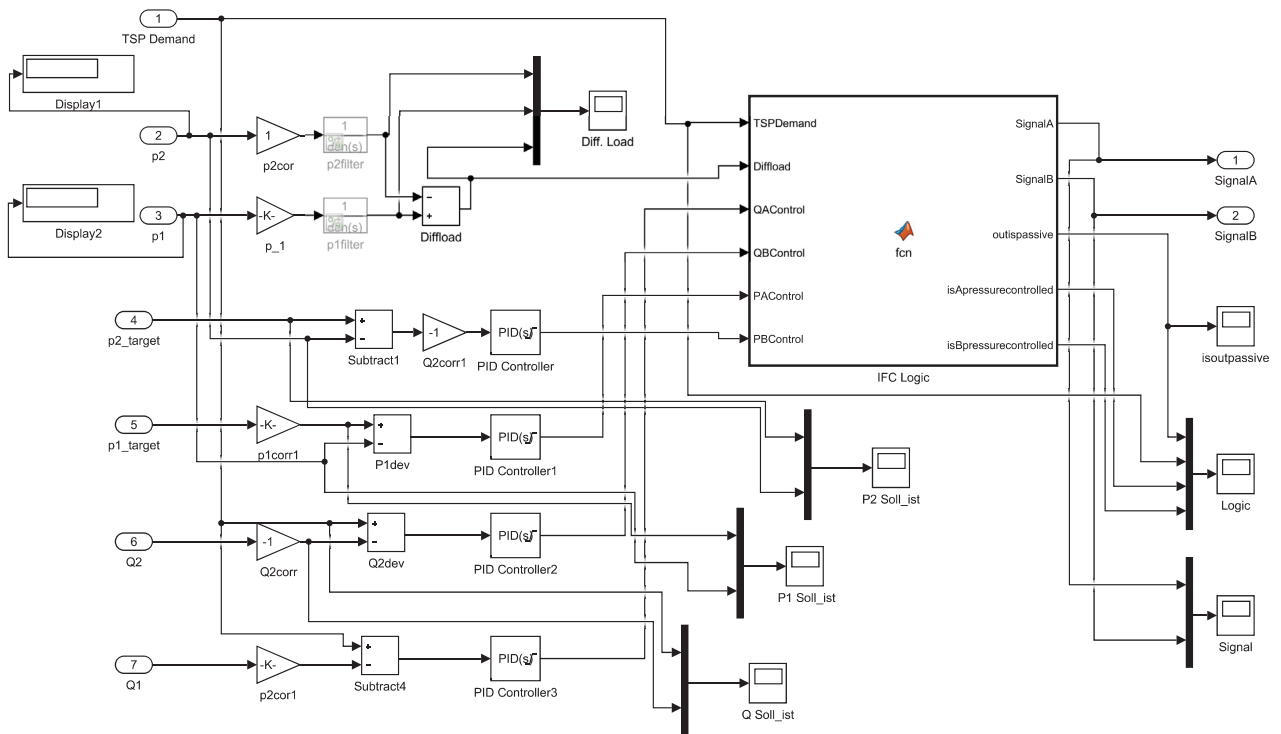


Figure 6.9: IFC control logic in Simulink®

Figure 6.9 shows the simulation block of the IFC. The input parameters in this block are the desired pressures ($P1_{target}$ and $P2_{target}$), the measured pressure in the cylinder ($p1$ and $p2$), the measured flow that enters and leaves the cylinder $Q1$ and $Q2$ and the demand of flow for the valve TSP Demand (the desired flow). The target values and the measured values are then compared with the feedback control loops and then controlled accordingly. Then they are sent in the IFC Logic block where they go through the control mode explained in Fig. 6.8 which after that sends the signals A and B to the valve where if we observe Fig. 6.4 they are one of the input values in the valve which are responsible for the position of the spools in the valve. A similar but not the same situation is for the UFC.

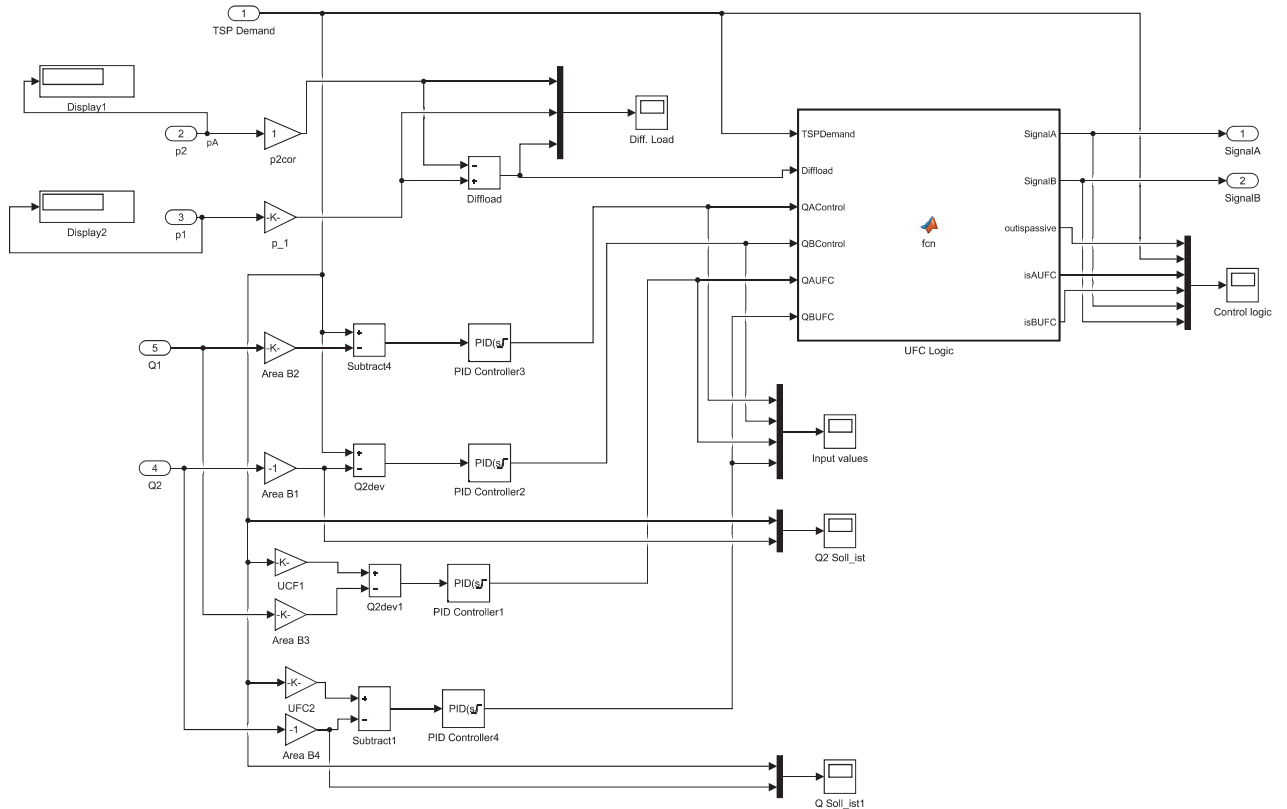


Figure 6.10: UFC control logic in Simulink®

The input parameters in the UFC differ from the ones in IFC as the UFC is only a flow control mode. Here we have a feedback control loops only for the flow which are compared with the target values and then sent into the UFC logic block. This block controls the values as shown in Fig. 6.7 and gives the signals A and B as outputs accordingly. The correction for the flows and pressures is done with the Eqn. 4.17.

The last part of the simulation is the load sensing variable displacement pump which is explained in Chapter 3.3.1. In order to simplify this model and the simulation process a non - physical pump is modelled which will give the needed pressure and the load sense margin.

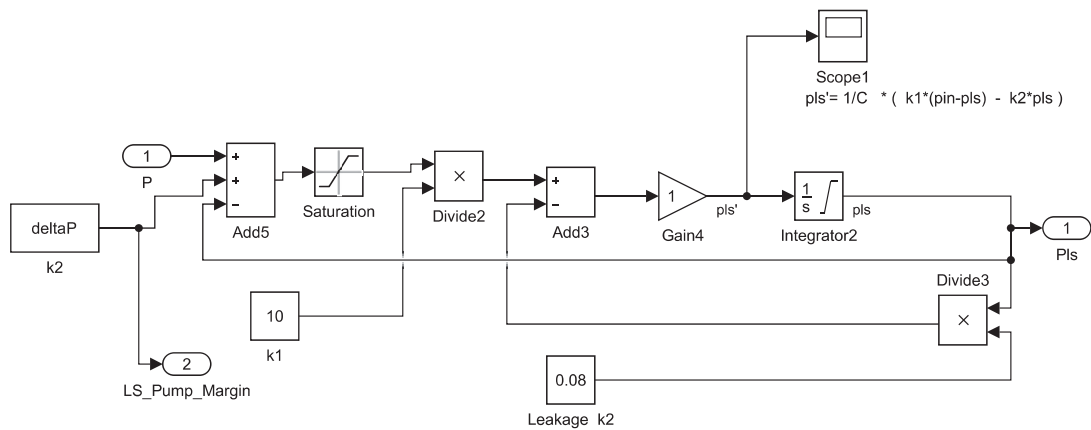


Figure 6.11: Simulink® model of load sensing pump

Figure 6.11 shows that the input values at the load sensing pump are the load sensing pressure P and the pressure difference Δp . The value of $k1$ represents the time delays that can be modified to our need in order to achieve the flow curve needed for our system and $k2$ represents the leakage coefficient. As we have previously described all mechanical, hydraulic and control subsystems that are included in this system, Figure 6.12 shows the simulated model of the test rig with the IFC control mode and Fig. 6.13 shows the simulated model of the test rig with the UFC control mode. It is important for the further simulation to mention that the piston side is referred to as number two and the rod side is referred to as number one in the given parameters.

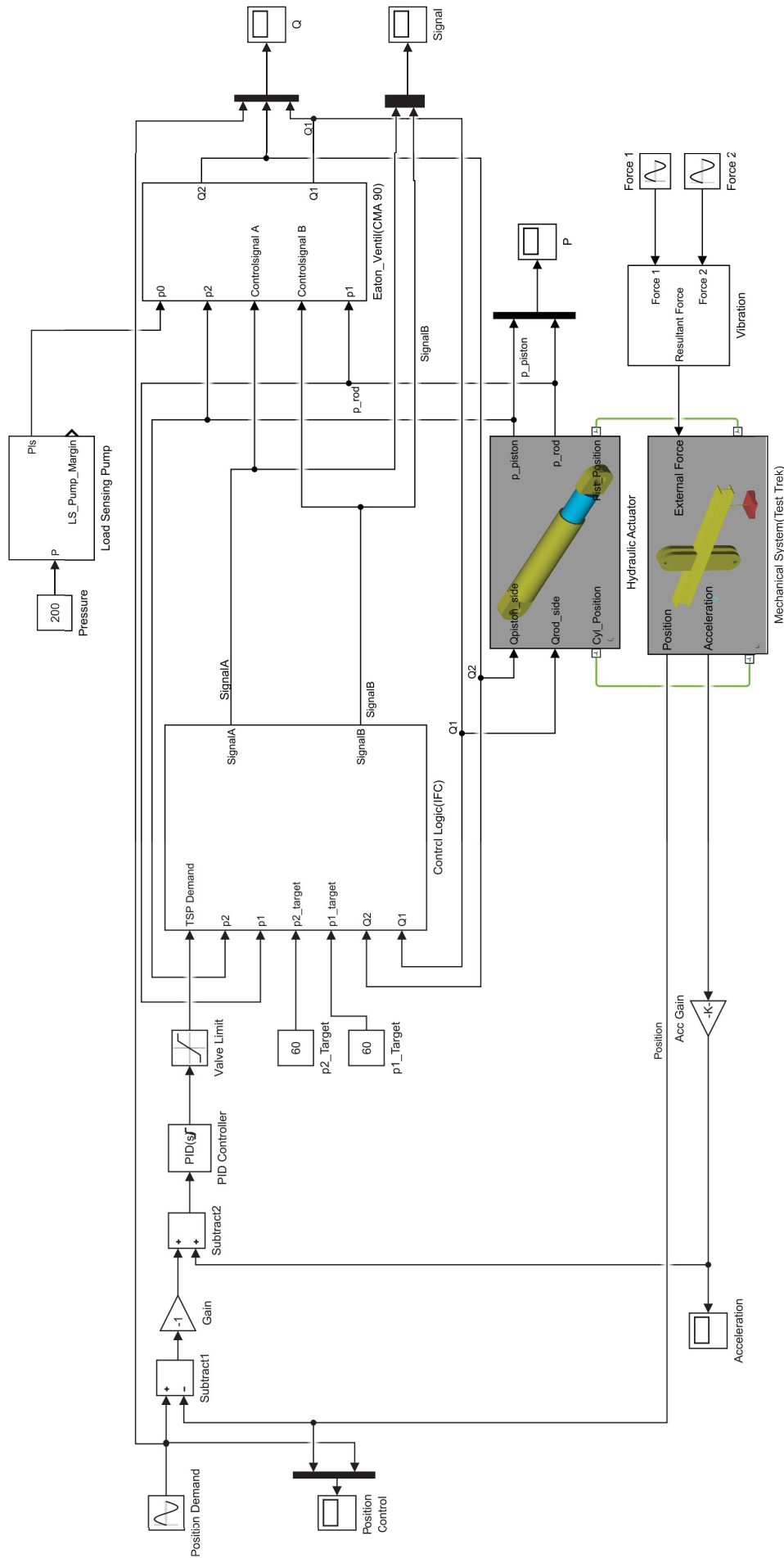


Figure 6.12: Simulink® model of the test trek with IFC control mode

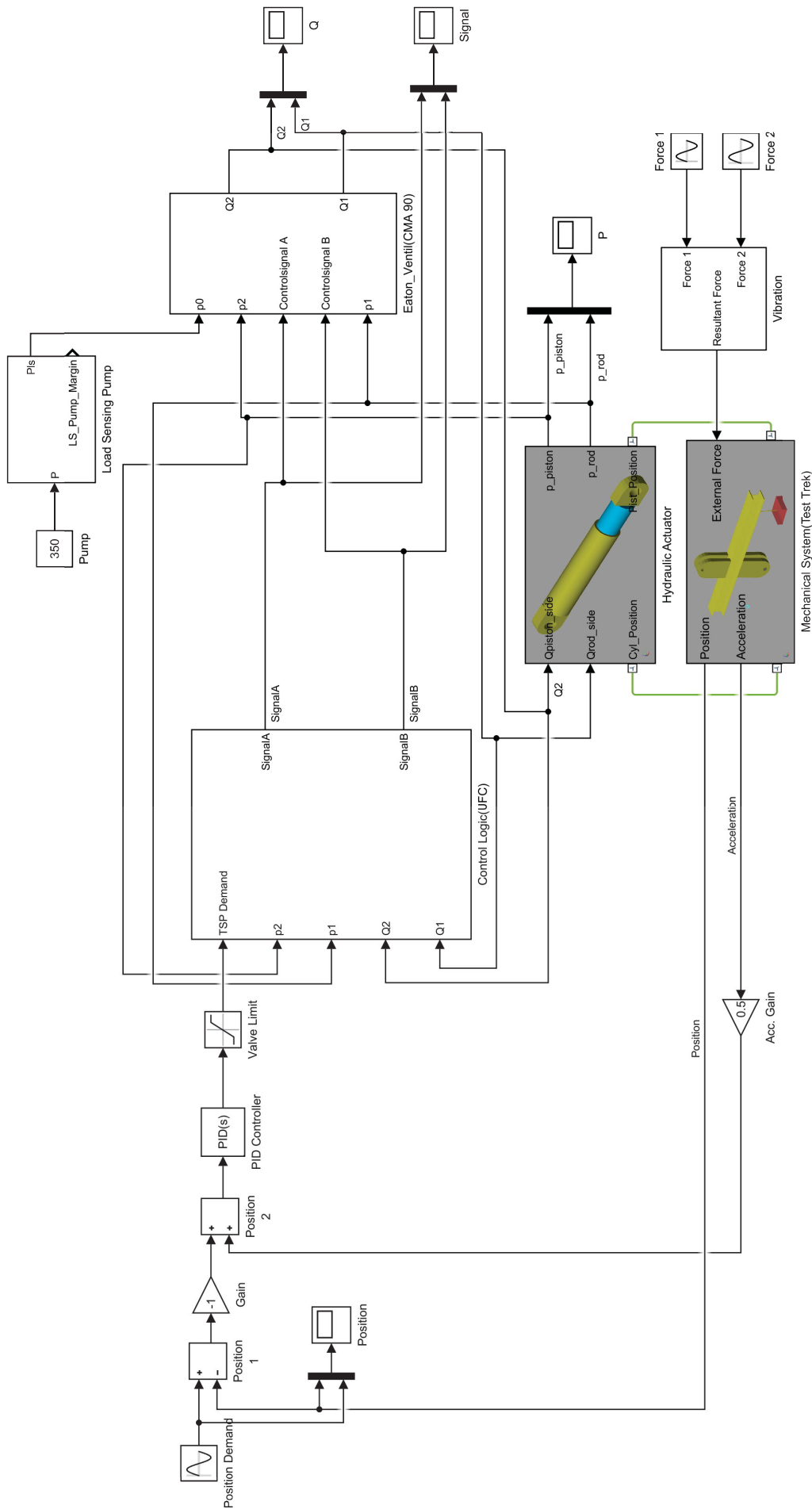


Figure 6.13: Simulink® model of the test rig with UFC control mode

Chapter 7

Simulation and Results

This chapter summarizes all chapters in which the basic parameters implemented in the simulations will be given as well as how the change in some of the parameters will influence the simulation model. The simulation of the two control modes with the relevant results will be given and explained. Finally, both models will be compared in order to see their advantages and disadvantages.

7.1 Test Rig Model with UFC Control Mode

In the previous chapter, I explained the basic principles of the hydraulic servo systems and the way in which the simulation model is built. In order to explain the effects of this system properly it is very important to include and explain the control parameters that are used in the simulation as well as their values.

As mentioned and explained before we will simulate and observe both twin spool modes that this valve offers, the IFC and the UFC.

The UFC control mode is the basic flow control method that this valve offers. Figure 6.7 shows that it uses only flow controllers without taking into account the pressure. In the simulation model we can see that we have implemented 4 PID controllers which control the flows Q_1 and Q_2 , which are corrected with the UFC gains and the Area ratio. Although the load control is very significant for these types of systems, the implemented UFC algorithm is designed in such way that the valve acts equally the same in passive and overrunning load.

Table 7.1 shows the PID controller gains and the UFC gains implemented in the model. Gain Q is the proportional action gain, QI is the integral action gain, Qd is the derivative action gain and UFC1 and UFC2 gains are the flow control gains explained in Chapter 6.2. The friction force is set at $3 \cdot 10^6$ N and there is no weight connected to the I beam.

The first tests will be of the UFC control mode where we will have flow input with the use of the step function block. First and foremost we must tune the PID control for optimal performance. Figure 7.1 shows how the valve reacts to step input with step time of 1 second and final value of 40 l/min. It is very clear that by the low gains ($K_p=0.001$) the controller is not so aggressive and we cannot achieve the desired value. But with the increase of ($K_p = 0.01$ and 0.1) we have

Parameters	Values
Gain Q	0,001
Gain QI	0,05
Gain Qd	0,008
UFC1 Gain	0.50
UFC2 Gain	0.50
Area 1[cm^2]	137
Area 2[cm^2]	201

Table 7.1: UFC control block parameters

much better and aggressive controller which reaches the desired value. But when we increase the proportional gain as mentioned in Chapter 5.2.1 and shown with Figure 7.1 we have oscillations which can have a very negative effect on the system.

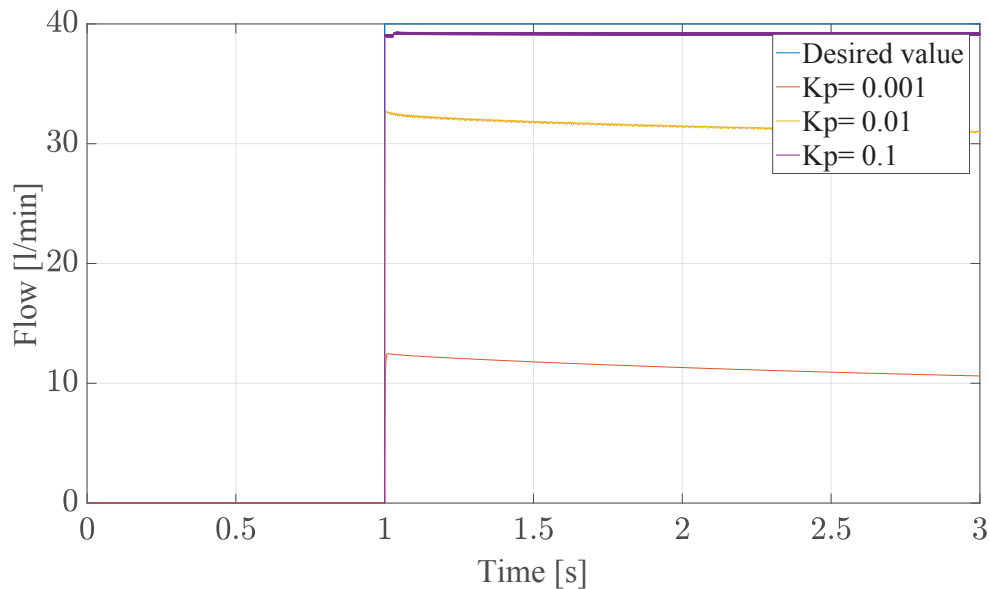


Figure 7.1: UFC Flow control Kp

This leads to the conclusion that further increase of the P gain will only have negative effect on the system and can lead to overshoot and instability. One of the possible ways in which we can decrease the oscillations is with the implementation of the derivative part of the PID controller 5.2.3.

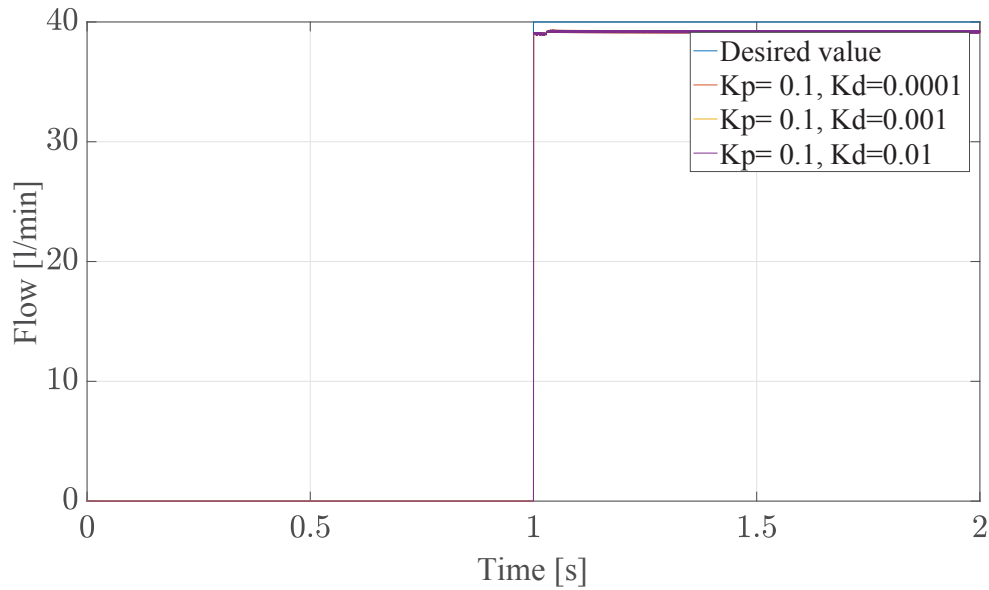
Figure 7.2: UFC Flow control K_p , K_d

Figure 7.2 shows the effect of the proportional and derivative controller by this type of systems. The input is again a step with 40 l/min final value and step time of 1 second. Although it was expected the derivative part to eliminate the oscillations, it had no effect whatsoever on the oscillations. On the other hand, by increasing the derivative part it had also had negative effect on the time needed to simulate the model. If we take the last two figures, Fig. 7.2 and Fig. 7.1 we can conclude that the P controller will be the most suitable for this type of system. The integral part was not used because we can see that the P action is doing great job by reaching the desired value, so implementation of the integral action is not needed.

However, in reality the machine normally uses a position controller which needs to follow the path implemented for cutting the desired piece. In order to simulate that we have implemented a position controller which has a feedback signal measured on the revolute joint on the I beam Fig. 2.7. The position is measured in degrees. In order to try and simulate this mode to its full capabilities we have implemented a weight on the beam of 10000 kg. We will start by implementing a P position controller with step function input with 1 degrees position change and 1 second step time.

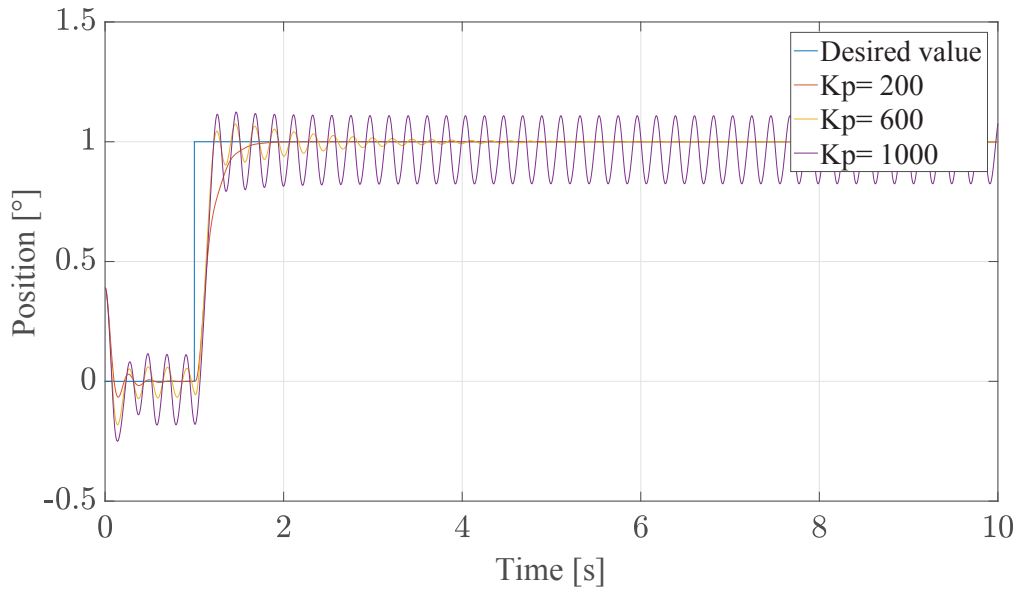


Figure 7.3: UFC position control

Figure 7.3 shows how the controller reaches the desired value of the position. We can see that with very low gains ($K_p=200$) the controller needs more time to achieve the desired value. But by increasing the value to $K_p=600$ the controller reaches the desired value much faster. Further increasing of the K_p gain leads to oscillations and overshoot. Similar results we will get if we change the input signal to sinus with an amplitude of 1 degree and frequency of 2rad/sec . It is important to notice that in order for the position controller to follow the desired path the valve flow control proportional gain was increased to 0.005.

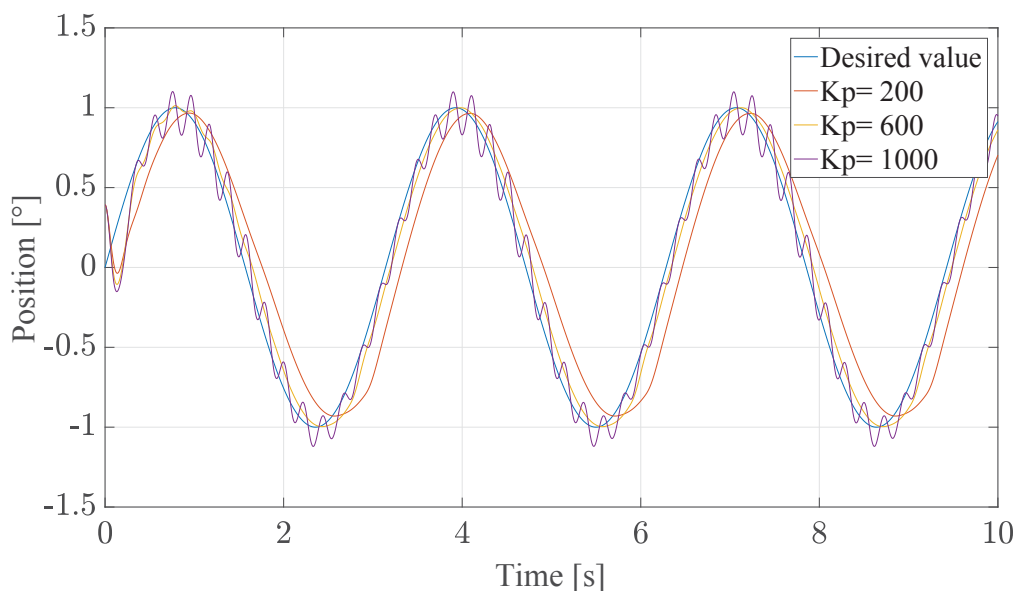


Figure 7.4: UFC position control (sinus input)

So as shown in Fig. 7.4, we have the same issue. As soon as we increase the K_p gain above unity then we have oscillations which can lead to overshoot. In order to solve this problem an

acceleration feedback is implemented, which as explained in Chapter 5.3 should have a damping effect on the whole system. The same conditions are going to be used for the previous two figures, Fig. 7.3 and Fig. 7.4 so we can compare and discuss the effect of the acceleration feedback. The acceleration feedback gain is $Ka = 0.1$.

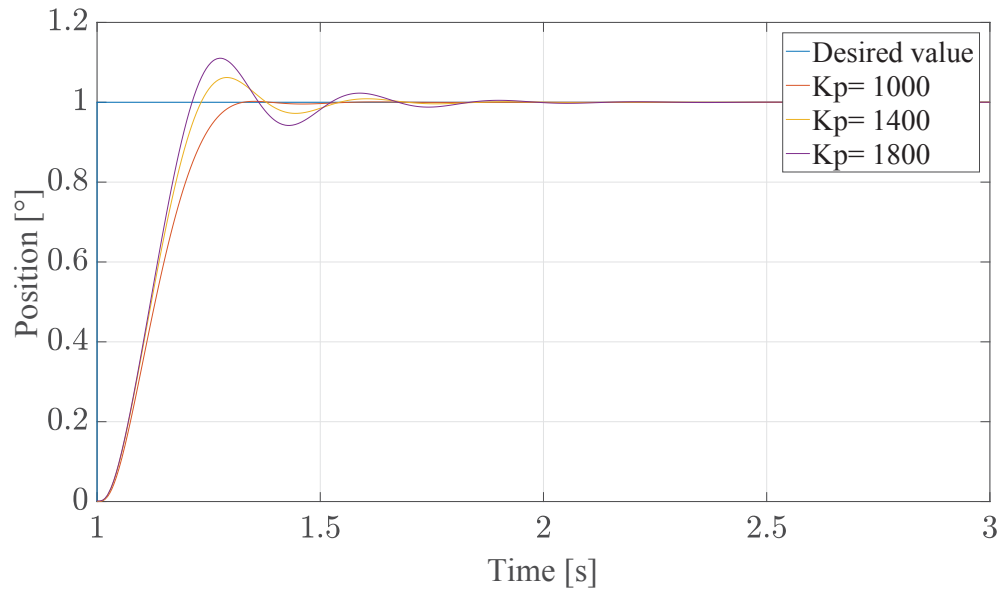


Figure 7.5: UFC position control with acceleration feedback

Figure 7.5 shows the damping effect of the acceleration feedback. We can see that when we compare the signals in Fig. 7.3 and Fig. 7.5 the effect is obvious.

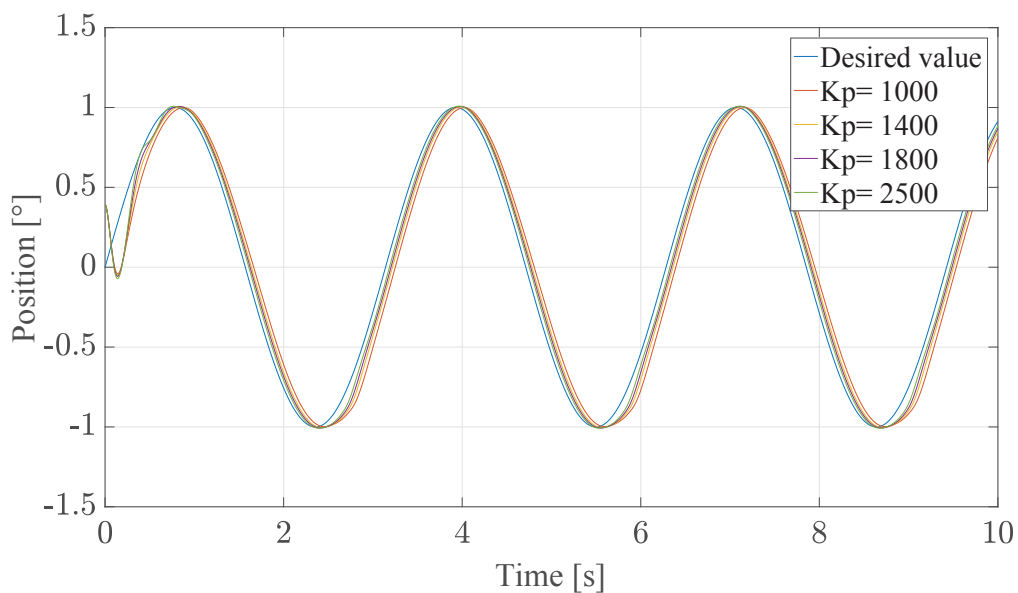


Figure 7.6: UFC position control with acceleration feedback (sinus input)

This gives us the possibility of increasing the proportional gain and achieving better performance. The same simulation was done for the sinus input also with the same properties as in

Fig. 7.4. Figure 7.6 shows the incredible damping effect of the acceleration feedback. The oscillations are fully damped and the controller follows the desired values without any disturbances. After achieving the desired control for the position, we can now focus on the advantages and disadvantages that this control mode offers.

Chapter 6.2 explains the basic principle on which this control mode is based. Figure 6.6 shows that the flow in and the flow out of the cylinder can be regulated with the help of the two UFC gains. These gains are normally set at low values in order to achieve stiffer performance. But as explained in Chapter 6.2 this leads to low energy efficiency of the system overall. We start with the values for the gain at the rod side 0.5 which means that we will restrict the flow out of the cylinder for half and increase to 1 and to 1.5 which means that we will require more flow out than we can possibly supply. As an input value we use a step function with step time of 1 and final value of 1 degree.

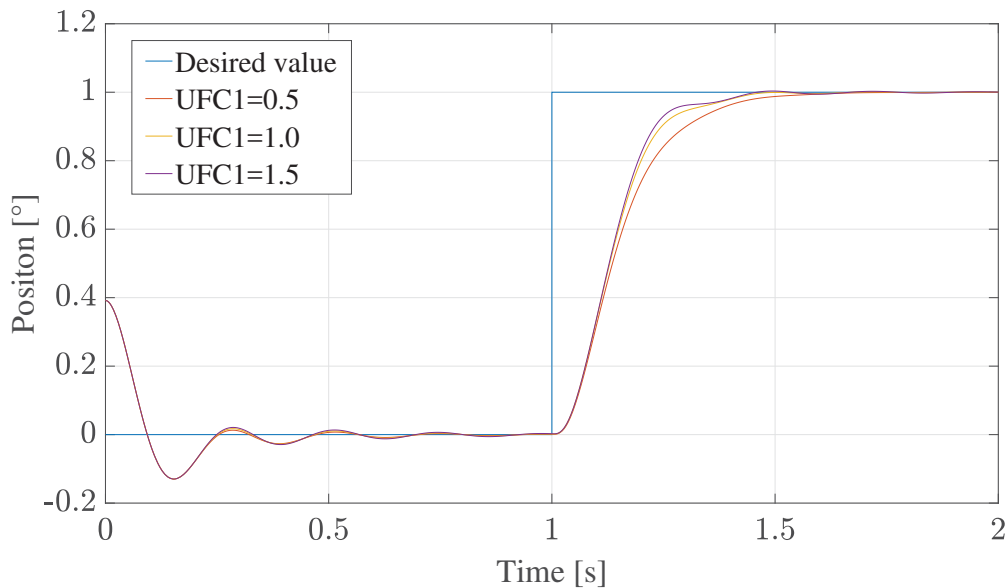


Figure 7.7: Position control UFC=0.1-1.5

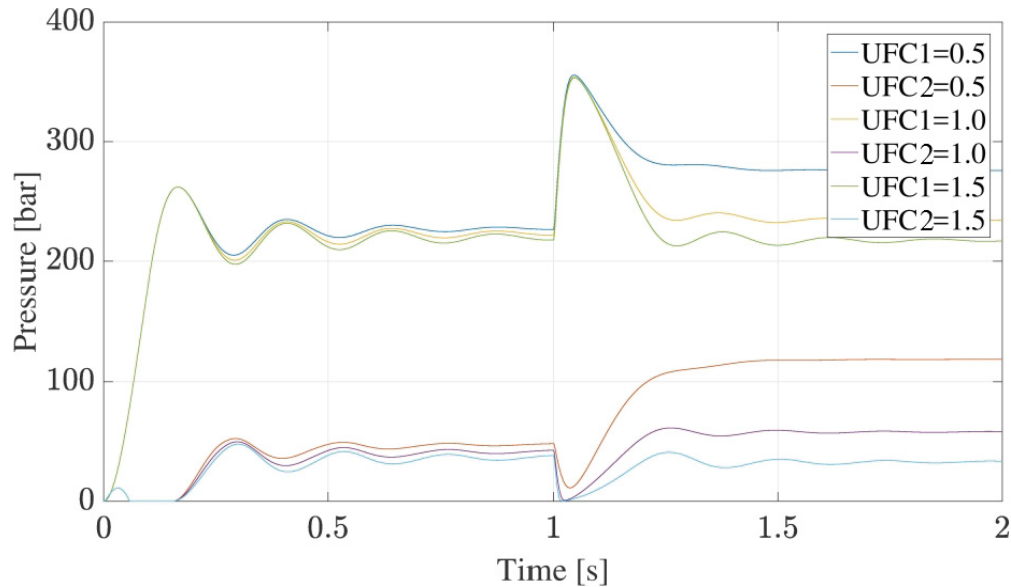


Figure 7.8: Pressures UFC=0.5-1.5

In Fig. 7.8 and Fig. 7.7 we can see that as we increase the UFC gain of the rod site the pressure falls and it can lead to cavitation. On the other hand, the position control is not as smooth as before and oscillations occur. From the previous tests we can conclude that the UFC is a control mode that can be used by application where the system efficiency is not an imperative.

7.2 Test Rig with IFC Control Mode

The IFC control mode is the main control mode used with this valve. It has the ability to control the pressure and the flow at the ports simultaneously. The main advantage is also that it has the possibility to pre-set the pressure values on both sides in order to avoid cavitation and to achieve stiffer performance. The other very important advantage is that this control mode takes into account the load condition and acts accordingly. So the passive and overrunning margins need to be pre-set in the control settings. The tests will be done in a similar manner as by UFC.

The IFC control mode is much more complicated and much more efficient than the UFC. Table 7.2

Parameters	Values
Gain P	0,02
Gain QI	0,02
Gain Pd	0
Gain QI	0
Gain PI	0
Area 1[cm^2]	137
Area 2[cm^2]	201

Table 7.2: IFC control block parameters

shows the main controller parameters that were used in this control mode. There are the propor-

tional part gains for the flow and the pressure (Gain P, Gain Q) then the areas which are used to calculate the area ratio and the integral derivative parts of the pressure and flow controllers. Similarly to UFC we also used the proportional action of the controller. The differential load is calculated according to Eqn. 6.1 and Eqn. 6.2 and the passive margin is set to be 2 and the over-running to 7 bars. These margins can be easily changed and the values are dependent on how big the load is. The friction force is set at $4 \cdot 10^4$ N and there is no weight connected on the I beam.

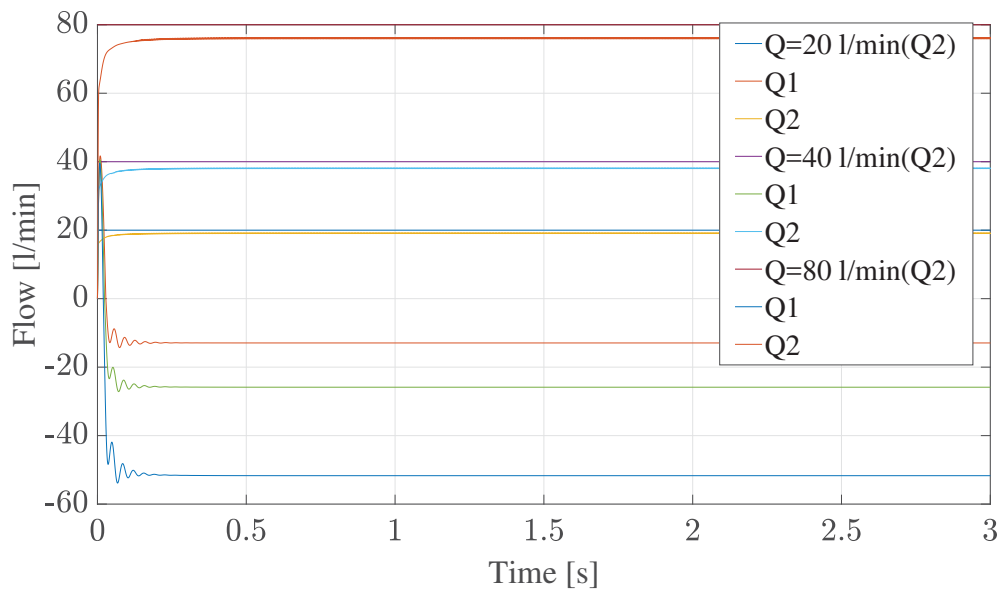


Figure 7.9: IFC flow control 20 - 80 l/min

Figure 7.9 shows that the set value for the flow is set at 20 - 80 l/min. We can see that in all cases the flow control goes smoothly and the proportional controller can easily achieve the flow desired value. In order to see the reaction of P controllers to change, there are similar simulations for the pressure change in both chambers. The flow demand will be set at 80 l/min.

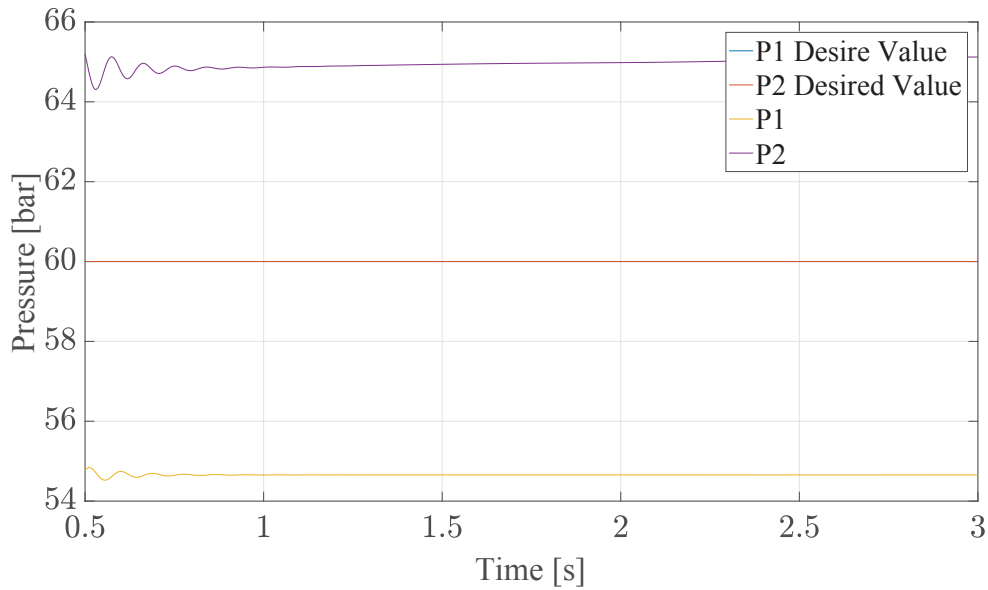


Figure 7.10: IFC pressure control [60bar]

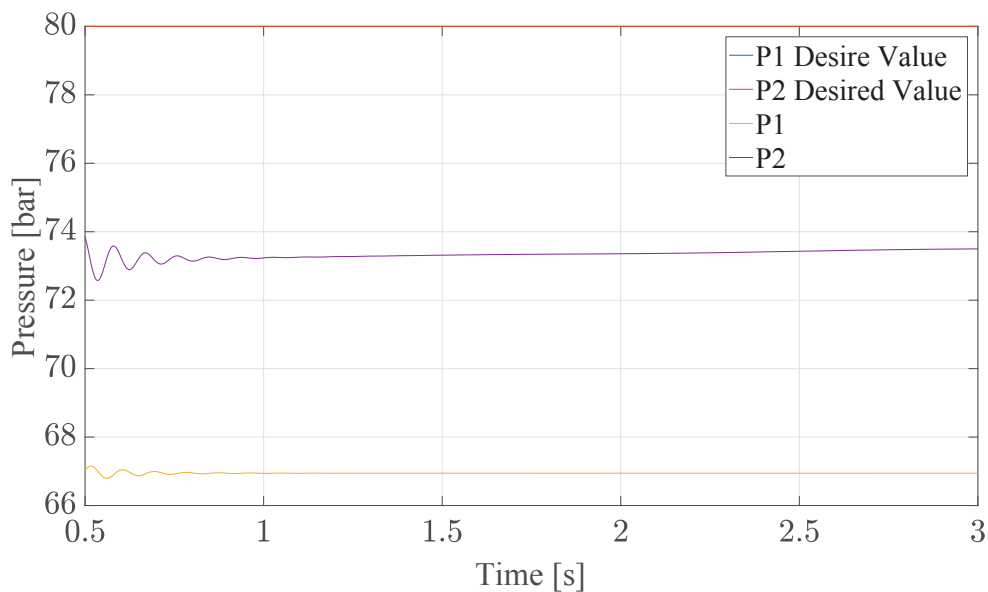


Figure 7.11: IFC pressure control [80bar]

Figure 7.10 and Fig. 7.11 show how the pressure control reacts to two different values. In Fig. 7.10 we can see that the desired value is set at 60 bar. The rod side is capable of achieving this value but it is smaller than this value because it is corrected with the area ratio. The piston side pressure exceeds this value because the load on the system is bigger and we need bigger pressure in order to achieve the desired moving path.

After testing the flow and pressure controllers we can now implement the position controller which is the controller that is used by the machine and in the test rig. The position controller proportional gain will be set at 50 and will be increased according to the demands of the system. The input

function will be a sinus function with an amplitude of 2 degrees and frequency of 3rad/s. The weight connected to the system is 3000 kg.

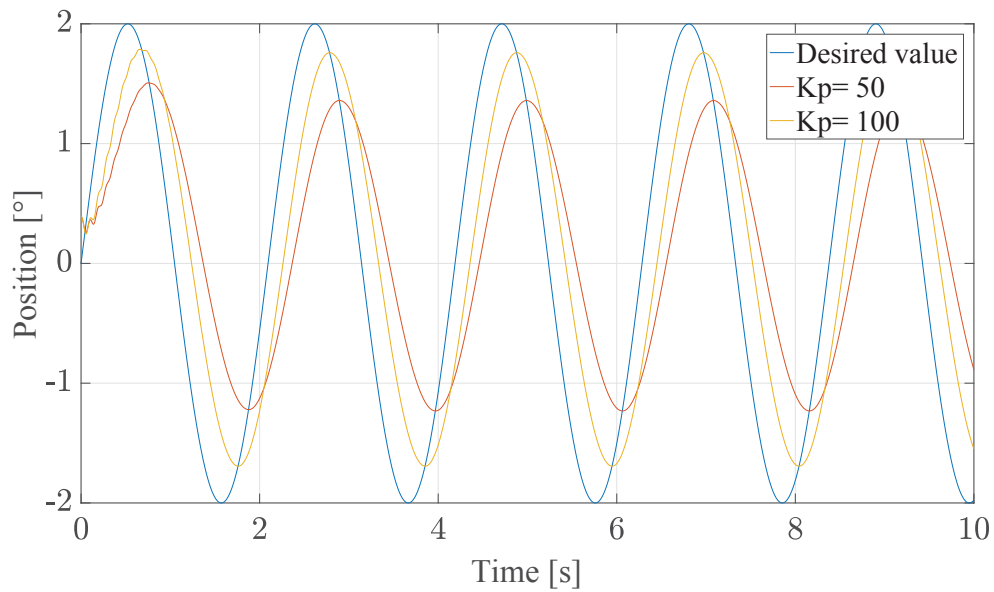


Figure 7.12: IFC position control $K_p=50,100$

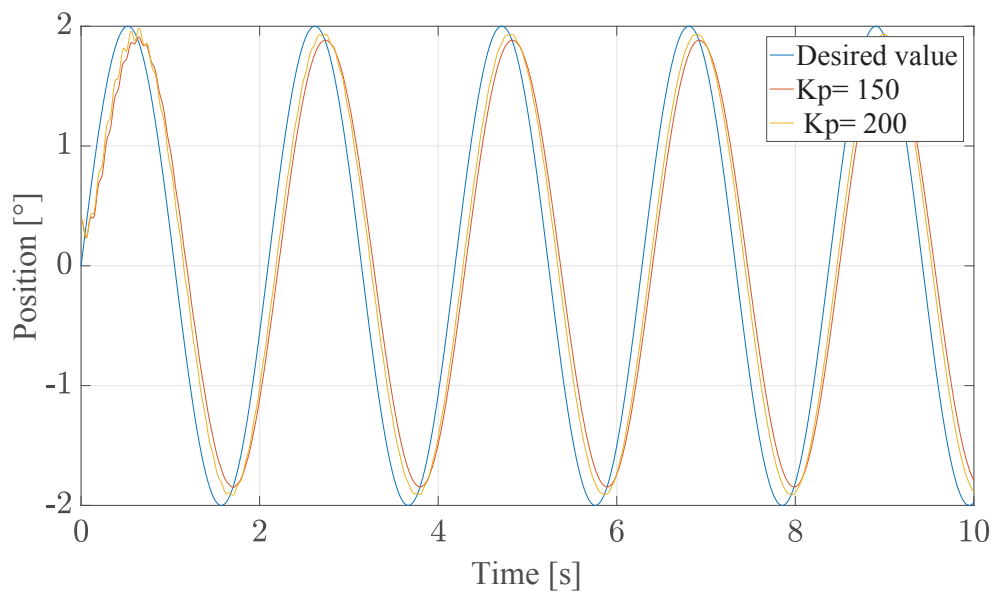
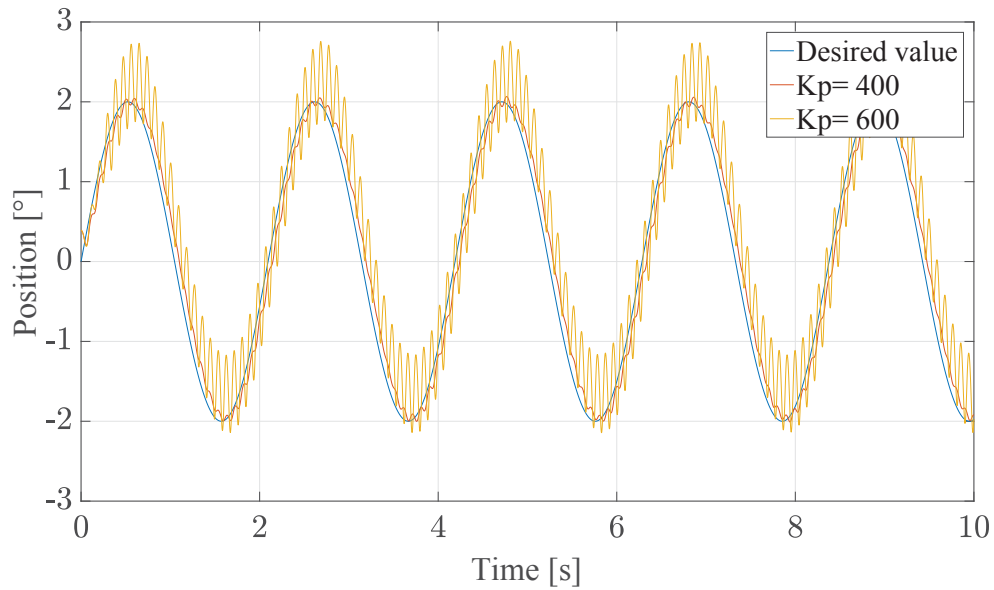
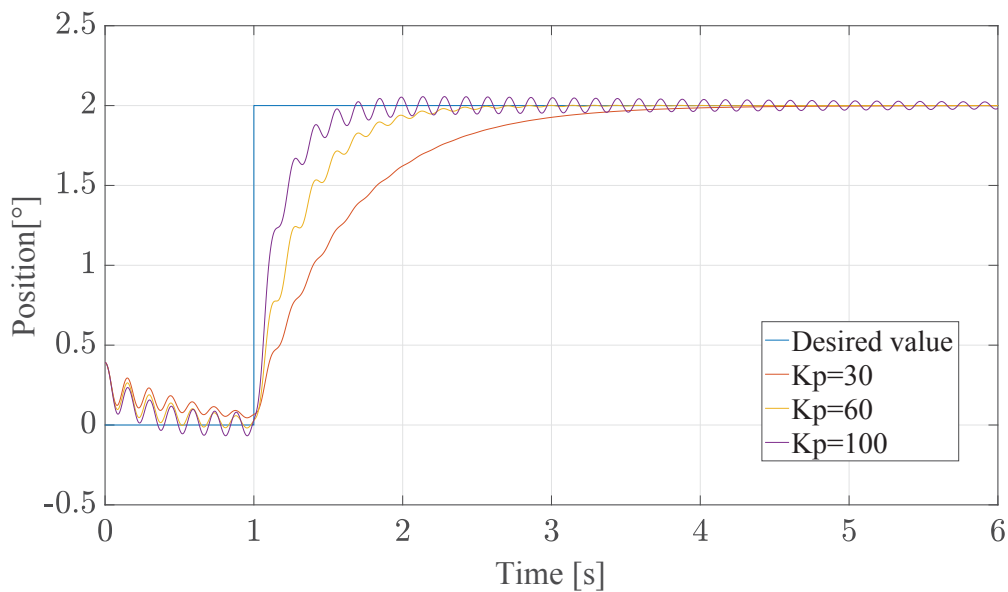


Figure 7.13: IFC position control $K_p=150,200$

Firstly, we start with low proportional gains as shown in Fig. 7.12. We can see that the controller has difficulty to achieve the desired values. With further increase of the gains, shown in Fig. 7.13 we are getting near the desired value but we can see that by $K_p = 200$, oscillations occur.

Figure 7.14: IFC position control $K_p=400,600$

The same will occur if we use different type of input, for example a step function with final value of two degrees and one second rise time. First the proportional gain at the position controller will be set at 30 and increased till 100.

Figure 7.15: IFC position control with step function input $K_p=30, 60, 100$

In order to achieve more accurate system the gain is increased at values of 400 and 600. At 400 the oscillations are still reasonably high but at value of 600 there is an overshoot and an unstable system. This leads us to the conclusion that in order to achieve better performance we need to try to damp the oscillations of the position controller which occur at high gain values. Similarly

to UFC the damping effect is achieved with the help of the implementation of the acceleration feedback. The acceleration gain $K_a = 0.1$.

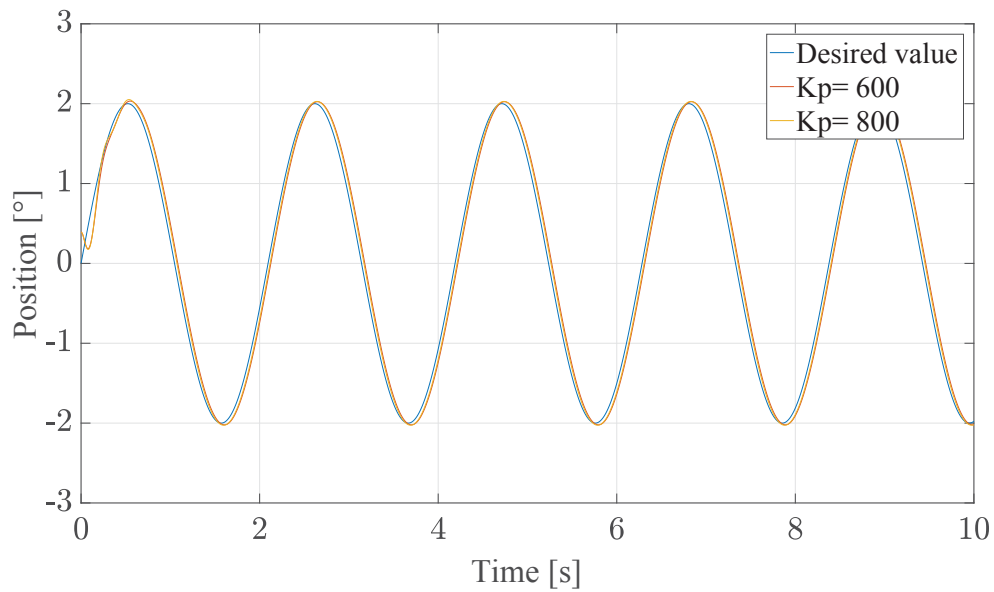


Figure 7.16: IFC position control with acceleration feedback $K_p=600, 800$

Figure 7.16 shows the damping effect of the acceleration feedback. We can see that this type of feedback control helps in getting stable and satisfactory results. The acceleration feedback has the same effect on the system with step function input Fig. 7.17.

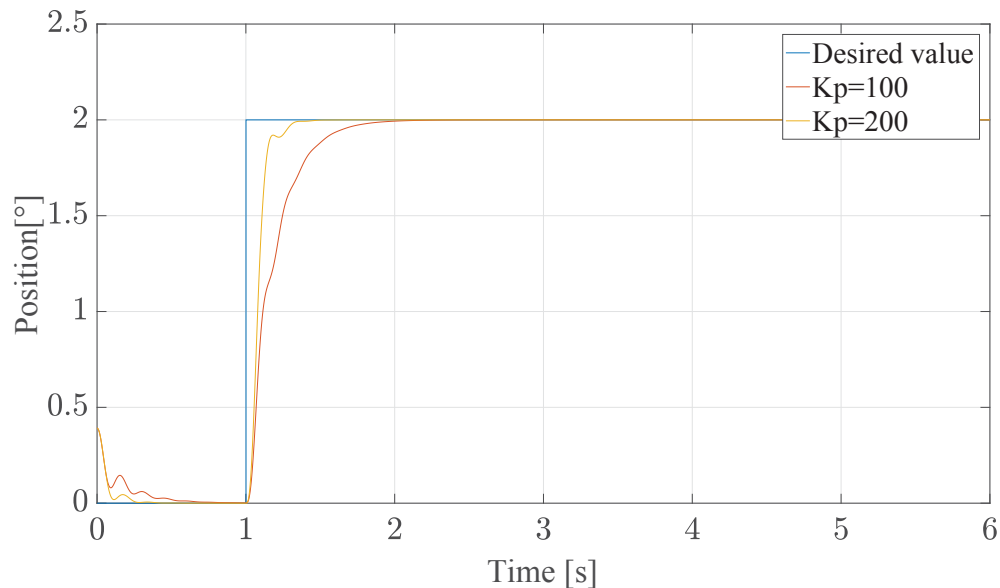


Figure 7.17: IFC position control with acceleration feedback (step function input)
 $K_p=100, 200$

Even by further increasing of the proportional gain the systems will stay stable and the oscillations will be damped, Fig. 7.18.

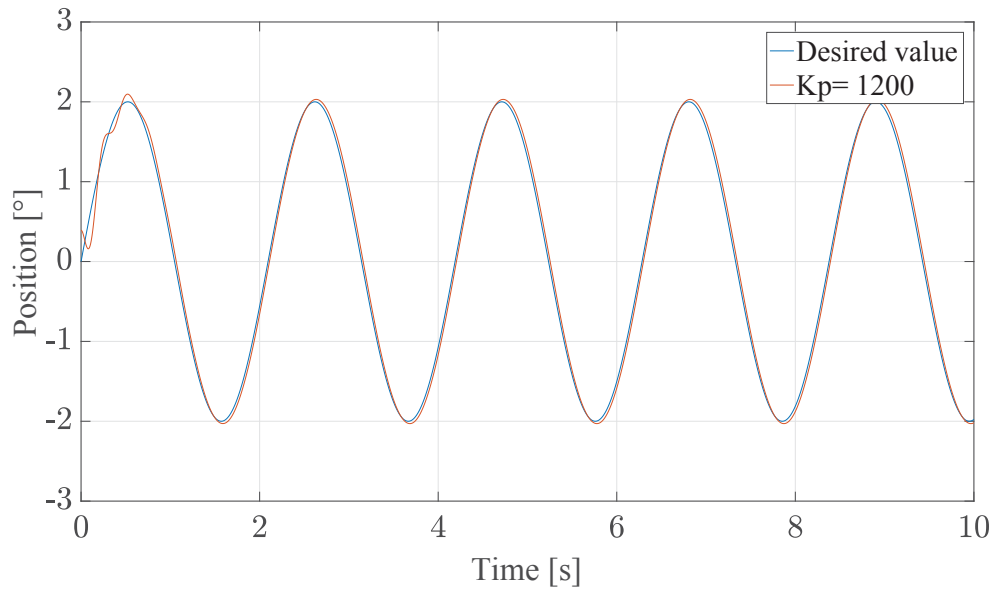


Figure 7.18: IFC position control with acceleration feedback $K_p=1200$

Figure 7.18 gives us confidence that this control mode is able to perform really good in even harsher environment with far bigger load and disturbance, which is the environment in which the road cutting machines usually find themselves. In order to simulate that we will firstly try to increase the weight on the Beam. While doing so we will take a closer look at the pressures, the position control as well as the control logic. Firstly, we will increase the weight on the system at 4000 kg. The proportional gain will stay at $K_p = 800$ and the pre-set pressures for the piston and rod side are set at 60 bar.

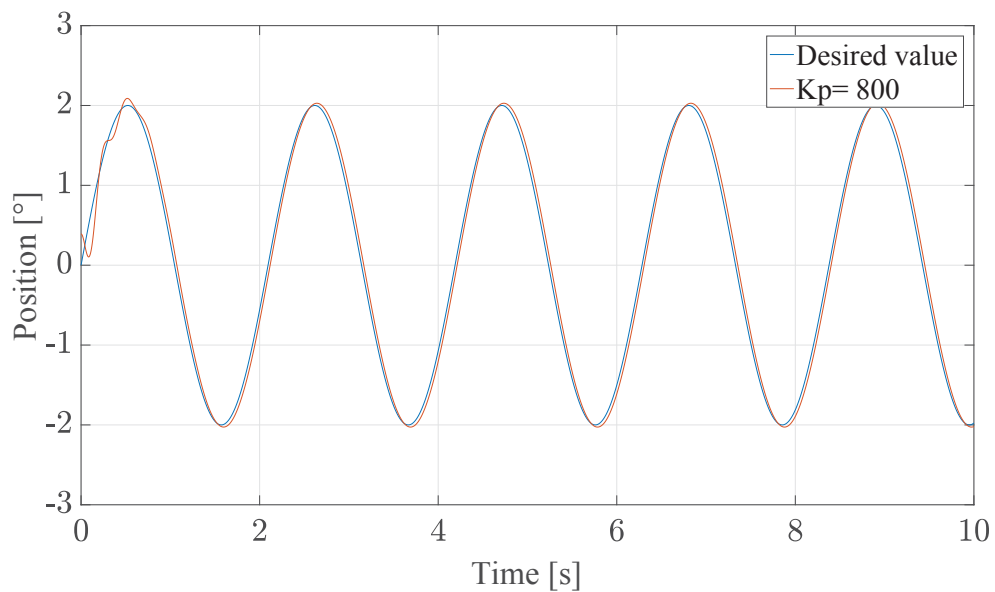


Figure 7.19: IFC position control with acceleration feedback $K_p=800$, $m=4000\text{kg}$

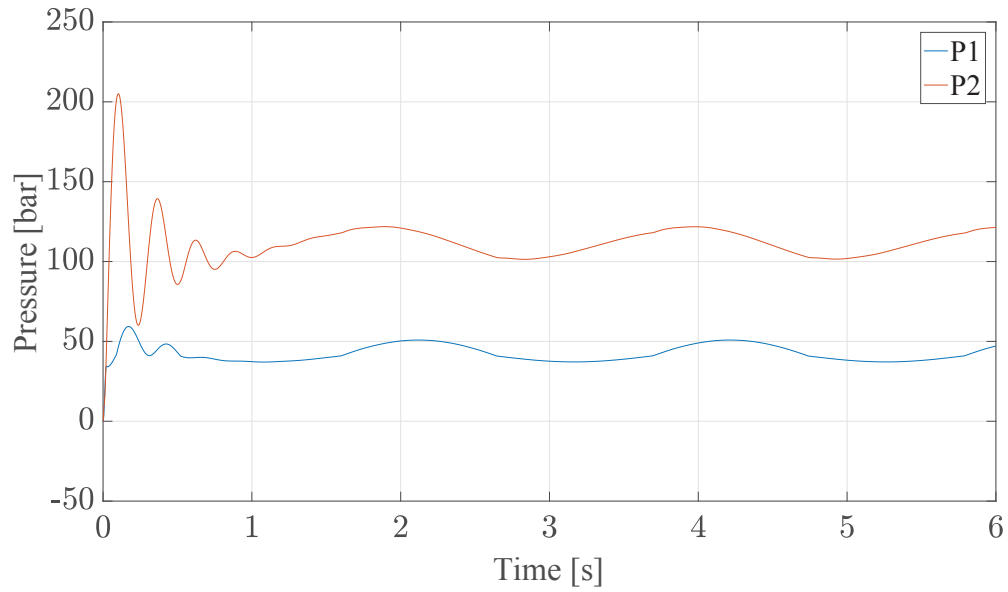


Figure 7.20: IFC pressure control with acceleration feedback $K_p=800$, $m=4000\text{kg}$

Figure 7.19 shows that the valve can rather easily achieve the desired value for the position at these values. The pressure at the piston side is increased which is expected as the load on the system is much bigger. The mass will be increased to 8000 kg. All other parameters will stay the same.

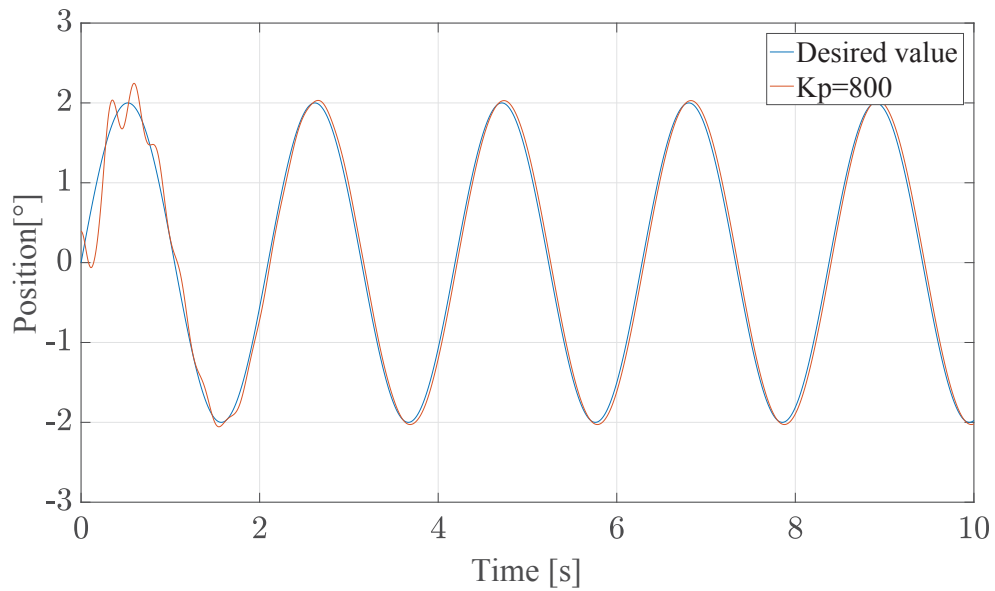


Figure 7.21: IFC position control with acceleration feedback $K_p=800$, $m=8000\text{kg}$

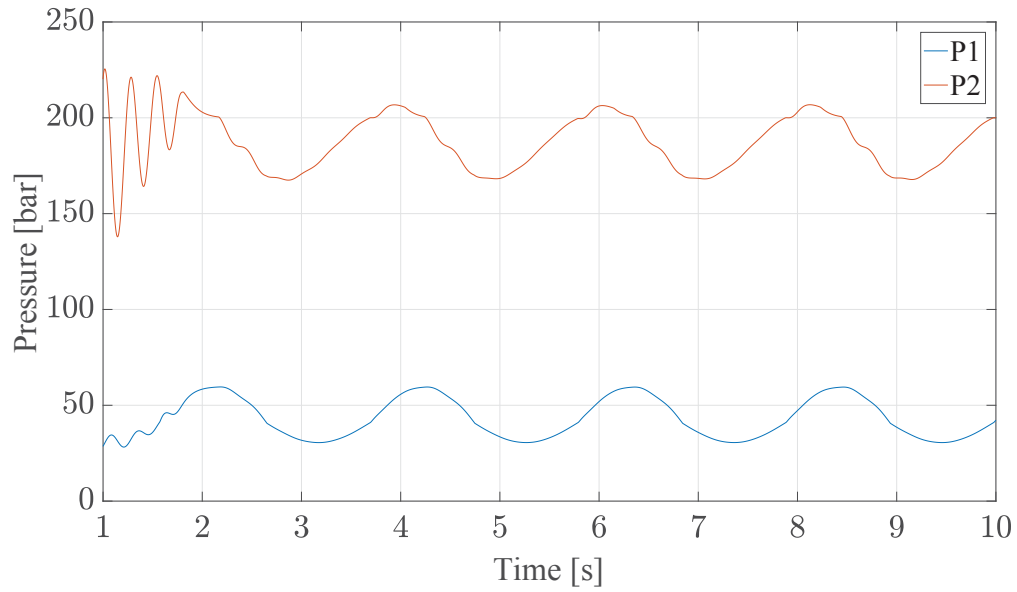


Figure 7.22: IFC pressure control with acceleration feedback $K_p=800$, $m=8000\text{kg}$

Figure 7.21 and Fig. 7.22 show that the system has no difficulties achieving the desired position with this load. The pressure value for the piston side is increased significantly as a result of the increased load. The further and last increase of the load on this system will be at weight of 12000 kg.

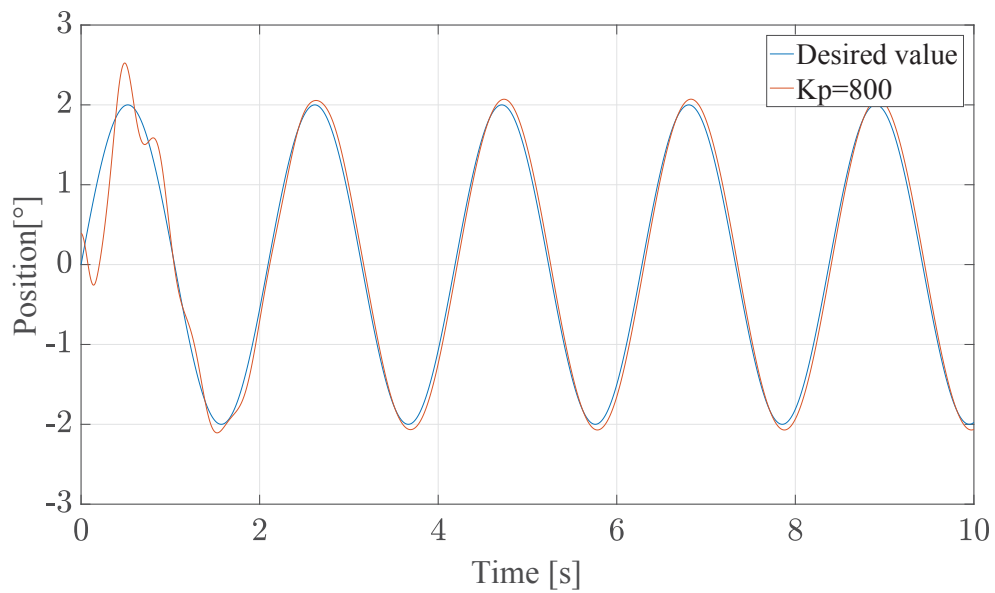


Figure 7.23: IFC position control with acceleration feedback $K_p=800$, $m=12000\text{kg}$

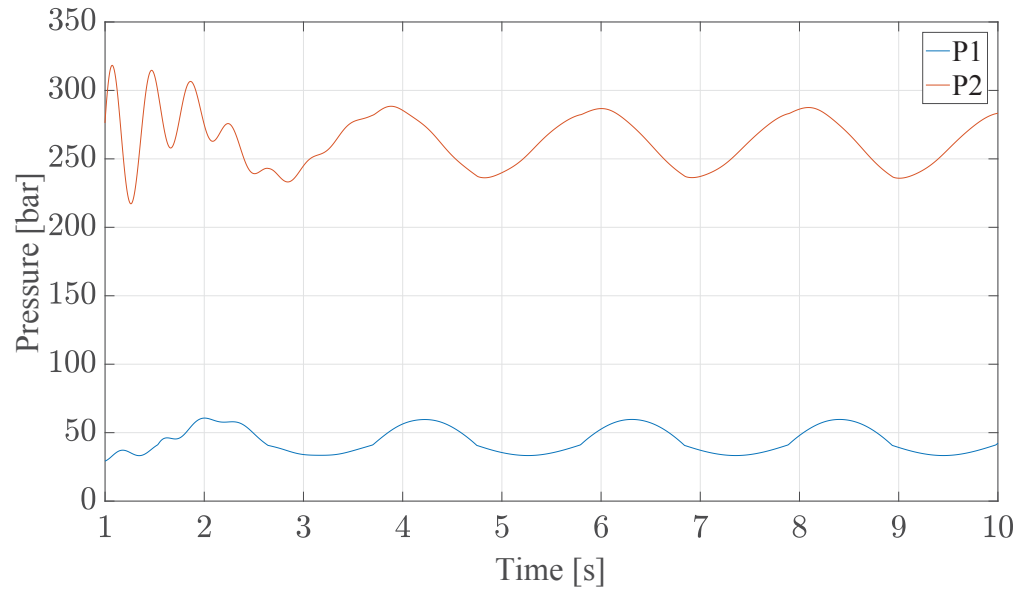


Figure 7.24: IFC pressure control with acceleration feedback $K_p=800$, $m=12000\text{kg}$

When the load is so big the oscillations of the systems are increased. In order to damp them and get stiffer performance the acceleration gain was increased at $K_a = 0.2$. In order to see how the valve reacts at so big values for the load we need to have closer look at the control algorithm.

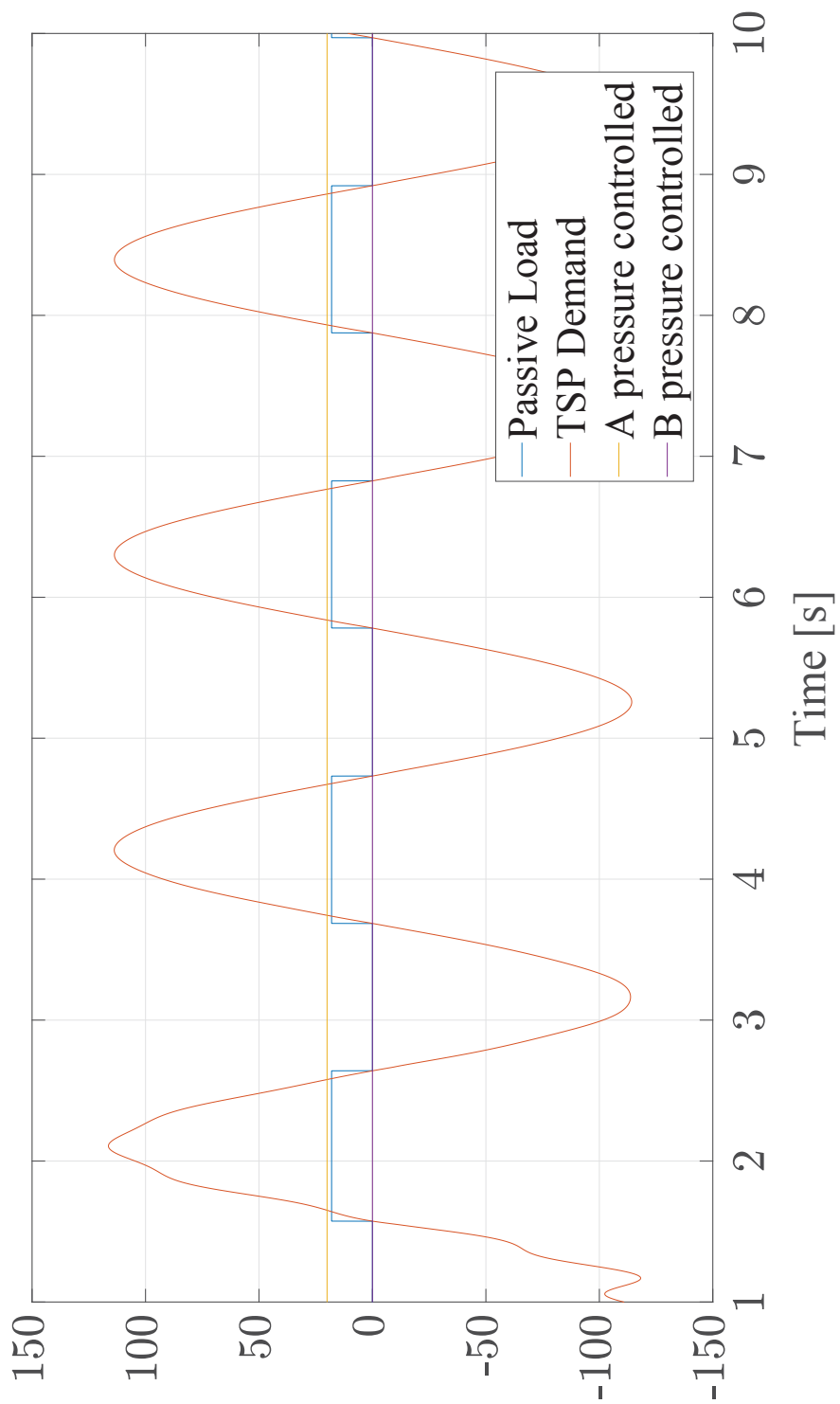


Figure 7.25: IFC control logic

Figure 7.25 shows the control of the system with IFC. The first two output values on this graph are the passive load and the TPS Demand. The passive load is set so that every time the load is passive it receives a value of 18 on the graph and every time it is active it is zero. The TPS Demand is already known and it represents the flow demand of the valve. As this valve offers pressure control on both sides, in order to see if the valve follows the right control logic given in Fig. 6.8 it is always set in that way that the A(rod side) is pressure controlled to be at zero and the B (piston side) is pressure controlled to show value of 19.

We can clearly see that every time the system moves up we get passive load which is expected, and every time the system moves in the opposite direction the load is active. That is also confirmed with the pressure control of the piston and the rod side. This leads us to the conclusion that the IFC control mode is well followed.

The last simulations done with this control mode show how this control mode will react when we apply vibration on the top of the beam. This block is shown in Fig. 6.9 as a vibration block. The force is implemented at the end of the beam at 3.4 meter distance. The input will be sinus with amplitude of 2 degrees and frequency of 3 rad/s. The acceleration gain is set at $K_a = 0.2$ and the weight on the beam is 3000 kg. The force that is implemented has the purpose of simulating the role of the vibration motor that was positioned on a similar location at the real test rig. The amplitude of the force is 15 kN and the frequency is 50 rad/s. The input is also a sinus function.

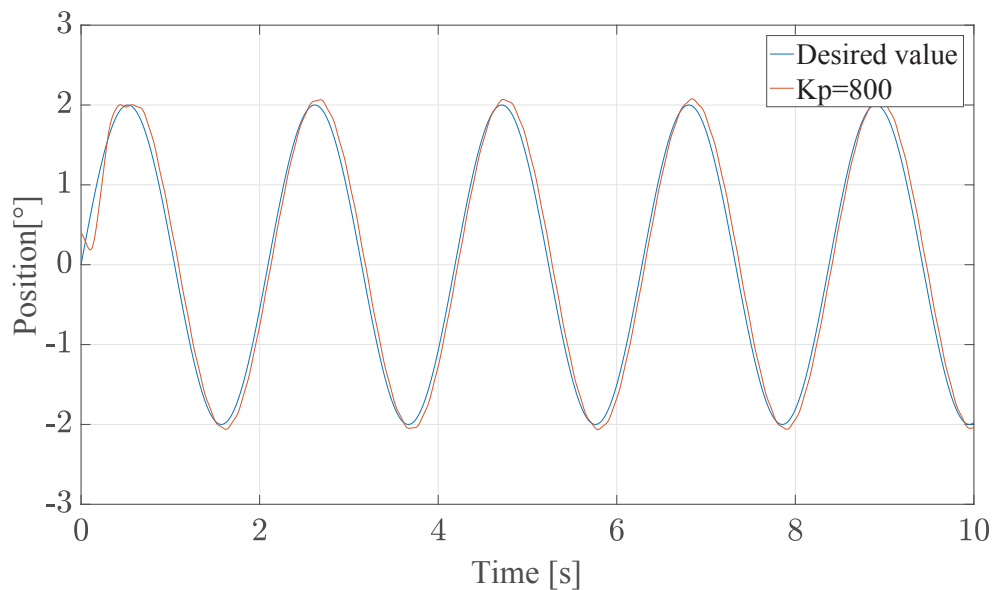


Figure 7.26: IFC position control with acceleration feedback and vibration $K_p=800$, $m=3000\text{kg}$

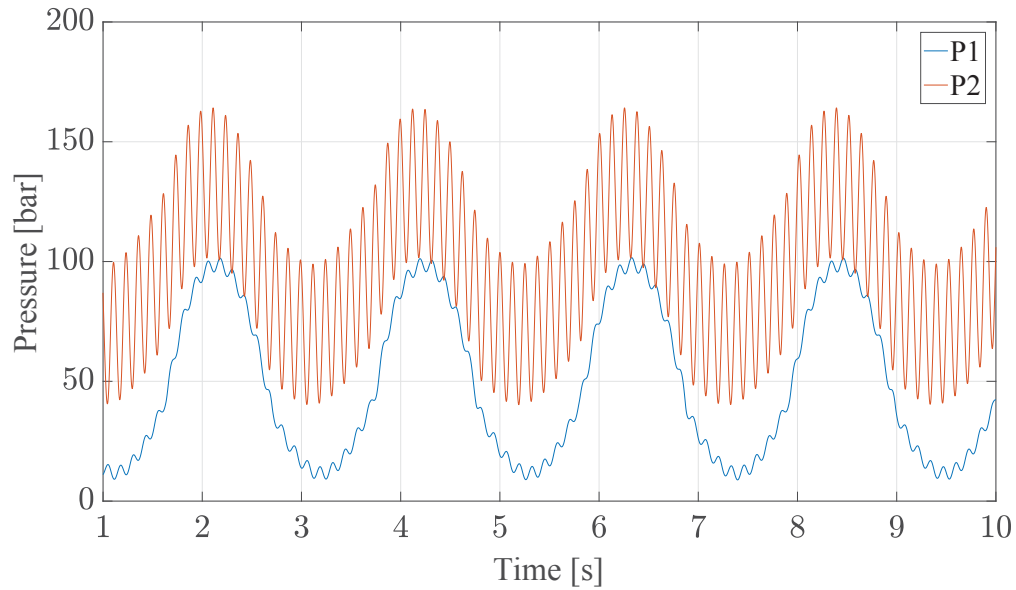


Figure 7.27: IFC pressure control with acceleration feedback and vibration $K_p=800$, $m=3000\text{kg}$

Figure 7.26 and Fig. 7.27 show the pressure and position control of the system by the given load. When we take a closer look at Fig. 7.26 we can see that it the desired value for the position is well followed and that the bigger part of the oscillations are damped. The pressure control on Fig. 7.27 shows that the pressure has a pick value of around 160 bar and that the system has a stiff response.

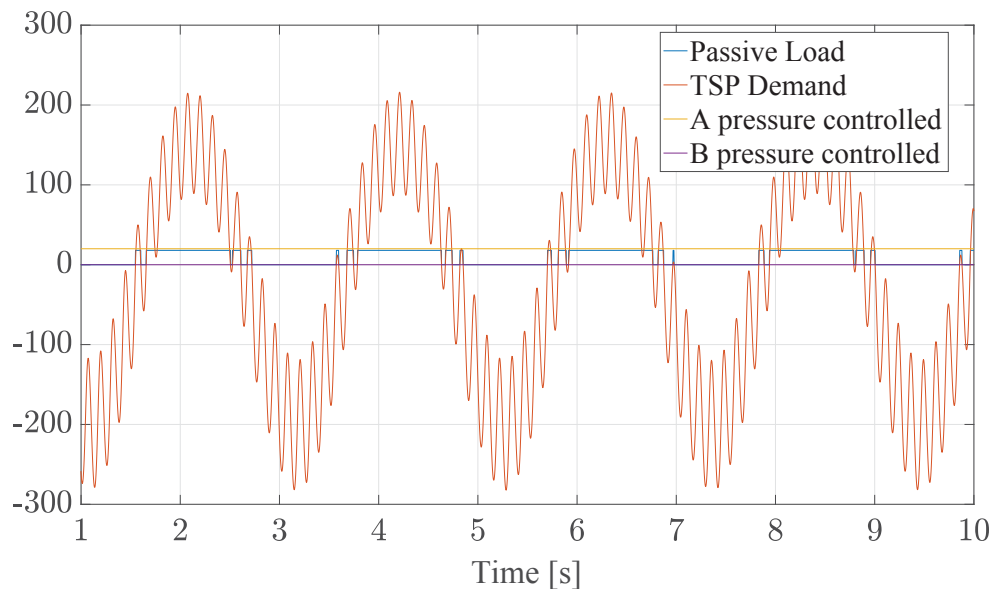


Figure 7.28: IFC control logic with acceleration feedback and vibration $K_p=800$, $m=3000\text{kg}$

In order to confirm the following results we will take a closer look at the control logic block for this simulation. As explained in Fig. 7.25 we can see in Fig. 7.28 that the control of the valve

is satisfactory and that the valve rather easily handles the change between active and passive load. With the fast response and the set passive and overrunning margins it is expected that the system will have stiffer response. This shows us that the system will not have problems for working in harsh environments and achieving the predicted cutting path.

Chapter 8

Verification of the Results

In order to verify the model simulated, numerous measurements at the real test rig were done. During the measurements similar desired values to the input were set and tested on the real system. Chapter 2.1.1 explains the parts which this model consists of. The parameters that were measured are:

1. Pressure on piston side
2. Pressure on rod side
3. Cylinder position
4. Spool position
5. Acceleration

In this chapter we will explain the instruments that are used for the measurements 8.1 and the results comparison in Chapter 8.2.

8.1 Measurement Instruments

In order to acquire all the necessary data during our tests we used the 'Sandvik aquisition system'. The values that we measure are actual pressure, flow, acceleration and we also have outputs of the position controller desired and actual value. The pressure was measured with the help of 'P3IC' pressure transducer, which is normally used to measure the static or dynamic pressure variance. The pressure limits are between 10 and 3000 bar. The acceleration was measured with the Kistler acceleration sensor from the 8630C series. It has a sensitivity of 1000 mV/g.

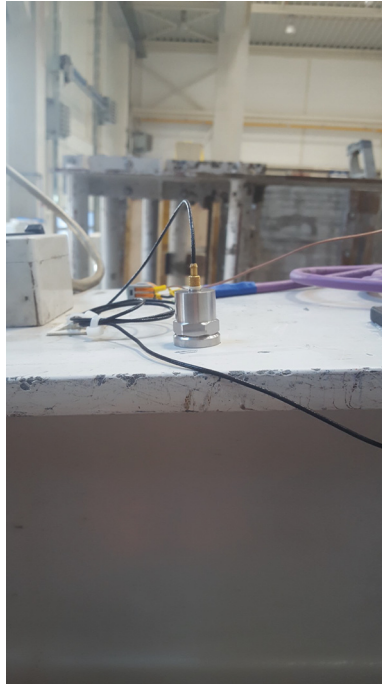


Figure 8.1: Acceleration sensor on test rig

The flow data was measured in the valve and sent to the controller with the help of the CANopen communication principle used in this system. This communication consists itself of 'SDOs' and 'PDOs' which are located in the object dictionary. A 'SDO' is a service data object which contains requests or answers from/to the object dictionary. But for most applications the 'SDO' communication is not efficient to handle the exchange of real process data [21]. The process data object 'PDO' implements an optimized solution for placing multiple process data variables from the object dictionary into a single CAN message [20]. The spool position data was sent to the controller in the same way as the flow data.



Figure 8.2: Eaton block



Figure 8.3: Test rig

8.2 Verification of the Model

In order to verify this model we used few measurement and simulation data. The measurements were done in few points. First the position of of the system was measured and verified and then the pressures on the piston and rode side were measured and compared with the simulation results.

Firstly we defined the inputs of the simulation and the measurements. By the position control we used a step-function input with a step time of 1 second and a step size of 1 degree. The weight on the system is 1t.

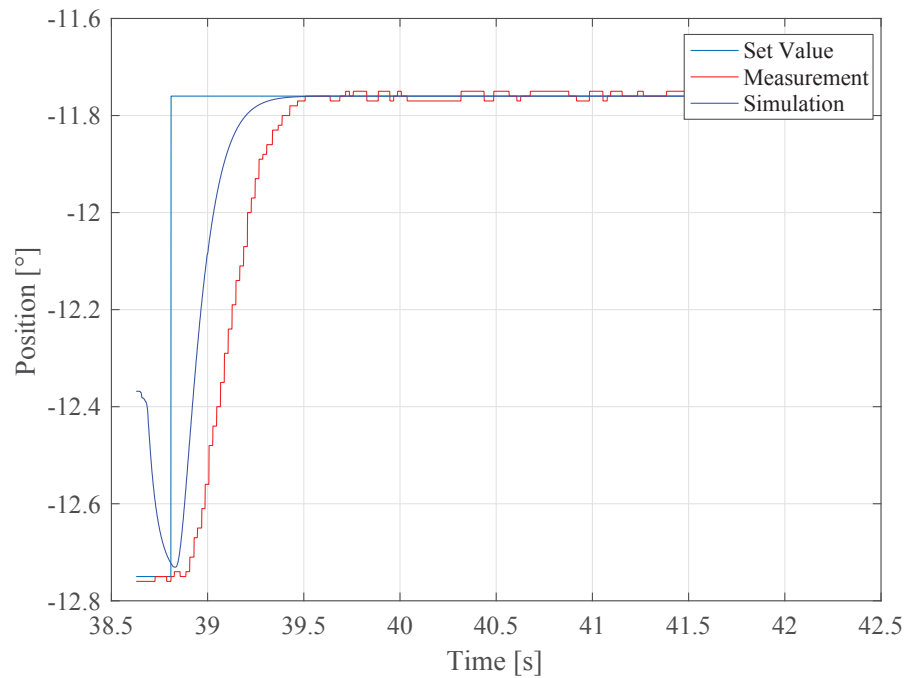


Figure 8.4: Verification of the position

Figure 8.4 shows the position signals for the simulation and the model. We can clearly see that in the both cases the position can be achieved quite fast and easily. At the beginning we have faster response at the simulation which at the end helps it to achieve the desired value a little bit faster.

In order to verify the model completely we needed to see the pressures for both sides at specific situation. As input value here we used a sinus function with the amplitude of 1 degree and the frequency of 1 rad/s. The weight was disconnected from the system and we were moving weightless.

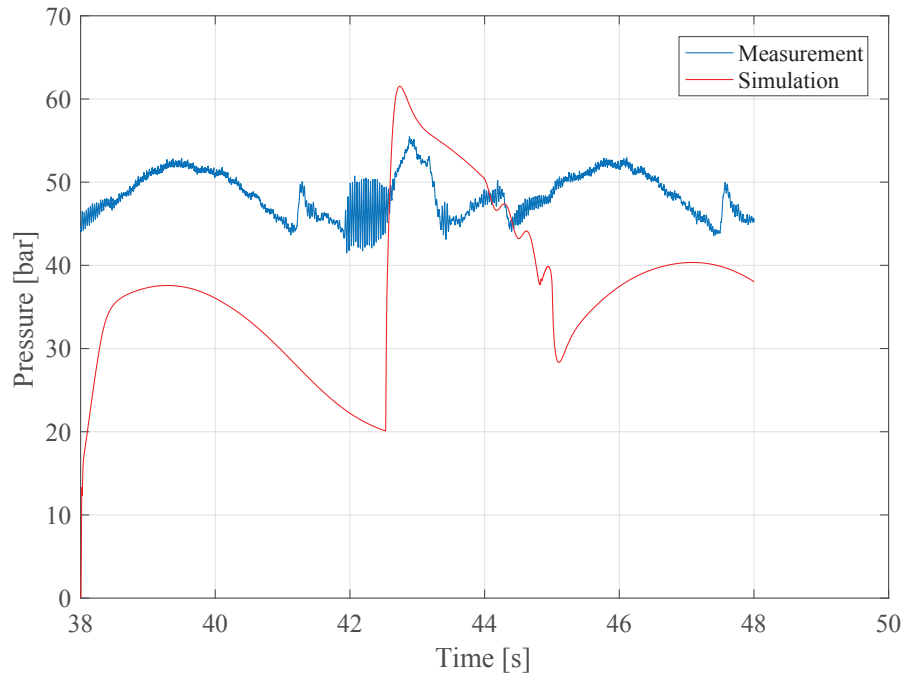


Figure 8.5: Pressure piston side verification

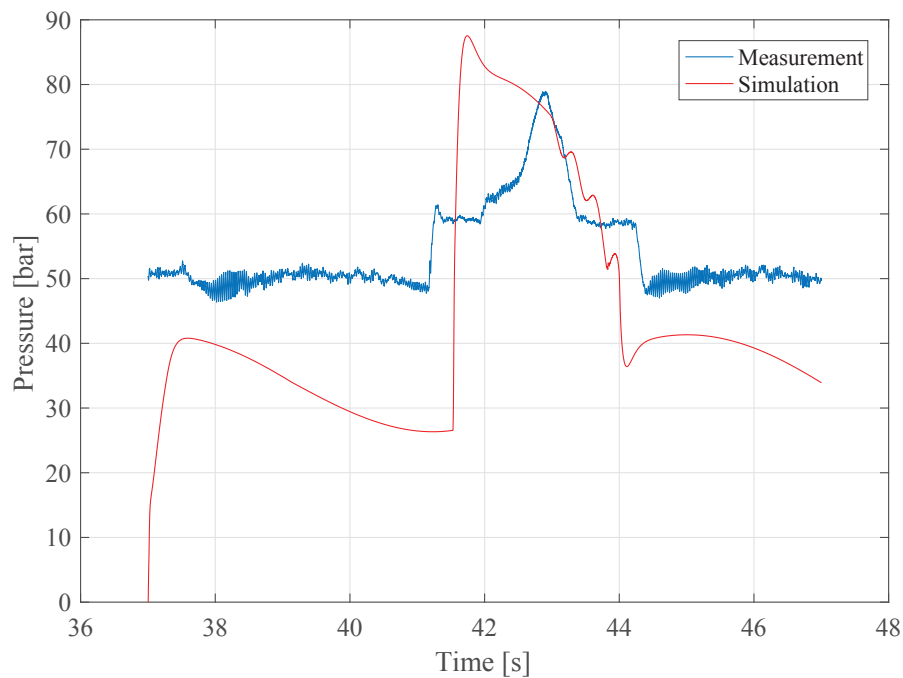


Figure 8.6: Pressure rod side verification

If we observe the both figures, Fig. 8.5 and Fig. 8.6 we can clearly see some similarities. In both cases the cylinder is moving up and then down. We can see that while moving down the pressure on the rod side is bigger from the pressure on the piston side which is expected. As when we move the we have an active load which the valve recognizes and as a result the pressure is increased in order to achieve constant velocity and no oscillations. There is a small differences in the pressure values as the result of the friction model. For our simulation a specific friction

model was not designed as it was not big importance to the system results.

Chapter 9

Conclusion and Future Recommendations

In this thesis a dynamic system of the test rig was created. In order to simulate the whole model the system was separated in three parts. First the mechanical model of the test rig. With the help of the Simscape[®] libraries which include bodies, joints the dynamic variables like forces, speed, acceleration, inertial moments were calculated.

Second the hydraulic model was created with the help of the differential state equations. The hydraulic model consists of hydraulic cylinder and hydraulic valve. A very advanced independent metering type of valve was used in the simulation.

At last, control system was designed in order to achieve better performance and energy efficiency. Two types of control system were simulated and tested. Flow control system, where both sides were flow controlled independent of the load and a pressure-flow controlled system where one side was always pressure controlled and the other side was always flow controlled dependent on the load status.

All three systems were combined with the help of the 'Prismatic Translational Interface', where the force that was responsible for the movement of the cylinder was calculated in the hydraulic system and as a result we measured the velocity of the prismatic joint. A weight was connected to the mechanical system in order to observe how the valve will react under more harsh conditions.

The dynamic system was simulated and tested for different types of inputs, in our case a sinus and step function and under different conditions. It is found that the flow control mode is has much lower energy efficiency of the flow-pressure control system and that loads (active or passive) or the inertia loads can have big influence on the system and that their control is very important.

The dynamic model simulation results were then compared with the real measurement data and the model was verified. It was found that the model accuracy can be increased by implementing a

specific friction model for the system.

We can conclude that dynamic models of the hydraulic systems can be used to determine what type of system will suit our application and can help to see the advantages and disadvantages of the different types of control systems used in our application. It can also help to determine which kind of controller is most suitable for our system.

This model can be used in future to determine the which type of valve or control system will suit the real system depending on the initial requirements. The application of different system can be done easily with few modifications.

Specific friction model for the hydraulic system can help to achieve better and more accurate analysis. The friction in the revolute joints in the mechanical system can be also calculated and implemented for further improvement of the system analysis.

Pipes, hydraulic relief valves, hydraulic pump and other hydraulic components which are not modelled in this system but can be simulated and implemented for better accuracy. The new Simscape® consists itself of a lot of complete hydraulic blocks for different types of hydraulic parts which can help constructing a more complex system.

The control systems implemented in this model and on the machine can be further improved by implementation of more complex algorithms and which will include more variables that can be controlled for better optimization of the system.

Appendix A

Code

Listing A.1: IFC control mode function block.

```
%%IFC control block function

function [SignalA,SignalB,outispassive,isApressurecontrolled,...
        isBpressurecontrolled] = fcn(TSPDemand,Diffload,QAControl,...
        QBControl,PAControl,PBControl)

%#codegen
OverrunningMargin=7;
PassiveMargin=2;
persistent ispassive
if isempty(ispassive)
    ispassive=false;
end
if TSPDemand>0
    Diffload=-Diffload;
end

if ispassive
    if Diffload>OverrunningMargin
        ispassive=false;
    end
else
    if Diffload<PassiveMargin
        ispassive=true;
    end
end
if TSPDemand>0
    if ispassive
        SignalA=QAControl;
        SignalB=PBControl;
```



```

    isApressurecontrolled=0;
    isBpressurecontrolled=19;

    else
        SignalA=PAControl;
        SignalB=QBControl;
        isApressurecontrolled=20;
        isBpressurecontrolled=0;
    end
elseif TSPDemand<0
    if ispassive
        SignalA=PAControl;
        SignalB=QBControl;
        isApressurecontrolled=20;
        isBpressurecontrolled=0;
    else
        SignalA=QAControl;
        SignalB=PBControl;
        isApressurecontrolled=0;
        isBpressurecontrolled=19;
    end
else
    SignalA=0;
    SignalB=0;
    isApressurecontrolled=0;
    isBpressurecontrolled=0;
end
outispassive=18*double(ispassive);

```

Listing A.2: UFC control mode function block.

```

%%UFC control block funciton

function [SignalA,SignalB,outispassive,...
    isAUFC,isBUFC] = fcn(TSPDemand,Diffload,QAControl,...
    QBControl,QAUFC,QBUFC)
%#codegen
OverrunningMargin=10;
PassiveMargin=5;
persistent ispassive
if isempty(ispassive)
    ispassive=false;
end
if TSPDemand>0
    Diffload=-Diffload;
end

```

```
if ispassive
    if Diffload>OverrunningMargin
        ispassive=false;
    end
else
    if Diffload<PassiveMargin
        ispassive=true;
    end
end
if TSPDemand>0
    if ispassive
        SignalA=QAControl;
        SignalB=QBUFC;
        isAUFC=0;
        isBUFC=18;

        else
            SignalA=QAControl;
            SignalB=QBUFC;
            isAUFC=0;
            isBUFC=18;
        end
elseif TSPDemand<0
    if ispassive
        SignalA=QAUFC;
        SignalB=QBControl;
        isAUFC=20;
        isBUFC=0;

        else
            SignalA=QAUFC;
            SignalB=QBControl;
            isAUFC=20;
            isBUFC=0;
        end
else
    SignalA=0;
    SignalB=0;
    isAUFC=0;
    isBUFC=0;
end
outispassive=18*double(ispassive);
```

Listing A.3: Mathematical model of I beam.

```

%I Beam Mask

W_I_Beam=300;           %mm
H_I_Beam=300;           %mm
T_I_Beam=11;           %mm
Tf_I_Beam=19;          %mm
D_I_Beam=H_I_Beam/2-Tf_I_Beam;
rho=7800;               %kg/m^3

%I Beam General Extrusion Model
A=[W_I_Beam/2, -H_I_Beam/2];
B=[W_I_Beam/2, -D_I_Beam];
C=[T_I_Beam/2, -D_I_Beam];
D=[T_I_Beam/2, D_I_Beam];
E=[W_I_Beam/2, D_I_Beam];
F=[W_I_Beam/2, H_I_Beam/2];
HalfCS = [W_I_Beam/2, -H_I_Beam/2; W_I_Beam/2, ...
          -D_I_Beam; T_I_Beam/2, -D_I_Beam; ...
          T_I_Beam/2, D_I_Beam; W_I_Beam/2, ...
          D_I_Beam; W_I_Beam/2, H_I_Beam/2];
I_Beam_CS=[HalfCS; -HalfCS];

```

Listing A.4: Mathematical model of the bracket form.

```

%% Mathematical model of the bracket
bracketForm = [];

%% Bracket Form
y = Hbracket - (Wbracket/2);
angle = linspace(0,pi,Nc/2)';
bracketForm = [(Wbracket/2)*cos(angle) (y+(Wbracket/2)*sin(angle))];
bracketForm = [bracketForm; ...
              -Wbracket/2 0;0 0];

%% Hole
angle = linspace(3*pi/2,-pi/2,Nc)';
bracketForm = [bracketForm; ...
              Rhole*cos(angle) (Hhole+(Rhole*sin(angle)))]];
bracketForm = [bracketForm; ...
              0 0;Wbracket/2 0];

```

Bibliography

- [1] Aleksandar T. N. *Hidraulicni Volumenski Mashini*. Skopje, 2011.
- [2] Amir S. *Quasi-Static Hydraulic Control Systems and Energy Savings Potential Using Independent Metering Four-Valve Assembly Configuration*. Phd, Woodruff School of Mechanical Engineering, August/2006.
- [3] Andersen O.T., editor. *Fluid Power Systems: Modeling and Analysis*. 2 nd edition edition, 2003.
- [4] K. J. Åström and T. Hägglund. *PID controllers*. ISA, Research Triangle Park, N.C., 2nd ed. edition, 1995.
- [5] BORAN K. *DYNAMIC MODELLING OF A BACKHOE-LOADER*. Master thesis, METU, Ankara, Turkey, September/2009.
- [6] Brain A.H., Pierre D., Carlos C.W. A survey of models, analysis tools and compensation methods for the control machines with friction. 1994.
- [7] Eaton. Cma user manual(v1.1) valve sw version 3.8 od version 3.2, 12/2015.
- [8] B. Eriksson and J.-O. Palmberg. Individual metering fluid power systems: Challenges and opportunities. *Proceedings of the Institution of Mechanical Engineers, Part I: Journal of Systems and Control Engineering*, 225(2):196–211, 2011.
- [9] H. E. Exner. *Hydraulics: Basic principles and components*, volume Vol. 1 of *The hydraulic trainer*. Bosch Rexroth, Erbach [Germany], 3rd rev. ed. edition, 2004.
- [10] FitzSimons P. M., Palazzolo J. J. Part ii: Control of a one-degree-of-freedom active hydraulic mount. II(J. Dyn. Sys., Meas., Control 118(3)):6, 1996.
- [11] G. F. Franklin, D. J. Powell, and Abbas E.N. *Feedback control of dynamic systems*. 5th ed. edition, 2006.
- [12] Hu Z., Xu D., Liu G., Jia C. Study on co - simulation technology based on adams and matlab. 2015.
- [13] M. Jelali and A. Kroll. *Hydraulic servo-systems: Modelling, identification, and control / Mohieddine Jelali and Andreas Kroll*. Advances in industrial control. Springer, London, 2003.

- [14] John F., Peter G. L. *Collaborative design for embedded systems: Co-modelling and co-simulation*. Springer, New York, 2014.
- [15] S. R. Majumdar. *Oil hydraulic systems: Principles and maintenance*. McGraw-Hill, New Delhi, 7th ed. edition, 2005, ©2001.
- [16] Mannesmann Rexroth. Hydraulic - training axial piston units.
- [17] H. E. Merritt. *Hydraulic control systems*. Wiley, New York and Chichester, 1967.
- [18] Moog INC. A brief hystory of electrohydraulic servomechanisms. 1978.
- [19] Olsson H. *Control Systems with Friction*. Phd, Lund Institute of Technology, Lund, Sweden, 1996.
- [20] O. Pfeiffer, A. Ayre, and C. Keydel. *Embedded networking with CAN and CANopen*. RTC, San Clemente, CA, 2003.
- [21] O. Pfeiffer, A. Ayre, and C. Keydel. *Embedded networking with CAN and CANopen: [Requirements for understanding embedded networking code and communications, the underlying CAN technology, selecting CAN controllers, implementation options, application-specific examples of popular device profiles]*. Copperhill Technologies Corp, Greenfield, Mass., rev. 1. ed. edition, 2009.
- [22] R. Braun, A. Asghar, A. Pop, D. Fritzson. An open - source framework for efficient co - simulation of fluid power systems. 2017.
- [23] Rydberg K.E., editor. *Hydraulic Servo Systems - Dynamic Properties and Control*. Linköping, Sweden, 2016.
- [24] Sena T., Semih Y., Semih G. P, pd, pi, pid controllers.
- [25] Welch T. R. The use of derivative pressure feedback in high performance hydraulic servomechanisms. (J. Eng. Ind 84(1), 8-14):7, 1962.
- [26] D. Will, H. Ströhl, and N. Gebhardt. *Hydraulik: Grundlagen, Komponenten, Schaltungen*. Springer, Berlin and New York, 2., neu bearb. aufl. edition, 2004.
- [27] Yuken Kogyo CO. LTD. *Basic Hydraulics and Components*. Minato-ku, Tokyo, Japan, 2005.
- [28] E. Zaev. *Hardware in the Loop for real - time simulation of complex mechanical systems and their control*. Doctoral dissertation, Faculty of Mechanical engineering, Skopje, 02/2013.
- [29] ZHAW University of applied science. Capacitance (hydraulic).